

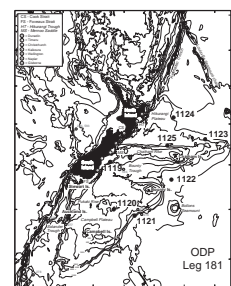
## 1. LEG 181 SUMMARY: SOUTHWEST PACIFIC PALEOCEANOGRAPHY<sup>1</sup>

Shipboard Scientific Party<sup>2</sup>

### INTRODUCTION

The circulation of cold, deep Antarctic Bottom Water (AABW) is one of the controlling factors in the Earth's heat budget and, ultimately, climate. Today, 40% of the flux of cold bottom water entering the major ocean basins does so through the Southwest Pacific Ocean, as a thermohaline Deep Western Boundary Current (DWBC) (Warren, 1981). The cold water in the DWBC is derived through dense waters sinking around Antarctica and through the entrainment and mixing of deep Atlantic and Indian ocean waters by the wind-driven Antarctic Circumpolar Current (ACC). At the approach to the Pacific Ocean, filaments of the ACC pass around and through gaps in the Macquarie Ridge to reunite further east and flow northeast along the eastern edge of the New Zealand microcontinent (Fig. F1). Early in its journey, where it flows along the edge of the Campbell Plateau, the DWBC is reinforced by the ACC. At 56°S, and at the southern edge of the Bounty Trough (46°S), branches of the ACC veer east and continue across the Pacific, whereas the DWBC flows on north at depths between ~4500 and ~2000 m, across the Bounty Fan, around the eastern end of the Chatham Rise, northward across the eastern boundary of the Hikurangi Plateau, to finally turn north and flow toward the equator along the Tonga-Kermadec Ridge. Higher in the water column, north-spreading Antarctic Intermediate Water (AAIW), formed by subduction near the Antarctic Polar Front (APF), bathes the top and eastern upper flank of the Campbell Plateau in depths of 400–1500 m.

F1. Bathymetric map of the eastern New Zealand region, [p. 39](#).



<sup>1</sup>Examples of how to reference the whole or part of this volume.

<sup>2</sup>Shipboard Scientific Party addresses.

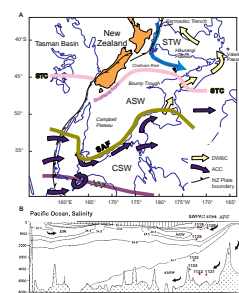
## EARLIER RESEARCH

Despite the key location of eastern New Zealand at the gateway for major water flows into the Pacific Ocean, no previous Ocean Drilling Program (ODP) drilling has been accomplished in the region. Of the four earlier Deep Sea Drilling Project (DSDP) sites (Fig. F1), only one was cored with the advanced hydraulic piston corer (APC)—Site 594 in the inner Bounty Trough, which penetrated a thick sequence of hemipelagic muds and nannofossil chinks, dated back to the late early Miocene (Kennett, von der Borch, et al., 1986). Results from this site yielded important information regarding the synchronicity of glaciations between the hemispheres (Nelson et al., 1986b), the history of supply of AAIW, and the historic properties and evolution of the Subtropical Convergence (STC) and the Subantarctic Front (SAF) (Nelson et al., 1986b, 1993; Dersch and Stein, 1991; Kowalski and Meyers, 1997) (Fig. F2). The three other DSDP sites were Sites 275 and 276, which were rotary drilled at locations on the edge of the Campbell Plateau where active erosion had removed a large part of the record, and Site 277, on the western edge of the Campbell Plateau, where an exceptional Paleogene–Neogene isotope record was recovered (Shackleton and Kennett, 1975). In addition to the DSDP Site 594 results, new research into the late Quaternary oceanographic, climatic, and sedimentary history of offshore eastern New Zealand has burgeoned since the early 1980s (e.g., Griggs et al., 1983; Carter and Carter, 1988, 1993; Carter and Mitchell, 1987; Barnes, 1992; Fenner et al., 1992; Carter et al., 1994; Carter and McCave, 1994, 1997; L. Carter et al., 1990, 1995, 1996; R. Carter et al., 1996; Lean and McCave, 1998; Lewis, 1994; Lewis et al., 1998; Nelson et al., 1986a, 1986b, 1993, 1994; McCave and Carter, 1997; Thiede et al., 1997; Weaver et al., 1997, 1998). This work notwithstanding, the lack of cored offshore drill holes means that we remain ignorant of the post-mid-Cenozoic paleoceanography for most of the region, apart from occasional studies from the western shallow water and onland edge of the basin (Ward and Lewis, 1975; Carter, 1985; Fulthorpe et al., 1996; R. Carter et al., 1996). Recent seismic studies have delineated the offshore structure moderately well (Lewis et al., 1986; R. Carter, 1988a, 1988b; R. Carter et al., 1994, 1996; Lewis, 1994; Barnes and de Lepinay, 1997), and this is the region that we must now search for the record of the inception and evolution of the large ACC and the Pacific DWBC current systems.

## BACKGROUND AND OBJECTIVES OF LEG 181

In summary, our knowledge of Southwest Pacific Ocean history, and, in particular, the development of the ACC-DWBC system, is extremely poor. Leg 181 researchers, therefore, drilled seven holes in the eastern New Zealand region to attempt to reconstruct the stratigraphy, paleohydrography, and dynamics of the DWBC and related water masses (Figs. F1, F2A). The sites composed a transect of water depths from 393 to 4460 m and spanned a latitudinal range from 39°S to 51°S (Fig. F2). Leg 181 drilling has provided the data needed to study a range of problems in Southern Ocean Neogene paleohydrography, sedimentology, paleoclimatology, and micropaleontology.

F2. Bathymetry, meridional salinity cross section, and water masses, p. 40.



## Tectonic Creation of the Southern Ocean

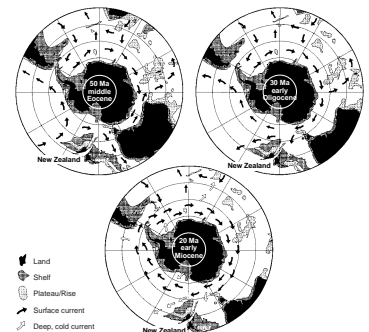
The origin of the modern thermohaline ocean circulation system must postdate the tectonic creation of a continuous Southern Ocean. Particularly important for the origin of the ACC-DWBC was the opening of the Australian-Antarctic (South Tasman) and South American-Antarctic (Drake Passage) deep-water flow gateways (Molnar et al., 1975; Lawver et al., 1992). The South Tasman gateway, including the Balleny Fracture Zone, opened to deep water in the early Oligocene (~32 Ma), thereby allowing connection between the Indian and Pacific Oceans for the first time (Kennett et al., 1972; Kennett, 1977). Later, at ~20 Ma (earliest Miocene), the opening of Drake Passage (Boltovskoy, 1980) allowed the establishment of the full circum-Antarctic oceanic circulation. During the critical late Eocene to Miocene period, the New Zealand microcontinent was located downcurrent from the evolving South Tasman gateway (Watkins and Kennett, 1971, 1972), directly in the path of the evolving ACC-DWBC system (Fig. F3).

## Geologic Setting

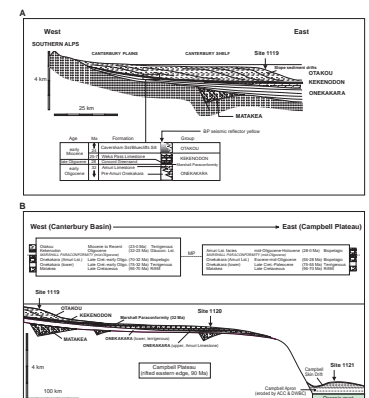
The evolution of the ACC-DWBC system took place during the Oligocene and earliest Miocene (32–20 Ma), when plate movements created the first deep-water oceanic gaps south of Australia and South America. The stratigraphic record of these events, and of the development of the modern ACC-DWBC, occurs in Cenozoic sediments located on and just east of the New Zealand microcontinental plateau (Fig. F4). South Island, New Zealand, is today transected by the Alpine Fault boundary between the colliding Australian and Pacific plates, but the greater part of eastern New Zealand has been unaffected by major tectonic events since the phase of Late Cretaceous rifting that created the South Pacific Ocean and first delineated the New Zealand Pacific continental margin. In short, since the Late Cretaceous, eastern New Zealand—which includes the submerged continental crust of Campbell Plateau and Chatham Rise, separated by the rift re-entrant of the Bounty Trough—has been a trailing-edge passive margin and subject to thermotectonic subsidence and marine transgression (Cotton, 1955; Carter, 1988b).

The geological history of eastern New Zealand therefore consists of Late Cretaceous rift-valley fill (Bishop and Laird, 1976), followed by peneplanation and a marine transgression that reached its climax in the Oligocene, when almost the entire New Zealand plateau was submerged, terrigenous sources were flooded or buried, and regional carbonate sedimentation reigned supreme (Fleming, 1975; Suggate et al., 1978). In the west, tectonic activity, associated with the development of the transform plate boundary through New Zealand, started in the late Eocene (Turnbull, 1985; Turnbull and Uruski, 1995; Sutherland, 1995), and, by the early Miocene, copious volumes of terrigenous sediment from mountains along the Alpine Fault were being shed eastward into the Canterbury Basin, where they built the progradational sedimentary prism that underlies the modern coastal lowland and continental shelf of eastern South Island (Carter and Norris, 1976; Norris et al., 1978). Mountain building accelerated, and, presumably, sediment yields increased, at ~6.5 Ma in the late Miocene, when a shift in the pole of rotation resulted in a stronger element of collision across the Alpine Fault boundary (Walcott, 1998). These various plate boundary events had only minor effects in the eastern (offshore) parts of the New Zealand

F3. Southern Hemisphere plate tectonic reconstructions, p. 42.



F4. Geologic cross sections, p. 43.



plateau (Fig. F4B). Apart from localized episodes of volcanism and mild folding-faulting associated with changes in regional stress patterns (e.g., Oliver et al., 1950; Carter, 1988a; Carter et al., 1994; Campbell et al., 1993), stasis or very slow postrift subsidence continued, and major sources of terrigenous sediment were absent. Sediment accumulation on bathymetric highs was either precluded by strong water motion (e.g., Chatham Rise) or consisted of biopelagic ooze and chalk (e.g., Campbell Plateau). In contrast, terrigenous sedimentation was restricted mainly to bathymetric lows (e.g., Bounty Channel-Fan complex) or to sites adjacent to the prograding eastern New Zealand sediment prism (e.g., DSDP Site 594; Kennett, von der Borch, et al., 1986).

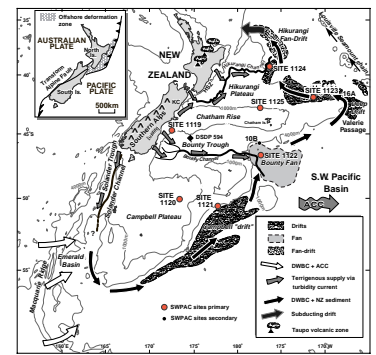
Modern New Zealand is transected by the plate boundary between the Pacific and Australian plates (Fig. F5). In South Island, the boundary is marked by the Alpine Fault transform, which passes north into the active arc volcanism of central North Island, east of which the Hikurangi subduction complex marks the subduction of the Pacific Plate under eastern North Island. The geology of eastern North Island (the East Coast Basin) is therefore complex and largely allochthonous (Stoneley, 1968), within which individual tectonic slices represent the emplacement of forearc shelf and slope-basin sediments throughout the Neogene (Ballance, 1976; Lewis, 1980; Pettinga, 1982; Lewis and Pettinga, 1993). The tectonic activity, basin formation, and enhanced terrigenous sedimentation rates that relate to the modern plate boundary commenced in the late Oligocene at ~25 Ma (Field et al., 1997).

All Leg 181 sites are located on the Pacific Plate and penetrated the typical eastern New Zealand rift-drift, or passive margin, succession. However, the results from sites that transected Paleogene sediments (e.g., Sites 1121 and 1124), and also those that are located north of Chatham Rise and contained abundant Miocene and younger tephras (e.g., Sites 1123, 1124, and 1125), are extremely relevant to the interpretation of North Island East Coast Basin geology. The Leg 181 Paleogene successions include deep-marine siliceous mudstone, brown mudstone, and nannochalks, which have close counterparts, respectively, in the Whangai Shale, Waipawa Black Shale, and Amuri Limestone facies onland. The succession of siliceous shale-black shale-nannofossil ooze may be regionally homotaxial and results partly from the postrift subsidence of the margin and partly from change in oceanographic factors through time (cf. Andrews, 1979). Particular sediment facies may therefore be of different ages offshore and onshore, but, in all cases, the occurrence of Leg 181 Paleogene facies within the North Island allochthon represents the accretion onto the Australian Plate of former Pacific Plate deep-marine continental margin sediments. This is an important conclusion, given that there has been a protracted controversy over a shallow vs. a deep-water origin for the onland East Coast Basin Paleogene sediment facies (e.g., Field et al., 1997). Finally, study of the tephra-rich Miocene and younger sediments from Leg 181 sites will help establish a greatly improved timetable of volcanic and tectonic activity for the Hikurangi margin.

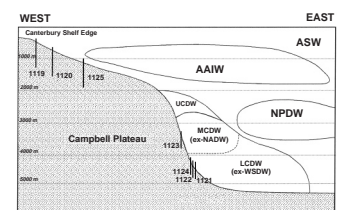
## Oceanography: Deep Currents

The supply of deep water to the Pacific Ocean is dominated by a single source, the DWBC, which flows north out of the Southern Ocean along the east side of the Campbell Plateau–Chatham Rise–Hikurangi Plateau, east of New Zealand (Figs. F2, F6). The volume transport of the

F5. Eastern New Zealand Oceanic Sedimentary System (ENZOSS), p. 44.



F6. West to east cross section through major water masses, p. 45.





DWBC is  $\sim 20 \times 10^6 \text{ m}^3 \text{ s}^{-1}$  (Sv), which composes  $\sim 40\%$  of the total input of deep water to the world's oceans (Warren, 1973; 1981). A secondary, but minor, deep flow of  $\sim 3$  Sv passes north into the Peru-Chile basin (Lonsdale, 1976). The magnitude of DWBC flow and the low temperature of the water involved are major determinants of the oceanography of the Pacific Ocean and of the global heat balance. Monitoring the DWBC flow at its entry into the Pacific is a key area where the "global thermohaline conveyor" hypothesis (Gordon, 1986; Broecker et al., 1990; Schmitz, 1995) can be tested, as the flow thereafter is believed to spread out to fill the Pacific. Some water upwells and returns at shallower depths across the Indian Ocean and on to the Atlantic, whereas other waters return south as North Pacific Deep Water (NPDW).

The supply of cold water to the deep Pacific from the main generating regions in the Weddell and Ross Seas is modulated by the ACC, which mixes these waters with North Atlantic Deep Water (NADW) in the Atlantic sector of the Southern Ocean to form Circumpolar Deep Water (CDW). Deep water output to the Pacific therefore carries the combined signatures of Southern Ocean processes in the region of deep water formation, chemical composition related to Southern Ocean gas exchange, and NADW. Despite its turbulent passage around Antarctica, CDW is not completely mixed, and a distinct NADW salinity maximum can be recognized at depths of 2800 m (at 55°S), deepening northward to 3400 m (at 28°S). In the Southwest Pacific, the DWBC comprises three main divisions: lower CDW, a mixture of bottom waters generated around Antarctica, in particular cold Weddell Sea Deep Water (Pudsey et al., 1988); salinity-maximum middle CDW, representing the NADW core; and strongly nutrient-enriched and oxygen-depleted upper CDW, mainly derived from Indian Ocean outflow added to Pacific outflow returning through Drake Passage (Fig. F6). The DWBC has its upper boundary at depths around 2000–2500 m. On the eastern side, the DWBC is overlain between 2500 and 3500 m depth by south-flowing NPDW, marked by an oxygen minimum and high silica content. Regionally, both DWBC and NPDW are overlain by low-salinity AAIW (Figs. F2B, F6).

The ACC-DWBC enters the Southwest Pacific around and through gaps in the Macquarie Ridge complex before passing along the 3500-m-high margin of the Campbell Plateau. Near the mouth of the Bounty Trough, the ACC uncouples and continues its eastward path, whereas the DWBC flows north around the eastern end of Chatham Rise and through Valerie Passage, where a small part of the flow diverges along the eastern margin of the Louisville Seamount chain (McCave and Carter, 1997; cf. Lonsdale, 1988). Valerie Passage, the 250-km-wide gap between the Chatham Rise and the Louisville Seamount chain, therefore marks the gateway to the Pacific for the DWBC (Warren, 1973).

### **Oceanography: Shallow Fronts**

In the shallower ocean, the seas east of South Island are crossed by two major frontal systems that exhibit intensified meridional gradients in temperature, salinity, and density (Fig. F2). At around 55°S, the east-flowing ACC is bounded to the north by the SAF (Orsi et al., 1995), but it then curls north around the southeastern corner of the Campbell Plateau to almost 50°S. South of the SAF, the annual mean surface-water temperature is  $<10^\circ\text{C}$ , and the nutrient-rich polar ocean is rich in both phosphate and silica. The observations of Bryden and Heath (1985), together with global circulation models (Carter and Wilkins, in press),

indicate that another unnamed front may extend east into the Pacific from the south side of the Bounty Trough. This front, at about latitude 46°S, probably marks the northern limit of the ACC east of New Zealand, rather than the 56°S SAF that is usually taken as the ACC limit (e.g., Orsi et al., 1995).

About 10° of latitude north of the SAF, the STC separates subantarctic water of salinity 34.5 and an annual surface-temperature range of 8°–15°C from subtropical water with salinity >35 and annual temperatures of >15°C. East-flowing currents occur on both sides of the STC, the warm East Cape Current (ECC; a continuation of the East Australian current) on the north side, and the cold West Wind Drift on the south. Interaction of the ECC with the bathymetry, the strong density gradients of the STC, and tides all interact to produce a strong, variable current regime (e.g., Chiswell, 1994a; Heath, 1985). Eastward flow on the south side of the STC is augmented by the Southland Current, which passes around the south end of South Island and then flows north along the eastern South Island continental margin before splitting, with one branch flowing north through Mernoo Saddle and the other branch turning east along the southern side of the crest of Chatham Rise (Heath, 1985).

Heat transfer from the equator to the pole takes place across the SAF and STC by a combination of wind drift and dynamic eddying, with a cold return flow at depth in the DWBC. In the open ocean, as demonstrated in the Indian sector of the Southern Ocean, these fronts may migrate backward and forward by up to 6° of latitude during a glacial/interglacial cycle (e.g., Howard and Prell, 1992). However, modern seasonal movements of the front of at least 2° of latitude occur also, as for example for the STC east of New Zealand (Chiswell, 1994b). In contrast to the seasonal oceanic mobility of the STC, several authors have shown that, over the long term, the STC has probably remained in the vicinity of the shallow Chatham Rise throughout at least the most recent climatic cycle (Fenner et al., 1992; Nelson et al., 1993; Weaver et al., 1998).

The pronounced bathymetry around New Zealand exercises a controlling influence on the disposition of both deep currents and oceanic frontal zones. Notably, the ACC and DWBC are steered around or through gaps in Macquarie Ridge and are then guided northward along the eastern escarpment of the Campbell Plateau. Concomitantly, in near-surface waters, the ACC bounded by the SAF is forced north around and along the southeastern corner of the Campbell Plateau, whereas the position of the STC is probably regulated by the eastward currents flowing along north and south flanks of Chatham Rise. Some Leg 181 sites were chosen to track whether or not past changes in the position of these fronts have occurred.

### **Sedimentary Record of the ACC-DWBC**

Sediments on the eastern New Zealand margin at shelf to upper bathyal depths (50–1000 m) are known to have been strongly affected by currents since at least the late Oligocene (Ward and Lewis, 1975; Carter, 1985; Fulthorpe and Carter, 1991; R. Carter et al., 1996). This evidence for strong paleoflows, together with the confirmation that substantial Antarctic glaciation commenced at least as early as the early Oligocene (Shackleton and Kennett, 1975; Barrett, 1996; Barron, Larsen, et al., 1989), implies that Pacific hydrography has been funda-

mentally affected by an evolving circumpolar current and western boundary current system since the middle Cenozoic.

To reconstruct the paleoflow of the DWBC and overlying current system requires drill sites through thick, undisturbed, fine-grained sediment masses constructed under the influence of the current. Seismic records indicate the presence of candidate sediment drifts at many points along the eastern edge of the New Zealand microcontinent, in water and paleo-water depths between ~300 and 5500 m (Fulthorpe and Carter, 1991; Carter and McCave, 1994; L. Carter et al., 1996). There are, however, five possible origins for any particular body of sediment: (1) deposition as part of the deepening- and fining-upward rift-drift cycle that characterizes New Zealand's Cretaceous to Oligocene history (i.e., Matakaea and Onekakara Group equivalents [Carter, 1988b]; cf. Fig. F4); (2) transport into the area via the DWBC (e.g., subantarctic diatoms present in the drifts at 40°S; Carter and Mitchell, 1987); (3) biopelagic snow (Nodder, 1998); (4) airfall rhyolitic and andesitic tephra, which derives from explosive Miocene–Holocene arc volcanism in New Zealand (Ninkovich, 1968; van der Lingen, 1968; Lewis and Kohn, 1973; Nelson et al., 1986a; Froggatt et al., 1986; Froggatt and Lowe, 1990; Shane, 1990; Shane and Froggatt, 1991; Alloway et al., 1993; Carter et al., 1995; Shane et al., 1995, 1996), and which, over the last 20 k.y., has been input at rates up to one-third that of fluvial terrigenous sediment (L. Carter et al., 1996); and (5) terrigenous sediment that is derived from uplifting mountains in New Zealand, after the inception of the modern Alpine Fault plate boundary (i.e., Miocene–Holocene Otakou Group equivalents [Carter, 1988b]; cf. Fig. F4A) and transported into the path of the DWBC by turbidity currents traveling down the Solander, Bounty, and Hikurangi Channel systems. Each of these sediment sources can be constrained, and the sedimentary dynamics and transport paths of the modern system are moderately well delineated (e.g., Carter and Carter, 1993; Carter and McCave, 1997; Lewis, 1994). In contrast, little is known regarding the geologic record or history of the DWBC.

### **The Eastern New Zealand Oceanic Sedimentary System**

The available seismic records suggest that the DWBC has been active along the eastern New Zealand margin since at least the Miocene, and probably since the middle Oligocene (32 Ma) (Carter and McCave, 1994). Starting at ~24 Ma, abundant terrigenous material was shed from rising mountains along the Alpine Fault plate boundary (Vella, 1962; Norris et al., 1978) and fed through the eastern South Island shelf into the Solander, Bounty, and Hikurangi Channel systems. Sediment supply accelerated at ~6.5 Ma in the late Cenozoic, when collision increased along the plate boundary (Walcott, 1998; cf. Kennett, von der Borch, et al., 1986), and supply to the deep sea was probably enhanced again from the start of major glacial lowstands at ~2.6 Ma onward. Much of this sediment ultimately became entrained in the DWBC drift system, which carries it northward to be eventually subducted into the Kermadec Trench (L. Carter et al., 1996).

Sediment is delivered into the DWBC through two newly described transport conduits, the Bounty (Carter and Carter, 1993) and Hikurangi (Lewis, 1994) channel-fan systems. A third feeder channel, Solander, is poorly known, but it extends for >450 km before discharging into the DWBC at Emerald Basin between Macquarie Ridge and the western side of Campbell Plateau (L. Carter et al., 1996; Carter and McCave, 1997;

Schuur et al., 1998). The Hikurangi Fan has been termed a “fan-drift” by Carter and McCave (1994) because it apparently represents the extreme case of a fan whose thickness and facies pattern are directly remolded by a deep current into the form of a sediment drift. In contrast, the Bounty Fan, located within a bathymetric embayment, has retained its fan morphology and has developed directly across the path of the DWBC, the only evidence of modern drift formation being scour of the upper fan and redeposition of material on the middle to lower fan as a series of small, discrete ridges (Carter and Carter, 1993, 1996). Compared to Hikurangi Fan-Drift, Bounty Fan has formed in a region where the DWBC is inferred to be slowed (1) by the lack of forcing by the ACC, which branches east across the Pacific just south of Bounty Trough; and (2) the loss of the topographic steering, and current acceleration, provided by the steep eastern slope of the Campbell Plateau, which ceases abruptly at Bollons Seamount, again at the southern edge of the Bounty Trough. However, 6 yr of satellite sea-surface temperature data, summarized by Carter et al. (1998), indicates that meanders from the ACC periodically affect the outer Bounty Trough, and the water motions that accompany them may also play a role in current-winnowing on the Bounty Fan.

During the later Cenozoic, the two described abyssal fans have been supplied with sediment by turbidites passing through the Bounty and Hikurangi Channels, each of which is over 1000 km long. Hikurangi Channel heads in the Kaikoura Canyon, only a few hundred meters from shore, and less than 10 km from the rapidly rising, 2.5-km-high Seaward Kaikoura Mountains (Lewis, 1994). The Hikurangi system is therefore active today, in interglacial times. In contrast, the Solander and Bounty Channels head in a number of canyons that indent the edge of the continental shelf. The Bounty and Solander Systems may therefore be sea-level (i.e., climatically) controlled, with most sediment being fed into them during glacial lowstands, whereas in interglacials the same sediment stream is diverted along the inner shelf, some of it reaching the Hikurangi System via the Kaikoura Canyon (Carter and Herzer, 1979).

Eastern New Zealand is thus the site of a major recycling system, whereby sediment is shed from uplifting mountains along the Australian/Pacific plate boundary and provided to the deep sea via several major submarine channel systems. Once at abyssal depths, the sediment is re-entrained by the ACC and DWBC and passed north along the edge of the Campbell Plateau, around the tip of the Chatham Rise, northwestward along the foot of the Hikurangi Plateau, to finally arrive in the Hikurangi-Kermadec trench, where it is subducted, melted, and returned to the surface as juvenile volcanic rock. Remarkably, and largely because of the effects of the plate boundary, the two small islands of New Zealand supply roughly 2% of the world’s sediment load to the oceans (Milliman and Syvitski, 1992); it is this sediment load that is then entrained in what L. Carter et al. (1996) have termed the Eastern New Zealand Oceanic Sedimentary System (ENZOSS) (Fig. F5).

Recent publications (Carter and Carter, 1993; Lewis, 1994; Carter and McCave, 1994; L. Carter et al., 1996) have delineated the ENZOSS region, between the Solander Trough and the Kermadec Trench, east of the modern Australian-Pacific plate boundary, as an integrated sediment source-transport-sink area. During the latter half of the Cenozoic, sediment from mountains along the New Zealand plate boundary was transported through deep-sea channel/fan systems, delivered into the

path of the DWBC, entrained northward within this current system, and finally consumed by subduction at the same plate boundary after a transport path of up to 4500 km.

### **Research Themes and Drilling Objectives**

ODP Leg 181 targeted drill sites located in the eastern New Zealand region and the key Southwest Pacific gateway because

1. The Pacific DWBC is today one of the largest single contributors to the deep waters of the world's oceans, and, therefore, deciphering its history is of fundamental importance to global ocean paleohydrography.
2. The stratigraphic record of the eastern New Zealand microcontinent and its abyssal margins is the best available for deciphering the history of development of Southern Ocean water masses in the Pacific sector and of the sediment drifts that they deposited.
3. The gateway region includes two major oceanic fronts, the STC and the SAF (Fig. F2). Thus, the region is in a prime position to allow determination of the migration of these boundaries, the forcing processes that caused them to move, and the environmental response to their movement. Sedimentary sequences beneath the STC are a record of oceanic productivity variability and causal processes.
4. The stratigraphic record from ENZOSS is of interest in its own right, as a major geological and sedimentary system within which sources, sinks, and material fluxes can all be quantified. The ENZOSS record is also directly relevant to one of the most important unresolved problems of Cenozoic climatology, namely the timing and precise nature of the development of widespread glaciation on the Antarctic continent (e.g., Barrett, 1996). In turn, it is, of course, these same glacial events that contribute source water to the DWBC and affect the flow of the ACC, which forces the boundary current south of 49°S.

The Leg 181 drilling schedule included 51 days at sea with drilling operations at seven sites. We began by drilling shallow-water sediment drifts on the upper continental slope near South Island, New Zealand, moved south in difficult weather conditions to drill sites on the central Campbell Plateau, and, at its eastern foot, turned north to drill a deep hole through the levee sediments of the Bounty Fan. The leg finished with two holes through sediment drifts on the north side of the Chatham Rise and one into the shallow rise itself. Overall, we recovered 3600 m of core and made over a million shipboard measurements. The material collected on Leg 181 will lead to a better understanding of the history and evolution of the Pacific ACC-DWBC system and nearby oceanic fronts, and will highlight the important role they play in global ocean circulation and production. Finally, that the stratigraphic and paleontologic information retrieved on the cruise contained many surprises was itself predictable, given the paucity of previous drilling in the Southwest Pacific region. This information will serve as a vital database for the targeting of future drilling legs in the Southern Ocean.



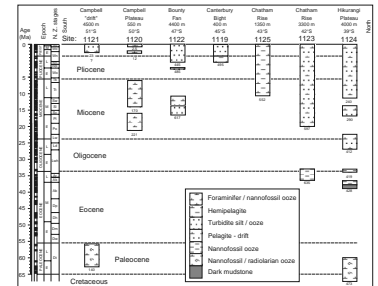
## PRINCIPAL RESULTS

The principal shipboard results of Leg 181 drilling are encapsulated by summary plots of stratigraphy, sediments, and average sedimentation rates at each site (Figs. F7, F8, F9). The main scientific target of the leg was the high-resolution study of Neogene sediments in the context of ACC-DWBC evolution. However, drilling in the Southwest Pacific is still in a state of reconnaissance, and, unsurprisingly, Leg 181 sites intersected sediments that range widely in age from Late Cretaceous to Holocene. Together with the results of earlier drilling, which transected sediments of early-middle Eocene and early Oligocene age (Site 277, 278; Fig. F8), a complete deep-marine stratigraphic record between the Late Cretaceous and Holocene is now available for the first time. Detailed study of this data set will undoubtedly lead to significant advances in our understanding of regional Southwest Pacific stratigraphy, micropaleontology, and paleoceanography, as well as helping delineate the origin and evolution of the world's modern thermohaline ocean circulation system.

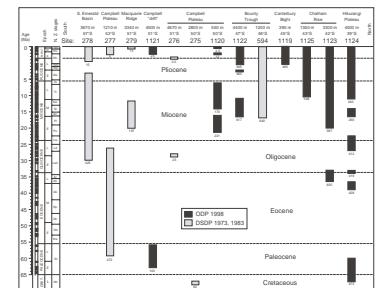
The principal results from Leg 181 include the following:

1. In composite, Leg 181 retrieved an almost-complete stratigraphic succession of largely deep-marine sediment back to the late Eocene (37 Ma), together with two high-quality cores (Sites 1121 and 1124) of late Cretaceous to Paleocene (67–56 Ma) age. Sedimentation rates range widely from a low of ~1.25 cm/k.y. for Site 1120 on the current-swept, shallow-water Campbell Plateau, to a high of 40 cm/k.y. at Site 1122 on the turbidity current-supplied levee of the abyssal Bounty Fan. Significant paraconformities, lasting up to many million years, occur at many sites and indicate phases of erosive bottom-water flow within the ACC-DWBC system.
2. Sites 1121 and 1124 contain a stratigraphic record of paleoceanographic events of the early postrift phase of evolution of the Southwest Pacific Ocean. Sites 1123 and 1124 contain a mid-Oligocene (~33–27 Ma) gap in sedimentation, which corresponds to the regional Marshall Paraconformity (Fulthorpe et al., 1996) and to the initiation of the ACC-DWBC system of deep cold-water circulation into the world ocean.
3. Sites 1123 and 1124 are located on DWBC sediment drifts and contain a high-resolution record of climatic cyclicity and probably also of bottom-current variability for the last 20 m.y. Uniquely in the world ocean, Site 1124 may have retrieved a complete Miocene to Holocene sedimentary record of uniform sedimentation rate, which is richly microfossiliferous and contains every magnetic reversal since Chron C6r of early Miocene (~20.5 Ma) age. Additional correlation control for Sites 1123 and 1124 will be provided by the macroscopic airfall tephra that they contain, >50 and >140 macrotephras, respectively. Also, these tephras (also present at Site 1125) will delineate an accurate record of explosive volcanicity from the arc volcanoes of central North Island.
4. Site 1125, on the north flank of the Chatham Rise at 1350-m water depth, contains a thick, terrigenous sequence back to ~11 Ma, with sedimentation rates as high as 13 cm/k.y. during the latest Miocene. Situated just north of the STC, Site 1125 is a counterpart for DSDP Site 594, located south of Chatham Rise in 1200-

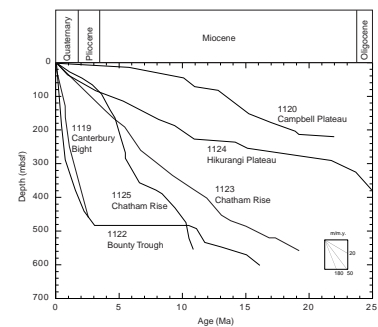
F7. Summary stratigraphy and sediment facies, p. 46.



F8. Summary thickness data, p. 47.



F9. Sedimentation rate summary curves, p. 48.



m water depth. The expanded sedimentation rates will allow high-resolution studies of paleoceanographic and paleoproductivity changes at the STC through time, including its positioning with respect to the crest of the Chatham Rise. These sites are also ideally situated for study of the ocean changes that accompanied the late Miocene (~6.5 Ma) carbon isotope shift.

5. Site 1122, on the north-bank levee of the Bounty Fan, establishes that the fan has been built over the last 2 m.y., during the time of marked glacioeustatic sea-level fluctuation that accompanied the intensification of polar glaciation during the late Cenozoic. Below a 450-m-thick sequence of spectacular fan turbidites, this site contains current-winnowed contourites of Miocene age, which contain a record of DWBC and perhaps ACC activity. Thus, Site 1122 is a vital link between southern Site 1121, where the Neogene record of DWBC activity is largely erosional, and northern Sites 1123 and 1124, which contain the expanded drift record necessary for high-resolution paleoceanographic studies.
6. Site 1119, at 395-m water depth on the eastern South Island upper continental slope, penetrated a Pliocene–Pleistocene rhythmic, sand-mud, shallow-water succession, which will help establish the nature of stratigraphic sequences (*sensu* Exxon) in the environment just seaward of the glacial lowstand shoreline. The deeper parts of Site 1119 transected AAIW drifts, which form part of the Canterbury (upper slope) drifts, and terminated in the top of a major drift in sediments of late Pliocene (~3.0 Ma) age. The base of the same drift can be seen on a seismic line to initiate in basal Otakou Group sediments of early Miocene age (~25 Ma). With a demonstrated longevity of >20 m.y., this drift may be the longest lived sedimentary bedform yet known on Earth.

### **Site 1119**

#### **Hole 1119A**

**Position:** 44°45.332'S, 172°23.598'E

**Start hole:** 0345 hr, 23 August 1998

**End hole:** 1020 hr, 23 August 1998

**Time on hole:** 6.58 hr

**Seafloor (drill pipe measurement from rig floor, mbrf):** 406.50

**Distance between rig floor and sea level (m):** 11.00

**Water depth (drill pipe measurement from sea level, m):** 395.50

**Total depth (from rig floor, mbrf):** 412.50

**Total penetration (mbsf):** 6.01

**Coring totals:** type: APC; number: 1; cored: 6.00 m; recovered: 100.17%

**Formation:** lithostratigraphic Unit I: olive-gray silty sand and greenish gray silty clay

#### **Hole 1119B**

**Position:** 44°45.332'S, 172°23.598'E

**Start hole:** 1015 hr, 23 August 1998

**End hole:** 0020 hr, 24 August 1998

**Time on hole:** 14.08 hr

**Seafloor (drill pipe measurement from rig floor, mbrf):** 407.80

Distance between rig floor and sea level (m): 11.00  
Water depth (drill pipe measurement from sea level, m): 396.80  
Total depth (from rig floor, mbrf): 563.60  
Total penetration (mbsf): 155.54 mbsf  
Coring totals: type: APC; number: 17; cored: 155.80 m; recovered: 105.56%  
Formation: lithostratigraphic Unit I: 0–92 mbsf; olive-gray silty sand and greenish gray silty clay; lithostratigraphic Unit II: 92–155.8 mbsf; olive-gray silty sand and greenish gray silty clay

### Hole 1119C

Position: 44°45.332'S, 172°23.614'E  
Start hole: 0020 hr, 24 August 1998  
End hole: 1915 hr, 26 August 1998  
Time on hole: 66.92 hr  
Seafloor (drill pipe measurement from rig floor, mbrf): 407.20  
Distance between rig floor and sea level (m): 11.00  
Water depth (drill pipe measurement from sea level, m): 396.20  
Total depth (from rig floor, mbrf): 902.00  
Total penetration (mbsf): 494.80  
Coring totals: type: APC; number: 17; cored: 160.30 m; recovered: 108.28%; type: XCB; number: 35; cored: 334.50 m; recovered: 80.32%  
Formation: Lithostratigraphic Unit I: 0–92 mbsf; olive-gray silty sand and greenish gray silty clay; lithostratigraphic Unit II: 92–404 mbsf; olive-gray silty sand and greenish gray silty clay; lithostratigraphic Unit III: 404–494.72 mbsf; greenish gray silty clay

Site 1119 is located 96 km east of the eastern shoreline of New Zealand's South Island, offshore from Timaru, within the Canterbury Basin (Fig. F1, p. 32, in the "Site 1119" chapter). The site was drilled in a water depth of 393 m on the upper slope, 5 km seaward of the edge of the continental shelf. Still further seaward, the slope levels out onto the southern edge of the Chatham Rise platform at 800–1000 m. Clinoform reflectors within the Miocene–Holocene represent earlier positions of the prograding shelf-slope. The reflectors define a shore-parallel zone of Pliocene–Pleistocene sediment drifts, each of which prograded landward and successively accreted to the edge of the shelf.

Site 1119 was drilled to sample the upper slope sediments and underlying sediment drifts. A copious source of sediment is required to build the drifts. Site 1119 samples will allow the provenance of the upper drift sediments to be established, paleocurrent velocities to be inferred, and the late Pliocene–Pleistocene history of the important AAIW water mass to be reconstructed close to its source. The sand-rich intervals encountered in the hole will allow inferences to be made regarding relative sea-level change during this period.

Hole 1119A comprised a single 6.01-m-long core taken for mudline sampling. APC penetration, with essentially full core recovery and little disturbance, was then achieved to a depth of 155.54 mbsf (Hole 1119B) and 160.3 mbsf (Hole 1119C) successively (Table T1, also in ASCII format). Hole 1119C continued to a depth of 494.8 mbsf using the extended core barrel (XCB). Throughout the APC core sections, core voids caused by gas expansion were common in the sands and silts. Core recovery was 105% for Hole 1119B and 89% for Hole 1119C.

---

T1. Site 1119 coring summary,  
p. 69.

---

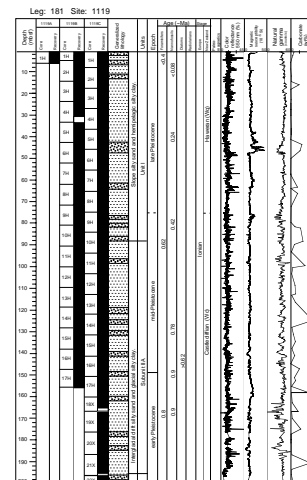
The 494.8 m of sediment cored is subdivided into three lithologic units (Fig. F10). The upper 88 m (Unit I) comprises repetitive, sharp-based, silty sand–silty clay couplets. Silty sand beds are usually <2 m thick and have an olive-gray color, coarse texture with shell debris, and small amounts of glauconite. Many microfossils are reworked. The silty clays form thick greenish gray beds (usually >4 m), with mica and scattered macrofossils (including double valves of the subantarctic scallop *Zygochlamys delicatula*). Nannofossils occur in most samples, radiolarians have sporadic distribution, pyrite is a common accessory mineral, and sponge spicules are prominent. Toward the bottom of lithostratigraphic Unit I, bathyal gastropods appear in the silty muds (e.g., *Elliecia*), perhaps indicating deepening conditions for the sedimentary couplets with depth in the hole: the sequence as a whole indicates shallowing-upward conditions. Foraminifers and nannoplankton indicate deeper, warmer conditions during deposition of the silty sands (sediment-starved upper slope during interglacial highstands), and deposition of silty-clay intervals during glacial lowstands, in relatively shallower, colder water on a nearshore upper slope. The basic nature of the Unit I sedimentary couplets was apparently controlled by sea-level change, but seismic records show that all but the uppermost parts of Unit I (shallower than 50 m) have a drift geometry. However, the marked sedimentary and environmental cyclicity of Unit I is similar to that already described from Pliocene–Pleistocene sediments nearby on land.

Lithostratigraphic Unit II comprises Subunits IIA from 88.2 to 196 mbsf, IIB from 196 to 285.2 mbsf, and IIC from 285.2 to 401 mbsf. It also contains sedimentary rhythms that differ from the couplets of Unit I. The upper part, Subunit IIA, contains doubly-graded silty sand–silty clay units in which the sand has gradational contacts with the silty clay both above and below. The sands also have a higher calcite content than their counterparts in Unit I and sometimes show incipient cementation. Nannofossils are more frequent than in Unit I. Subunit IIB contains sharp-based sand–silty clay couplets similar to those of Unit I, but in which the sands again have less terrigenous material and include significant amounts of broken shell, benthic foraminifers, and nannofossils. The sands have sharp bases, beneath which are muds displaying sand-filled burrows of *Thalassinoides* and *Planolites*. Whole-valve mollusks, conspicuous in the overlying unit, are rare.

The lowest double-graded motif occurs in the bottom part of Core 181-1119C-34X (near the top of Subunit IIC), below which the sharp-based sand-mud couplets continue downhole intermittently to Core 43X (401.0 mbsf, base of Subunit IIC). We interpret the double-graded motif as the deeper water manifestation of the climatic and sea-level changes that produced the sharp-based silty sand–silty clay couplets in Unit I. The sharp-based silty sand–silty clay couplets of Subunit IIB are more difficult to interpret. They may have a similar origin to their counterparts in Unit I, or they may be redeposited (i.e., turbidites). X-radiography may help in making this distinction.

Unit III occurs from 401.1 mbsf to the bottom of the hole at 494.8 mbsf and comprises mostly massive, pale olive-gray silty clay with occasional burrows, which is similar to the inferred glacial silty clays of Units I and II. Unit III contains very thin beds and laminae of light gray sediments that smear-slide analyses suggest are richer in carbonate nannofossils and therefore may be mud turbidites. The trace fossil *Zoophycos* is scattered throughout, macrofossils and shell fragments are almost absent, and interbeds of olive sand are completely absent. This unit cor-

F10. Summary log, Site 1119, p. 49.



responds with the presence of a large sediment drift on the deep seismic line through Site 1119, and we interpret Unit III sediments as deposits on the deeper slopes of the Canterbury drifts. Microfaunas are consistent with deeper water depths for Unit III than for Units I and II.

Preliminary paleontological data indicate that the Unit I/II boundary is ~0.6 Ma (early Castlecliffian), the Unit II/III boundary ~2.2 Ma (early Nukumaruan), and the bottom of hole ~2.8 Ma (late Pliocene, perhaps as old as late Waitotaran) in age. These ages are drawn from cycle counting and faunal evidence. A shipboard paleomagnetic reversal chronology could not be determined unambiguously because of a combination of low intensities and magnetic overprints. Based on the biostratigraphic ages, the average sedimentation rate across the section is ~20 cm/k.y., with lower rates during interglacials (sand) and considerably higher rates during glacials (silt and clay).

Despite the widely varying sedimentation rates and the presence of random core gaps resulting from degassing and possible washing of sand, an excellent spliced multisensor (MST) record for the two APC cores was achieved for Site 1119, based on magnetic susceptibility and natural gamma records. Cyclicity that matches the observed sediment couplets is apparent in both the smoothed magnetic susceptibility and, to a lesser degree, the natural gamma-ray records. Other physical properties data reveal a distinct increase in vane shear strength at ~85 mbsf, which may correlate with an observed seismic discontinuity and indicate a hiatus.

Carbonate concentrations are in the wide range of 0.5% and 75%, indicating strongly variable environmental conditions during sediment deposition (Fig. F10). In contrast, the average concentration of total organic carbon is 0.34% with small variations, which is low for coastal sediments. This may be a result of (1) dilution by either carbonate or terrigenous clastic material, and (2) decomposition, which is manifested in the high methane contents.

Interstitial water profiles show that the sulfate reduction zone occurs at 20 mbsf. There are increases in alkalinity, ammonium, and phosphate concentration across this zone. These increases are controlled by the degradation of sedimentary organic matter in a shallow marine environment. Sulfate concentrations are near zero from 20.15 through 472.3 mbsf, suggesting enhanced diagenetic processes, including the dissolution of magnetic minerals throughout the sequence. The decreases in calcium and magnesium concentrations in the sulfate reduction zone suggest that the precipitation of diagenetic carbonate was promoted by the rapid increase in alkalinity.

Downhole logging at Site 1119 included runs of the following tools: triple combination, Geologic High-Resolution Magnetic Tool (GHMT), and Formation MicroScanner (FMS-sonic). Downhole conditions were irregular below 160.3 mbsf because of damage to the wall during drilling, and some data dropouts are present. After the GHMT tool run, the bottom 20 m of the hole collapsed because of cavings or swelling mud, and, as a result, the data from the two later tool strings do not include this portion of the hole. The poor hole conditions affected the lithodensity and neutron porosity tools and make interpretation of the data difficult. The sonic tool was also affected by the poor hole conditions, but to a lesser degree, and the data obtained from it were used to create integrated travel times for interpretation of seismic survey data at this site. The resistivity, susceptibility, and gamma-ray tools recorded good logs with cyclic signals.



## Site 1120

### Hole 1120A

Position: 50°3.803'S, 173°22.300'E  
Start hole: 0045 hr, 28 August 1998  
End hole: 0600 hr, 28 August 1998  
Time on hole: 5.25 hr  
Seafloor (drill pipe measurement from rig floor, mbrf): 553.90  
Distance between rig floor and sea level (m): 11.00  
Water depth (drill pipe measurement from sea level, m): 542.90  
Total depth (from rig floor, mbrf): 558.50  
Total penetration (mbsf): 4.60  
Coring totals: type: APC; number: 1; cored: 4.60 m; recovered: 100%  
Formation: lithostratigraphic Unit I: 0–4.6 mbsf; foraminifer nannofossil ooze and nannofossil foraminifer ooze

### Hole 1120B

Position: 50°3.803'S, 173°22.300'E  
Start hole: 0600 hr, 28 August 1998  
End hole: 2020 hr, 28 August 1998  
Time on hole: 14.33 hr  
Seafloor (drill pipe measurement from rig floor, mbrf): 555.20  
Distance between rig floor and sea level (m): 11.00  
Water depth (drill pipe measurement from sea level, m): 544.20  
Total depth (from rig floor, mbrf): 743.20  
Total penetration (mbsf): 188.00  
Coring totals: type: APC; number: 8; cored: 68.30 m; recovered: 92.55%; type: XCB; number: 13; cored: 119.70 m; recovered: 69.59%  
Formation: lithostratigraphic Unit I: 0–4.3 mbsf; foraminifer nannofossil ooze and nannofossil foraminifer ooze; lithostratigraphic Unit II: 4.3–10.2 mbsf; foraminifer nannofossil ooze; lithostratigraphic Unit III: 10.2–54.9 mbsf; foraminifer nannofossil ooze; lithostratigraphic Unit IV: 54.9–188.0 mbsf; nannofossil ooze

### Hole 1120C

Position: 50°3.815'S, 173°22.299'E  
Start hole: 2020 hr, 28 August 1998  
End hole: 0613 hr, 29 August 1998  
Time on hole: 33.88 hr  
Seafloor (drill pipe measurement from rig floor, mbrf): 556.90  
Distance between rig floor and sea level (m): 11.00  
Water depth (drill pipe measurement from sea level, m): 545.90  
Total depth (from rig floor, mbrf): 601.50  
Total penetration (mbsf): 44.60  
Coring totals: type: APC; number: 5; cored: 44.60 m; recovered: 100.78%  
Formation: lithostratigraphic Unit I: 0–4.6 mbsf; foraminifer nannofossil ooze and nannofossil foraminifer ooze; lithostratigraphic Unit II: 4.6–11.2 mbsf; foraminifer nannofossil ooze; lithostratigraphic Unit III: 11.2–44.6; foraminifer nannofossil ooze

### Hole 1120D

Position: 50°3.822'S, 173°22.300'E

Start hole: 0613 hr, 29 August 1998  
End hole: 0600 hr, 1 September 1998  
Time on hole: 47.78 hr  
Seafloor (drill pipe measurement from rig floor, mbrf): 556.90  
Distance between rig floor and sea level (m): 11.00  
Water depth (drill pipe measurement from sea level, m): 545.90  
Total depth (from rig floor, mbrf): 777.60  
Total penetration (mbsf): 220.70  
Total length of drilled intervals (m): 157.40  
Coring totals: type: XCB; number: 9; cored: 63.30 m; recovered: 104.53%  
Formation: lithostratigraphic Unit IV: 157.4–220.7 mbsf; nannofossil ooze

Site 1120 is located ~650 km southeast of Stewart Island on the eastern flank of Pukaki Rise, near the middle of the Campbell Plateau, in 543-m deep water (Fig. [F1](#), p. 25, in the “Site 1120” chapter). The seismic succession is punctuated by seven conspicuous reflectors (R1–R7), several of which may represent unconformities. Few basement highs remained on the Campbell Plateau to shed terrigenous sediment after Late Cretaceous rifting of the eastern plateau margin and subsequent erosion, and the entire succession above reflector R6 (probably Paleocene) is apparently biopelagic carbonate. Times of water-mass change, perhaps accompanied by current activity and sublevation, are indicated by changes in seismic character that take place across younger reflectors D to A, the target of Site 1120 drilling.

Site 1120 was drilled to establish the age of the major unconformities in the Campbell Plateau sequence and to determine the evolution of the shallow circulation across the Plateau. The analysis of seafloor magnetic anomalies suggests that the ACC had its inception in the Oligocene, at ~32 Ma, when Australia separated from Antarctica, thus allowing partial circumpolar flow. At this time, the Campbell Plateau was situated immediately downcurrent from the opening southern ocean and was, therefore, exposed to vigorous current activity. It was anticipated that reflector R2/R3 would be of middle to late Miocene age and correlate with either or both the sharp cooling of Antarctica recorded isotopically at 15–14 Ma, and a phase of known volcanism and minor faulting in eastern South Island, New Zealand, between ~13 and 10 Ma.

Four holes that recovered a sedimentary section spanning the last 23 m.y. were cored with the APC/XCB at Site 1120 to a maximum depth of 220.7 mbsf (Table [T2](#), also in [ASCII format](#)). Hole 1120A consists of one single mudline core. Twenty-one cores were taken with the APC/XCB at Hole 1120B from 0 to 188.0 mbsf before operations were put on standby because of excessive heave. After waiting because of weather, five cores were taken with the APC at Hole 1120C to 44.6 mbsf before a broken wireline and deteriorating weather conditions ended operations. Hole 1120D was drilled to 157.4 mbsf and cored with the XCB to 220.7 mbsf when operations again had to be terminated because of the excessive heave.

Site 1120 penetrated a succession of calcareous biogenic oozes that downsection become nannofossil rich, and contain less distinct bedding. Bioturbation ranges from moderate to heavy throughout the core, with identifiable traces of *Zoophycos*, *Palaeophycus*, and *Planolites*. The lithostratigraphy is visually monotonous and featureless for most of the section. However, four units can be characterized, using subtle changes

---

T2. Site 1120 coring summary,  
[p. 71](#).

---

in composition determined from smear slides (Fig. F11). The upper unit (Unit I, 0–4.6 mbsf) comprises glacial/interglacial cycles in alternating beds of foraminifer-oozes and nannofossil-foraminifer oozes. Unit II (4.6–11.2 mbsf) is separated from Unit I by an unconformity and comprises a foraminifer nannofossil ooze with glauconite and rare pyrite concretions. Unit III (11.2–54.9 mbsf) is a foraminifer nannofossil ooze similar to Unit II. The lowermost Unit IV (54.9–220.7 mbsf) is a foraminifer-bearing nannofossil ooze. Foraminifers are less abundant in this unit than in overlying beds, and neither glauconite nor siliceous sponge spicules were observed.

The section is punctuated by a number of significant paraconformities, the first of which lies just below the seafloor at 4.6 mbsf and separates stratified cycles of darker and lighter white ooze of late Pleistocene age from slightly compacted, brownish foraminiferal ooze of middle Pleistocene age below. Another paraconformity may occur at around 13 mbsf, corresponding to a reflection on the site survey 3.5-kHz profile, and a change in microfaunas to latest Miocene forms (5–16 Ma). An expanded section of middle and late Miocene age (13.6–6 Ma) occurs between ~13 and 170 mbsf, apparently without breaks. Another probable unconformity at ~170 mbsf is perhaps marked by reflector R2 on the seismic reflection profile, where nannofossil evidence suggests a biostratigraphic break may occur.

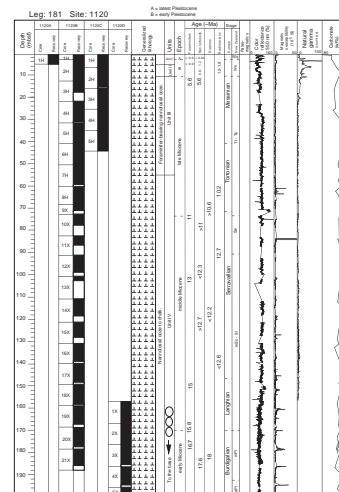
The Pliocene–Pleistocene section at Site 1120 is very thin, and the presence of probable hiatuses throughout the hole indicates that intensified water-mass movements occurred periodically across the Campbell Plateau during the late Neogene. The relatively complete middle to late Miocene section present corresponds to sedimentation rates of 1–2 cm/k.y. over the period ~5.5 to 16 Ma, and indicates quieter, undisturbed biopelagic conditions. The lowest part of the core is of early Miocene age (18–23 Ma) and has a slower sedimentation rate, again consistent with current influence. The occurrence of the usually long-ranging *Sphenolithus heteromorphus* in only one core (between 167 and 177 mbsf) suggests that up to 2–3 m.y. of late early Miocene and early middle Miocene sediment may be either missing at an unconformity or represented by condensed sedimentation.

Benthic foraminifers indicate that the site has been bathyal throughout the Neogene–Quaternary. Evidence from all planktonic microfossil groups consistently indicates that during the Pleistocene the surface waters and intermediate water masses above the Campbell Plateau were cold. In the Miocene section, changes in the composition of calcareous microfossils reflect cyclic alternations between warmer and colder conditions. The planktonic foraminifers and calcareous nannofossils show a general trend toward colder faunas and floras from the early–middle to the middle–late Miocene.

Physical sediment properties were determined both by high-resolution MST core logging and by index properties measurements. Magnetic susceptibility, gamma-ray attenuation porosity evaluator (GRAPE) density, natural gamma-ray intensity, and digital reflectance data measured with the Minolta Spectrophotometer reveal cyclicities, which were used for stratigraphic correlation in the top 50 mbsf. Detailed hole-to-hole comparisons demonstrated that a nearly complete sedimentary sequence was recovered down to 50 meters composite depth (mcd), with only one small gap at 19 mcd.

A shipboard paleomagnetic reversal chronology could not be determined because of a combination of low intensities and magnetic overprints.

F11. Summary log, Site 1120, p. 52.



The profiles of interstitial water constituents are controlled by simple diagenetic diffusion processes, which show slightly increasing alkalinity, chloride, calcium, lithium, and silica concentrations, and decreasing potassium and magnesium trends with depth, and no signatures of sulfate reduction. This results from the uniform lithology (carbonate oozes) throughout the hole. The dominant chemical reactions were dissolution of carbonate, silica diagenesis, the possible precipitation of dolomite, and ion-exchange reactions in clay minerals.

## **Site 1121**

### **Hole 1121A**

**Position:** 50°53.876'S, 176°59.862'E

**Start hole:** 2225 hr, 1 September 1998

**End hole:** 1555 hr, 2 September 1998

**Time on hole:** 17.50 hr

**Seafloor (drill pipe measurement from rig floor, mbrf):** 4503.10

**Distance between rig floor and sea level (m):** 11.10

**Water depth (drill pipe measurement from sea level, m):** 4492.00

**Total depth (from rig floor, mbrf):** 4511.50

**Total penetration (mbsf):** 8.40

**Coring totals:** type: APC; number: 1; cored: 8.40 m; recovered: 99.64%

**Formation:** lithostratigraphic Subunit IA (0–8.40 mbsf): yellow to yellowish brown silty or sandy clay and grayish brown and light yellowish brown silt, silty sand, and sand beds

### **Hole 1121B**

**Position:** 50°53.876'S, 176°59.862'E

**Start hole:** 1555 hr, 2 September 1998

**End hole:** 1045 hr, 4 September 1998

**Time on hole:** 42.83 hr

**Seafloor (drill pipe measurement from rig floor, mbrf):** 4499.00

**Distance between rig floor and sea level (m):** 11.10

**Water depth (drill pipe measurement from sea level, m):** 4487.90

**Total depth (from rig floor, mbrf):** 4638.70

**Total penetration (mbsf):** 139.70

**Coring totals:** type: APC; number: 3; cored: 23.00 m; recovered: 129.04%; type: XCB; number: 14; cored: 4.60 m; recovered: 49.85%

**Formation:** lithostratigraphic Subunit IA (0–15.2 mbsf): yellow to yellowish brown silty or sandy clay and grayish brown and light yellowish brown silt, silty sand, and sand beds; lithostratigraphic Subunit IB (15.2–32.7 mbsf): pale yellow and light yellowish brown clay with fragments of chert layers and nodules; lithostratigraphic Subunit IIA (32.7–132.7 mbsf): white nannofossil ooze with a subordinate content of diatoms, radiolarians, sponge spicules, and silicoflagellates; beds alternate with light greenish gray nannofossil diatom ooze; lithostratigraphic Subunit IIB (132.7–139.7 mbsf): greenish gray nannofossil-bearing clay

Site 1121 is located on the Campbell “drift,” which today lies under the DWBC and ACC (Fig. F1, p. 27, in the “Site 1121” chapter). Drilling at this site showed that, contrary to the pre-Leg 181 view, the sediment accumulation defined by topography and seismic reflection profiles is not a Neogene contourite drift, but rather represents a portion of the

original sediment apron that accumulated adjacent to the Campbell Plateau after Late Cretaceous rifting.

The sediment body drilled lies along the foot of the 3000-m-high eastern escarpment of Campbell Plateau and is ~800 km long. The underlying crust dates from the rifting of Campbell Plateau from Marie Byrd Land at ~95 Ma. Up to 1.1 s (~1000 m) of sediment overlies oceanic basement, and probably comprises a basal wedge of nonmarine clastics, followed by latest Cretaceous and Paleogene marine sediments and thin Neogene contourites. In particular, Carter and McCave (1997) surmised that the uppermost sequence of closely spaced reflectors (<160 m thick) was of Pliocene–Pleistocene age. A short gravity core from the site has yielded an abundant assemblage of late Pleistocene and reworked older foraminifers. This sequence, presumed to carry a record of ACC and DWBC history, was the drilling target. The objectives were to obtain well-dated records of isotopic properties of oxygen and carbon that would show possible shifts of the SAF, the onset of and changes in the inflow of Circumpolar Deep Water (CDW) and AABW, and, through grain-size analysis, document changes in the vigor of the deep circulation.

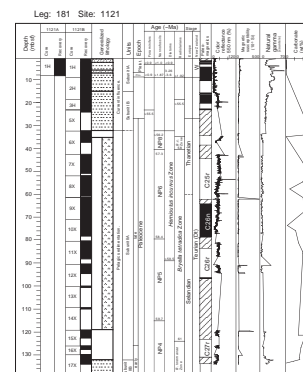
Two holes that recovered a sedimentary section spanning the last 63 m.y. were cored with the APC/XCB at Site 1121 to a maximum depth of 139.7 mbsf (Table T3, also in [ASCII format](#)). Hole 1121A consists of one single mudline core. Seventeen cores were taken with the APC/XCB at Hole 1121B from 0 to 139.7 mbsf with 62.9% recovery, when operations were terminated because of bad weather.

The cored section is divided into two units, each subdivided (Fig. F12). Subunit IA (0–15.2 mbsf) is mottled silty and sandy clay with conspicuous manganese nodules. Subunit IB (15.2–32.7 mbsf) is a relatively uniform yellow siliceous clay with cherts as nodules and (broken) layers. This unit is possibly of Neogene age and represents a residual deposit with a very slow net sedimentation rate (~1 m/m.y.). It is the residue of significant erosion by the ACC-DWBC some time after the Paleocene. Unit II includes two subunits dominated by varying mixtures of siliceous and nannofossil-bearing ooze and chalk with up to 50% carbonate. The unit is extensively bioturbated and contains common chert below 71 mbsf. The lithologic features indicate deep marine deposition of pelagic biogenic material close to the CCD at a rate of ~15–30 m/m.y. The inferred erosion in the upper part of the section is corroborated by the ratio of shear strength to overburden pressure which, with values over 0.5 in the upper 20 mbsf, is indicative of overconsolidation. Chert in the lower part of the section precludes similar measurements in the Paleocene Unit II, which is probably also overcompacted.

The uppermost 3 mbsf of the section contains a condensed sequence, with late Pleistocene over early Pleistocene over late Pliocene diatoms in the top meter, underlain by 2 m of early late Pliocene. Foraminifers and coccoliths in the top meter are also of middle to late Pleistocene age. The remainder of the upper 32 mbsf composing Unit I yielded a few late Neogene nannofossils and reworked (?) Paleocene radiolarians. From 32.7 mbsf to the bottom of the hole (Unit II), the sequence provides for the first time in the Southwest Pacific a continuous record of deep marine sediment of late early to late Paleocene age. The rich microfaunas have all major microfossil groups, including nannofossils, diatoms, radiolarians, and benthic foraminifers. Radiolarian Zones RP4, 5, and 6, nannofossil Zones NP4, 5, 6, and 8, benthic foraminiferal Zone CD1, and the diatom *Hemiaulus incurvus* Zone are present in the

T3. Site 1121 coring summary, p. 72.

F12. Summary log, Site 1121, p. 54.





record. This has provided tight control on an equally good magnetostratigraphic record in the Paleocene section where magnetochrons C27r, C27n, C26n, and C25r are recognized. The upper condensed section also contains a number of reversals, but, apart from the tentative recognition of the Gauss Chron, the biostratigraphic control is not adequate to identify them. The combined age data indicate sedimentation rates of up to 100 m/m.y. in the Paleocene and ~1 m/m.y. in the Neogene.

The profiles of interstitial water constituents show local fluctuations that are consistent with lithologic control rather than diffusion. The primary chemical reactions were probably silica diagenesis, dissolution of carbonate, and possibly ion-exchange reactions of clay minerals. In particular, relatively high concentrations of dissolved silica in the interval between ~35 and 120 mbsf are related to the dissolution of biosiliceous sediments.

## **Site 1122**

### **Hole 1122A**

**Position:** 46°34.781'S, 177°23.610'W

**Start hole:** 2254 hr, 5 September 1998

**End hole:** 0415 hr, 7 September 1998

**Time on hole:** 29.35 hr

**Seafloor (drill pipe measurement from rig floor, mbrf):** 4446.20

**Distance between rig floor and sea level (m):** 11.20

**Water depth (drill pipe measurement from sea level, m):** 4435.00

**Total depth (from rig floor, mbrf):** 4570.10

**Total penetration (mbsf):** 123.90

**Coring totals:** type: APC; number: 8; cored: 75.80 m; recovered: 96.97%; type: XCB; number: 5; cored: 48.10 m; recovered: 29.02%

**Formation:** lithostratigraphic Subunit IA (0–16.6 mbsf): light brownish gray silty clay; lithostratigraphic Subunit IB (16.6–95.0 mbsf): greenish gray silty clay with interbedded dark greenish gray and greenish gray sand and fine sand turbidites; lithostratigraphic Subunit IC (95.0–123.90 mbsf): dark greenish gray silt and very fine sand turbidites, which are intercalated in grayish green and greenish gray silty clay

### **Hole 1122B**

**Position:** 46°34.781'S, 177°23.610'W

**Start hole:** 0415 hr, 7 September 1998

**End hole:** 0625 hr, 7 September 1998

**Time on hole:** 2.17 hr

**Seafloor (drill pipe measurement from rig floor, m mbrf):** 4441.00

**Distance between rig floor and sea level (m):** 11.20

**Water depth (drill pipe measurement from sea level, m):** 4429.80

**Total depth (from rig floor, mbrf):** 4450.50

**Total penetration (mbsf):** 9.50

**Coring totals:** type: APC; number: 1; cored: 9.50 m; recovered: 103.26%

**Formation:** lithostratigraphic Subunit IA (0–9.5 mbsf): light brownish gray silty clay above gray silty clay and very fine sand

## Hole 1122C

**Position:** 46°34.780'S, 177°23.622'W

**Start hole:** 0625 hr, 7 September 1998

**End hole:** 0800 hr, 12 September 1998

**Time on hole:** 121.58 hr

**Seafloor (drill pipe measurement from rig floor, mbrf):** 4443.00

**Distance between rig floor and sea level (m):** 11.20

**Water depth (drill pipe measurement from sea level, m):** 4431.80

**Total depth (from rig floor, mbrf):** 5070.40

**Total penetration (mbsf):** 627.40

**Coring totals:** type: APC; number: 13; cored: 103.70; recovered: 103.33%; type: XCB; number: 55; cored: 523.70 m; recovered: 46.65%

**Formation:** lithostratigraphic Subunit IA (0–22.7 mbsf): light brownish gray silty clay; lithostratigraphic Subunit IB (22.71–109.35 mbsf): greenish gray silty clay with interbedded dark greenish gray and greenish gray sand and fine sand turbidites; lithostratigraphic Subunit IC (109.35–261.7 mbsf): dark greenish gray silt and very fine sand turbidites, which are intercalated in grayish green and greenish gray silty clay; lithostratigraphic Subunit ID (261.7–386.9 mbsf): greenish gray and gray silty clay interbedded with dark greenish gray very fine sand and silt turbidites; lithostratigraphic Subunit IIA (386.9–472.3 mbsf): greenish gray to light greenish gray silty clay with interbeds of dark gray or dark greenish gray fine sand and silt beds; lithostratigraphic Subunit IIB (472.3–494.5 mbsf): dark greenish gray to greenish gray silty clay interspersed with light brownish gray to gray, nannofossil-rich layers; lithostratigraphic Subunit IIC (494.5–550.4 mbsf): dark greenish gray to greenish gray silty clay interspersed with white nannofossil ooze layers; lithostratigraphic Subunit IIIA (550.4–580.62 mbsf): green to greenish gray clayey silt to silty clay with interbeds of greenish to greenish gray fine sand and silt beds and white to gray nannofossil-bearing foraminifer sands; lithostratigraphic Subunit IIIB (580.62–617.85 mbsf): greenish gray fine sand with intraclasts of silty clay and abundant wood fragments (debris flow) and greenish gray to dark greenish gray fine sand-bearing siltstones and light greenish gray foraminifer-bearing nannofossil chalks

Site 1122 is located ~830 km east of South Island, in a water depth of 4430 m on the north (left) bank levee of the abyssal Bounty Fan (Fig. F1, p. 38, in the "Site 1122" chapter). The fan is located in the most seaward axial deep of the Bounty Trough, a rift basin formed in the Late Cretaceous during the separation of New Zealand and Antarctica across the newly forming mid-Pacific Rise. The Bounty Channel feeds sediment along the axis of the trough and into the path of the Pacific DWBC, which flows north along ~95-m.y.-old oceanic crust of the Southwest Pacific abyssal plain. Subsidence calculations indicate that Site 1122 was situated at depths of ~4700 m in the early Miocene, subsequently shoaling to ~4400 m today because of late Cenozoic sediment deposition. The seismic line through the fan shows that the channel here has over 300 m of incision, with a higher north bank levee, of which the upper parts are composed of a spectacular series of climbing sediment waves, deposited from turbidity current overspill.

Three holes that recovered a sedimentary section spanning the last 16 m.y. were cored with the APC/XCB at Site 1122 to a maximum depth

of 627.4 mbsf (Table T4, also in [ASCII format](#)). Hole 1122A was cored with the APC to 75.8 mbsf and deepened with the XCB to 123.9 mbsf. One failed mudline core was taken at Hole 1122B. Thirteen cores were taken with the APC at Hole 1122C from 0 to 103.7 mbsf. The hole was deepened with the XCB to 627.4 mbsf. In an attempt to log Hole 1122C, the triple combination was deployed but was unable to pass the bit by more than 12 m. It was decided to recover the logging tool in rapidly deteriorating weather conditions and to terminate operations at the site because of the heavy seas and high winds.

Drilling confirmed that the upper ~300 m of the sediment pile is composed of rhythmic late Pleistocene sand turbidites (Fig. F13), deposited at a high rate of more than 40 cm/k.y. Recovery ranged from good when the turbidite sands were separated by regular muds and cored by APC, to very poor where they were inferred to be dominated by sand and cored by XCB. Between 300 and 450 mbsf, the turbidite sequence passed down into late Pliocene to middle Pleistocene current-worked sands and muds that are inferred to have been deposited under the influence of the DWBC, possibly reinforced by the ACC. A substantial 8-m.y.-long condensed sequence or unconformity exists at ~470–500 mbsf, below which current-influenced sands and muds of late Miocene age (10–18 Ma), with a sedimentation rate of ~5 cm/k.y., were penetrated. Accompanying microfaunas show a shift to less diverse foraminiferal assemblages, suggestive of the incursion of colder waters, an interpretation that is supported by the appearance also of subantarctic diatom floras. The lower part of the Miocene sediments contains abundant coarser grained sand, carbonized wood fragments, and transported shallow-water foraminifers, consistent with the onlap of these sediments onto the angular unconformity observed on the seismic profile. Because of drilling difficulties, the hole terminated just above this unconformity, though poor core recovery and the unfortunate lack of a sonic log makes it difficult to be certain how far above.

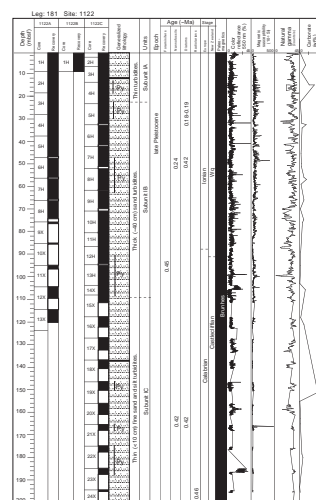
Site 1122 yielded an excellent high-resolution record of the input of middle upper Pleistocene sediment into the DWBC-ACC system. The site contained some significant surprises. Preliminary analysis shows that (1) turbidite deposition on the fan levee continued through both glacial and interglacial periods, although the frequency of turbidites was higher in glacials; (2) the major reflecting horizons seen on the seismic profile do not correspond to oxygen isotope stage stratigraphy; and (3) the change from DWBC-influenced sedimentation to New Zealand-derived turbidite/fan levee-influenced sedimentation is unexpectedly young (~0.7 Ma). Seven major tephra horizons were located at Site 1122, and, together with the excellent paleomagnetic record and close micropaleontologic controls, these will provide a tight chronostratigraphic framework for more detailed studies.

A complete magnetostratigraphy was determined in the uppermost 440 mbsf of the APC/XCB section at Site 1122 after AF demagnetization at 20 mT (Fig. F13). All chrons from the Brunhes (C1n) to the onset of C2r.1n (Reunion) at 2.14 Ma could be identified. In the upper Miocene section, below the major unconformity, Chrons C5r.1n and C5r.2n were determined.

Physical sediment properties were determined by high-resolution MST core logging and by index properties measurements. Natural gamma-ray intensity indicates that clay mineral concentration varies strongly between sand and clay layers. Magnetic susceptibility, GRAPE density, and digital reflectance data measured with the Minolta Spectrophotometer reveal cyclicities, which were used for stratigraphic correla-

T4. Site 1122 coring summary, p. 73.

F13. Summary log, Site 1122, p. 55.



tion. Detailed hole-to-hole comparisons demonstrated nearly complete recovery of the sedimentary sequence down to 83 mcd with a gap in the continuous record at 73 mcd.

The primary controlling factor on the interstitial water chemistry at Site 1122 is sulfate reduction and methane genesis, which governs alkalinity, phosphate, and ammonia concentrations. In contrast to the complete utilization of sulfate in the upper part of the core, the reappearance of increasing sulfate levels in the middle of the section represents an approach to the original sulfate concentration during sediment deposition, possibly because of a lack of sufficient metabolizable organic matter and low sedimentation rates. Other significant chemical profiles are magnesium and calcium, from the pattern of which we deduce that lateral transport of magnesium-rich fluid occurred during the dissolution of carbonate. The general chemical zonations of interstitial waters at Site 1122 correspond to the lithostratigraphic units and paleontological age divisions. In particular, the sharp reduction of methane at 260 mbsf coincides with the base of the highly pyritized turbidites of the mud-wave sequence. The calcium carbonate concentration varies between 0 and 77%, indicating strong environmental changes during sediment deposition. Organic carbon content averages 0.24%, and shows also strong variations with the sedimentary facies. The organic carbonate concentration is low for marine environments and may reflect the dilution of the organic matter by either marine carbonate or terrigenous detritus. Alternatively, organic matter is likely to have decomposed to generate the methane.

## **Site 1123**

### **Hole 1123A**

**Position:** 41°47.174'S, 171°29.940'W

**Start hole:** 1848 hr, 13 September 1998

**End hole:** 2355 hr, 14 September 1998

**Time on hole:** 29.12 hr

**Seafloor (drill pipe measurement from rig floor, mbrf):** 3301.40

**Distance between rig floor and sea level (m):** 11.30

**Water depth (drill pipe measurement from sea level, m):** 3290.10

**Total depth (from rig floor, mbrf):** 3459.50

**Total penetration (mbsf):** 158.10

**Coring totals:** type: APC; number: 17; cored: 158.10 m; recovered: 100.34%

**Formation:** lithostratigraphic Subunit IA (0–158.1 mbsf): greenish gray to white clayey nannofossil ooze

### **Hole 1123B**

**Position:** 41°47.1560'S, 171°29.939'W

**Start hole:** 2355 hr, 14 September 1998

**End hole:** 0955 hr, 19 September 1998

**Time on hole:** 106.00 hr

**Position:** 41°47.1598'S, 171°29.9387'W

**Seafloor (drill pipe measurement from rig floor, mbrf):** 3301.10

**Distance between rig floor and sea level (m):** 11.30

**Water depth (drill pipe measurement from sea level, m):** 3289.80

**Total depth (from rig floor, mbrf):** 3790.10

**Total penetration (mbsf):** 489.00

**Coring totals:** type: APC; number: 17; cored: 155.40 m; recovered: 102.79%; type: XCB; number: 35; cored: 333.60 m; recovered: 87.43%

**Formation:** lithostratigraphic Subunit IA (0–181.9 mbsf): greenish gray to white clayey nannofossil ooze; lithostratigraphic Subunit IB (181.9–256.59 mbsf): white clayey nannofossil chalk interbedded with greenish gray clayey nannofossil chalk; lithostratigraphic Unit II (256.59–450.8 mbsf): light greenish gray clayey nannofossil chalk; lithostratigraphic Subunit IIIA (450.8–489.00 mbsf): light greenish gray and greenish gray clayey nannofossil chalk and nannofossil mudstone

### Hole 1123C

**Position:** 41°47.147'S, 171°29.941'W

**Start hole:** 0955 hr, 19 September 1998

**End hole:** 1000 hr, 24 September 1998

**Time on hole:** 120.08 hr

**Seafloor (drill pipe measurement from rig floor):** 3301.50 mbrf

**Distance between rig floor and sea level:** 11.40 m

**Water depth (drill pipe measurement from sea level):** 3290.10 m

**Total depth (from rig floor):** 3934.30 mbrf

**Total penetration:** 632.80 mbsf

**Coring totals:** type: APC; number: 16; cored: 151.50 m; recovered: 101.45%; type: XCB; number: 17; cored: 158.40 m; recovered: 85.69%

**Formation:** lithostratigraphic Subunit IA (0–151.5 mbsf): greenish gray to white clayey nannofossil ooze; lithostratigraphic Subunit IIIA (484–542.9 mbsf): light greenish gray and greenish gray clayey nannofossil chalk and nannofossil mudstone; lithostratigraphic Subunit IIIB (542.9–550.5 mbsf): greenish gray plastically deformed clasts of clayey nannofossil chalk; lithostratigraphic Subunit IIIC (550.5–587.2 mbsf): light greenish gray and greenish gray nannofossil chalk and nannofossil mudstone; lithostratigraphic Unit IV (587.2–632.8 mbsf): white to light greenish gray micritic limestone

Site 1123 is located 410 km northeast of the Chatham Islands, on the deep northeastern slopes of Chatham Rise at a water depth of 3290 m (Fig. F1, p. 52, in the “Site 1123” chapter). The holes penetrated the North Chatham sediment drift, which is located between 169°W and 175°W at depths of 2200–4500 m. The drift is thicker than 0.6 s above 3500-m water depth and has been deposited where the DWBC decelerates after passing through Valerie Passage. The drift is well defined by three seismic reflectors. Before drilling, the basal reflector (707 ms two-way traveltime [TWT]) was interpreted to be of middle Oligocene age. The upper sediments at this site comprise a 0.2-s-thick sequence of sediments, which on 3.5-kHz records comprise a series of irregular, vertically climbing mud waves. Parallel reflectors within this drape probably represent hemipelagites and calcareous pelagites. The anticipated presence of a substantial carbonate record back to the middle Oligocene made Site 1123 a prime location at which to evaluate the evolution of the DWBC system, including information on the NADW component of flow. It was also expected that the upper part of the sequence would contain a record of volcanic tephras derived from North Island, New Zealand. The objectives of Site 1123 were thus (1) to test the coherence of the paleoclimatic record with Milankovitch cyclicity; (2) to determine



the evolution of circum-Antarctic ocean circulation, with particular reference to periods of tectonic opening of critical seaways and climatic events (e.g., growth of Antarctic ice at 15–14 Ma); (3) to evaluate isotopic and grain-size signals to determine the paleohydrography of CDW and to estimate the volume transport of the DWBC; and (4) to determine the paleoproductivity associated with the nearby STC.

Three holes that recovered a sedimentary section spanning the last 20 m.y. were cored with the APC/XCB at Site 1123 to a maximum depth of 632.8 mbsf (Table T5, also in [ASCII format](#)). Seventeen cores were taken at Hole 1123A with the APC to 158.1 mbsf. Hole 1123B was cored with the APC to 155.4 mbsf and deepened with the XCB to 489.0 mbsf. Logging was conducted from the bottom of the hole at 489 mbsf to the bit at 84 mbsf. Three standard tool-string configurations were run: the triple combination, the FMS-sonic (two passes), and the GHMT. The condition of the borehole was good and the quality of the data is excellent. Hole 1123C was cored with the APC to 151.5 mbsf and deepened by drilling ahead to 484.0 mbsf. One XCB core was obtained from 230.0 to 239.6 mbsf to provide overlap with an interval of poor recovery in Hole 1123B. XCB coring resumed and advanced from 484.0 mbsf to the modified depth objective of 632.8 mbsf with excellent recovery.

Triple APC coring resulted in a complete composite section for the upper 150 mbsf, which contained the major volcanic tephtras erupted from New Zealand over the last 4.2 m.y. (Fig. F14). Splicing between cores was based on color reflectance and magnetic susceptibility data. The tephtras are surprisingly variable in thickness over the 20-m distance between holes, which is probably a result of coring disturbance.

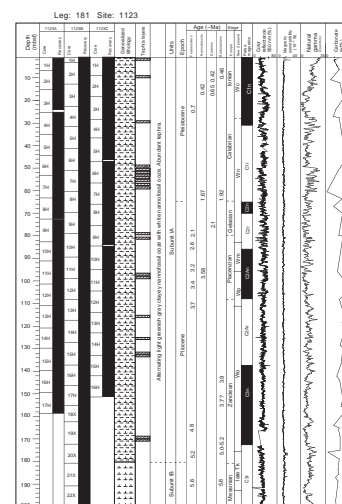
The stratigraphic sequence at Site 1123 is remarkably uniform over the upper 450 mbsf. Subdivision into Units I and II was made using the presence of tephtras in the upper section (above 182 m). Diffuse reflector R1, which before drilling was correlated with regional reflector Y, is in the drill core evidenced by only a small step in velocity and density at around 145 mbsf depth (i.e., corresponds to a lithification front). The dominant lithology of Unit I is a pale greenish gray ooze/chalk with a carbonate content oscillating around 65% ( $\pm 15\%$ ). In the upper 40 mbsf of the section, the color cyclicity (both visual and spectrophotometrically measured) is likely to be closely matched to isotopic stratigraphy and thereby dated. This cyclostratigraphic dating is consistent with the magnetostratigraphy, which recognizes the Matuyama/Brunhes boundary at 32 mbsf (Fig. F14). Units I and II, which have an average sedimentation rate of 4.1 cm/k.y., both show cyclicity in lithology, magnetic susceptibility, and/or reflectance, and/or GRAPE, and/or natural gamma-ray intensity. The lower part of the drift sequence, Unit III, has higher magnetic susceptibility and is darker green because of the presence of chlorite, but it retains the clear cyclicity seen in the Pleistocene. Unit III is punctuated by a 7.6-m-thick, plastically deformed mass flow subunit between 542.9 and 550.5 mbsf.

The Unit I–III sequence is extraordinarily well dated by 113 microfossil datum points and every magnetic polarity shift (plus two new ones) back to Chron C6n or 20 Ma on the scale of Berggren et al. (1995). There is ~100% core recovery over the 0–11 and 16–20 Ma intervals. Recovery of this sequence ended with a substantial hiatus from Chrons C6n to C12r, at ~32 Ma, with 12.5 m.y. missing.

Unit III rests with profound paraconformity on early Oligocene to Eocene micritic limestone, which was deposited at an average sedimentation rate of 2 cm/k.y. The contact between Units III and IV comprises an abrupt, *Chondrites*-burrowed surface, and represents the Marshall

T5. Site 1123 coring summary, p. 75.

F14. Summary log, Site 1123, p. 59.



Paraconformity, a regional marker of middle Oligocene environmental and stratigraphic change (Carter and Landis, 1972; Carter, 1985; Fulthorpe et al., 1996). Late Pleistocene foraminiferal assemblages show little influence of dissolution. Miocene and Pliocene samples are somewhat impoverished in planktonic and benthic taxa, and at some levels abundant test fragments occur, suggesting that the area was swept by corrosive cold bottom waters. In contrast, the Eocene and early Oligocene microfaunas from Unit IV comprise well-preserved planktonic-dominated assemblages. The Neogene planktonic foraminifers are clearly derived from the warmer waters north of the STC (*Globigerinoides conglobatus*, *G. ruber*). The light/dark sedimentary cyclicity reflects warm/cold cycles in planktonic foraminifers and possible productivity changes are mirrored in diatom abundances. Late Neogene diatoms show a mixture of local (warm water) forms and subantarctic forms from Bounty Trough or further south. This aspect to the flora is lacking in the beds below the Marshall Paraconformity. The evidence all points to the occurrence of major environmental change in the middle Oligocene, with the DWBC starting after ~30 Ma.

The physical properties records from Site 1123 are excellent and show cyclicity at several long and short wavelengths in magnetic susceptibility, density, gamma radiation, and color reflectance. Overall, most properties are uniform or gently increase down to 450 mbsf, and then increase again sharply in a unit overlying the unconformity at 587 mbsf. These characteristics occur in the downhole logs, which contain very good data on acoustic velocities, magnetic susceptibility, resistivity, gamma radiation, and density down to 486 mbsf.

Most of the recovered sediments are carbonate dominated, with carbonate concentrations between 10.3% and 84.3% and an average of 57.5% (Fig. F14). Organic carbon contents are twice the average for deep-sea sediments. The organic material seems to be heavily oxidized, probably by microbial reworking during sedimentation or early diagenesis. As a result of these processes, metabolizable organic matter is virtually absent, which results in low sedimentary methane concentrations and moderate sulfate concentrations in the pore water.

Interstitial water compositions are dominantly controlled by the high carbonate content of the sediments. Moderate reduction occurs in the upper part of the hole, probably because of a relatively high organic carbon content (~0.5%) there compared to normal deep-sea carbonate sediments. Sulfate content decreases gradually with depth to 13 mM at ~200 mbsf, below which it remains almost constant. Alkalinity shows a small maximum value of 8.5 mM at 107 mbsf. Carbonate diagenetic reactions are inferred from the profiles of dissolved calcium, magnesium, and strontium. The variation of dissolved silica in the lower part of the hole may imply changes of paleoproductivity.

Downhole logging measurements were taken in Hole 1123B, using the triple combination, the FMS-sonic, and the GHMT tools. Borehole conditions were good and the data were of high quality. A successful correlation was made between core and log-based magnetic susceptibility. The results were used to position missing sections of core. The sonic velocity data were used to construct a set of integrated travel times, to calculate the depth to major seismic reflectors. Distinct logging units were recognizable within the downhole measurements, reflecting fluctuating sedimentary conditions through time.

From all points of view, Site 1123 has the potential to become the Neogene standard section, and it will certainly provide an important reference site for the integration of Southwest Pacific microfaunas into

tropical zonation schemes. Results from the site will also help define the properties of the water flowing into the Pacific Ocean for the last 20 m.y.

## **Site 1124**

### **Hole 1124A**

**Position:** 39°29.901'S, 176°31.894'W  
**Start hole:** 1748 hr, 24 September 1998  
**End hole:** 0305 hr, 25 September 1998  
**Time on hole:** 9.28 hr  
**Seafloor (drill pipe measurement from rig floor, mbrf):** 3979.00  
**Distance between rig floor and sea level (m):** 11.50  
**Water depth (drill pipe measurement from sea level, m):** 3967.50  
**Total depth (from rig floor, mbrf):** 3988.50  
**Total penetration (mbsf):** 9.50  
**Coring totals:** type: APC; number: 1; cored: 9.50 m; recovered: 100.11%  
**Formation:** lithostratigraphic Subunit IA (0–9.5 mbsf): nannofossil silty clay

### **Hole 1124B**

**Position:** 39°29.901'S, 176°31.894'W  
**Start hole:** 0305 hr, 25 September 1998  
**End hole:** 1745 hr, 26 September 1998  
**Time on hole:** 38.67 hr  
**Seafloor (drill pipe measurement from rig floor, mbrf):** 3978.10  
**Distance between rig floor and sea level (m):** 11.50  
**Water depth (drill pipe measurement from sea level, m):** 3966.60  
**Total depth (from rig floor, mbrf):** 3988.00  
**Total penetration (mbsf):** 9.90  
**Coring totals:** type: APC; number: 2; cored: 9.90 m; recovered: 99.90%  
**Formation:** lithostratigraphic Subunit IA (0–9.88 mbsf): nannofossil silty clay

### **Hole 1124C**

**Position:** 39°29.901'S, 176°31.894'W  
**Start hole:** 1745 hr, 26 September 1998  
**End hole:** 1630 hr, 30 September 1998  
**Time on hole:** 94.75 hr  
**Seafloor (drill pipe measurement from rig floor, mbrf):** 3978.00  
**Distance between rig floor and sea level (m):** 11.50  
**Water depth (drill pipe measurement from sea level, m):** 3966.50  
**Total depth (from rig floor, mbrf):** 4451.10  
**Total penetration (mbsf):** 473.10  
**Coring totals:** type: APC; number: 14; cored: 132.00 m; recovered: 102.12%; type: XCB; number: 35; cored: 333.10 m; recovered: 89.76%  
**Formation:** lithostratigraphic Subunit IA (8–60.6 mbsf): nannofossil silty clay; lithostratigraphic Subunit IB (60.6–178.4 mbsf): silty clay grading into nannofossil silty clay intercalated with clayey nannofossil ooze grading into nannofossil ooze; lithostratigraphic Subunit IC (178.4–302.5 mbsf): clay-bearing nannofossil chalk intercalated with

clayey nannofossil chalk and nannofossil mudstone; lithostratigraphic Unit II (302.5–411.5 mbsf): nannofossil chalk with interbeds and laminae of clay-bearing nannofossil chalk that grades downcore through a nannofossil-bearing mudstone to a plain mudstone; lithostratigraphic Unit III (411.5–419.3 mbsf): clayey nannofossil chalk; lithostratigraphic Unit IV (419.3–429.09 mbsf): mudstone; lithostratigraphic Unit V (429.09–467.4 mbsf): nannofossil bearing mudstone; lithostratigraphic Unit VI (467.4–473.1 mbsf): nannofossil-bearing mudstone

## Hole 1124D

**Position:** 39°29.884'S, 176°31.892'W

**Start hole:** 1630 hr, 30 September 1998

**End hole:** 2330 hr, 1 October 1998

**Time on hole:** 31.00 hr

**Seafloor (drill pipe measurement from rig floor, mbrf):** 3978.00

**Distance between rig floor and sea level (m):** 11.50

**Water depth (drill pipe measurement from sea level, m):** 3966.50

**Total depth (from rig floor, mbrf):** 4133.60

**Total penetration (mbsf):** 155.60

**Coring totals:** type: APC; number: 14; cored: 133.00 m; recovered: 99.13%

**Formation:** lithostratigraphic Subunit IA (22.5–60.6 mbsf): nannofossil silty clay; lithostratigraphic Subunit IB (60.6–155.6 mbsf): silty clay grading into nannofossil silty clay intercalated with clayey nannofossil ooze grading into nannofossil ooze

Site 1124 is located ~600 km due east of New Zealand's North Island, on the 250-km-long north-south-trending ridge of Rekohu Drift (Fig. F1, p. 42, from the "Site 1124" chapter). The main Rekohu sequence, consisting principally of inferred Miocene drift sediments, overlies older sediments beneath seismic reflector R4 (= regional reflector X), and is on-lapped from the west by overbank turbidites from the Hikurangi Channel. Rekohu Drift has clearly acted as an effective barrier to eastward dispersal of terrigenous sediment from Hikurangi Channel, which turns abruptly to the left (north) against the drift. The channel is thought to have originally flowed to the north along the New Zealand margin toward Kermadec Trench and then to have been diverted eastward by a major slide off Hawke Bay in the early to mid-Pleistocene (Lewis et al., 1998). The drift sediments at this site were believed to be calcareous pelagites before drilling. It was hoped that Site 1124 would yield a mainly carbonate record of the Miocene paleohydrography of the DWBC, and, if it penetrated reflector R4, important information on the middle Cenozoic initiation deep-water circulation. The objectives of Site 1124 were thus to determine: (1) the Miocene evolution of the DWBC and associated water masses, (2) the provenance of sediment in the DWBC system, and (3) the Neogene volcanic history of the North Island.

Hole 1124A consists of a full core that failed to recover the mudline. The bit was raised by 5 m and Hole 1124B was spudded. The core barrel was retrieved with a shattered liner and no core. The second APC core achieved an incomplete stroke and required retrieval of the bottom-hole assembly with the stuck core barrel to the surface. Hole 1124C was washed to 8.0 mbsf where XCB coring was initiated. The hole was cored with the XCB from 8.0 to 27.2 mbsf, was deepened with the APC to 159.2 mbsf, and with the XCB to 473.1 mbsf (Table T6, also in ASCII

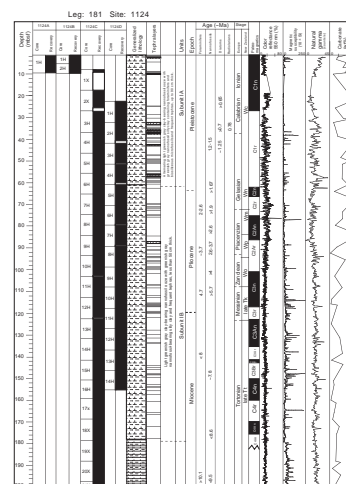
**format**). The hole was logged from total depth to 78 mbsf with the triple combination, the FMS-sonic, and the GHMT. Hole 1124D was drilled ahead to 22.6 mbsf with the XCB and deepened with the APC to refusal at 155.6 mbsf.

A high-quality and complete spliced record was obtained for 17.7 to 174 mcd from Holes 1124C and 1124D. The uppermost 11.7 mcd is also complete in Cores 181-1124A-1H and 181-1124B-1H and 2H, but coring difficulties caused by tephra resulted in the loss of a small section between 11.7 and 17.7 mcd. The Brunhes/Matuyama boundary is located at 33 mcd (Fig. F15), however, and it should therefore be straightforward to estimate the resulting time gap in the middle Pleistocene, which may be only ~100 k.y. long. The coring problems suggest that considerable lateral variability occurs in tephra thickness and cementation over the short distances between holes (~20 m).

The sequence at Site 1124 has been divided into six lithostratigraphic units. Units I and II, which compose the drift sequence, occupy the top 412 mbsf. These units are pale greenish gray ooze and chalk showing cyclicity in color, GRAPE, and magnetic susceptibility. Tephra beds are increasingly common from the upper Miocene upward, over the top 200 mbsf of the hole. The drift sequence is broken by a hiatus of ~4 m.y. within the lower Miocene (23–19 Ma). Beneath this, a thick (110 m) upper Oligocene section (Unit II) overlies the Marshall Paraconformity, which occurs at 412 mbsf and has similar characteristics to its occurrence at Site 1123 (see “**Lithostratigraphy**,” p. 4, in the “Site 1123” chapter) Microfaunas indicate that there is a 5-m.y. hiatus (32–27 Ma) across the Marshall Paraconformity at Site 1124. Beneath the paraconformity occur four thin units of contrasting character: lower Oligocene nannofossil chalk (Unit III), middle Eocene brown to dark brown mudstone (Unit IV), Paleocene nannofossil chalk with zeolitic interbeds (Unit V), and Upper Cretaceous cherty zeolitic mudstone with nannofossils (Unit VI), the first three being separated by two further profound paraconformities and the last two by the Cretaceous/Tertiary (K/T) boundary. Unfortunately, the boundary section itself is missing between cores, though it shows clearly on the FMS and other downhole logs as a resistivity high and magnetic susceptibility low. Carbonate contents are variable at Site 1124, averaging 36% but ranging from 0% to 88%. The lowest values are found in the middle and upper Miocene, between 100 and 300 mbsf. The organic carbon content is normal for deep-sea sediment, averaging 0.31%. The Eocene brown mudstone (Unit IV) is similar to the Waipawa Black Shale facies known from eastern North Island (e.g., Moore, 1988), but has a low organic carbon content of 0.26% to 0.44%.

Despite poor preservation of all groups in the Oligocene and Miocene, 66 microfossil datum points (49 above the middle Oligocene) have been recognized at Site 1124, giving a reasonably well-constrained age-depth curve. Planktonic foraminifers are too poorly preserved—only thick-shelled species have survived dissolution—for an assessment to be made of warm/cold assemblages. However, the diatoms represent a warm subtropical flora throughout. The upper Neogene, but not the upper Oligocene/lower Miocene, contains reworked Eocene taxa. As other indicators suggest the DWBC was flowing vigorously at this time, this may point to opening of a source to the south supplying Bounty Trough or scouring of Chatham Rise. Corrosion of foraminifers clearly intensifies after the formation of the Marshall Paraconformity compared with specimens in underlying strata, which is strong evidence for a new cold bottom-water source.

F15. Summary log, Site 1124, p. 63.





The magnetostratigraphy at Site 1124 was particularly good for the spliced interval of Holes 1124C and 1124D (30–170 mcd). All subchrons of the Matuyama, Gauss, Gilbert, and C3r–C4r inclusive were recognized in the upper part of the record. However, a strong magnetic overprint was encountered between 180 and 280 mbsf, which prevented unambiguous polarity determination over that interval. Magnetic intensities were very weak in the Oligocene, but increased in the Paleocene and around the Cretaceous/Tertiary boundary, where C29r was identified spanning the K/T boundary interval. Shore-based research should allow polarity and environmental magnetism to be determined for the whole record at Site 1124.

The Upper Cretaceous–Paleocene siliceous zeolitic mudstones were deposited at an average rate of 5 m/m.y. However, the rates for the succeeding two unconformity-bounded Eocene and lower Oligocene sections are indeterminate. Above the Marshall Paraconformity, the thick upper Oligocene–lower Miocene (~27–23 Ma) section accumulated at ~27 m/m.y. The middle and upper Miocene sections accumulated steadily at 10 m/m.y., slowing down (or possibly a brief hiatus) around 9.5 to 8.5 Ma. A sharp increase in sedimentation at 1.2 Ma to ~38 m/m.y. possibly records the Hikurangi Channel switching toward the drift and contributing fine tails of turbidity currents to it. This provides a possible age for the emplacement of the very large Ruatoria slide off eastern New Zealand.

Physical properties at Site 1124 are very uniform in two intervals, 20–178 and 178–280 mbsf, corresponding to lithostratigraphic Subunits IB and IC, respectively. The early drift and subdrift sequence shows down-hole increases in density and compaction. The brown mudstone unit, however, is of lower density than the chalk above and below. Temperature measurements yield a gradient of 51.9°C/km and an estimated heat flow of 0.049 W/m<sup>2</sup>.

Good logging results were obtained with all tools except the NMRS magnetic intensity instrument. All show signals of useful dynamic range, except for magnetic susceptibility between 318 and 419 mbsf, which is of very low amplitude, paralleling the core values. These values correlate very well between core and log over the whole hole. The brown mudstone unit stands out sharply in gamma, porosity, seismic velocity, photoelectric effect, and magnetic susceptibility. A 30-cm-thick layer at the correct position for the K/T boundary is evident in resistivity, magnetic susceptibility, and on the Formation MicroScanner display. The logs are vital for filling in the major features of a 17-m unrecovered interval just above 300 mbsf. The integrated travel times based on the sonic log suggest that reflector R4 (= regional reflector X) probably corresponds to the top of the brown mudstone.

The organic carbon concentrations average 0.3% and are in the normal range for deep-sea sediments. Carbonate contents show a high variability with values between 0.1% and 88.3%, and thus reflect a varying combination of fluctuating biological productivity, dilution by noncarbonate hemipelagic sedimentary components, and postdepositional carbonate dissolution.

The dominant chemical reactions that control the interstitial water element concentrations include organic matter degradation, carbonate dissolution/precipitation, silica dissolution, chert formation, and reactions with clay minerals. The element profiles of alkalinity, phosphate, and ammonia are typical of a situation without active sulfate reduction, and reflect organic matter oxidation and carbonate precipitation. The behavior of Ca, Mg, and Sr in the bottom of the section reflects a chem-

ical reaction other than carbonate diagenesis. The decrease of Sr is similar to the pattern of Li, which is related to Si utilization to form the chert in the lowermost part of the core. The low Si concentration in the middle of the section is attributed to poor preservation of biogenic siliceous sediments, probably caused by low paleoproductivity. The general chemical zonation of interstitial waters at Site 1124 can be related to the lithostratigraphic units, paleontological age divisions, and hiatuses.

Site 1124 will provide well dated and characterized material for paleo-oceanographic studies of the deeper levels of flow entering the Southwest Pacific Ocean, though bulk carbonate isotopic measurements may be necessary for some parts of the core. The stratigraphy of Site 1124 will be of particular importance for integrating the results from Leg 181 with the known onland geology of eastern North Island, New Zealand.

## **Site 1125**

### **Hole 1125A**

**Position:** 42°32.996'S, 178°9.989'W

**Start hole:** 2248 hr, 2 October 1998

**End hole:** 2000 hr, 3 October 1998

**Time on hole:** 21.20 hr

**Seafloor (drill pipe measurement from rig floor, mbrf):** 1376.20

**Distance between rig floor and sea level (m):** 11.60

**Water depth (drill pipe measurement from sea level, m):** 1364.60

**Total depth (from rig floor, mbrf):** 1579.70

**Total penetration (mbsf):** 203.50

**Coring totals:** type: APC; number: 22; cored: 203.50 m; recovered: 102.74%

**Formation:** lithostratigraphic Subunit IA (0–70.8 mbsf): clayey nannofossil ooze interbedded with nannofossil-bearing silty clay; lithostratigraphic Subunit IB (70.8–203.52 mbsf): nannofossil-bearing silty clay intercalated clay-bearing nannofossil ooze

### **Hole 1125B**

**Position:** 42°32.979'S, 178°9.988'W

**Start hole:** 2000 hr, 3 October 1998

**End hole:** 1730 hr, 6 October 1998

**Time on hole:** 69.50 hr

**Seafloor (drill pipe measurement from rig floor, mbrf):** 1377.20

**Distance between rig floor and sea level (m):** 11.60

**Water depth (drill pipe measurement from sea level, m):** 1365.60

**Total depth (from rig floor, mbrf):** 1929.30

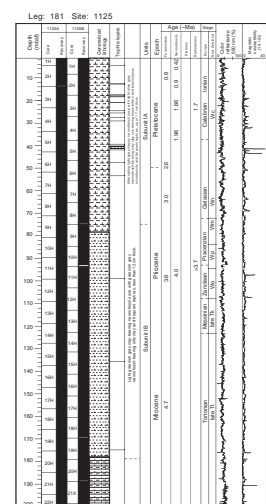
**Total penetration (mbsf):** 552.10

**Coring totals:** type: APC; number: 20; cored: 188.80 m; recovered: 101.49%; type: XCB; number: 38; cored: 363.30 m; recovered: 88.09%

**Formation:** lithostratigraphic Subunit IA (0–74.8 mbsf): clayey nannofossil ooze interbedded with nannofossil-bearing silty clay; lithostratigraphic Subunit IB (74.8–245.2 mbsf): nannofossil-bearing silty clay intercalated clay-bearing nannofossil ooze; lithostratigraphic Subunit IIA (245.2–331.5 mbsf): clayey nannofossil chalk; lithostratigraphic Subunit IIB (331.5–552.10 mbsf): clayey nannofossil chalk

Well-preserved and rich calcareous nannofossil, foraminiferal, and radiolarian floras and faunas are present throughout Site 1125, and rich diatom floras are present also below 160 mbsf. These microfossils have yielded 47 age datums between the early Miocene and late Pleistocene, thus providing a robust age-depth curve. The floras indicate subtropical

F16. Summary log, Site 1125,  
p. 66.



high-productivity conditions, whereas the faunas show some mixing of warm and cool subtropical species. Some cyclicity in warm/cold faunas in light/dark layers is also apparent, but no subantarctic species have been found.

Magnetic intensities are weak in the upper 200 mbsf, and deeper in the core they decline to the noise level of the machine. A reasonable magnetic stratigraphy can be detected in the upper 200 mbsf, with most reversals down to the base of C3n.4n at 5.23 Ma being present. After shore-based work, the paleomagnetic data will significantly aid the development of a tuned age model for the Pliocene–Pleistocene sediments at this site.

Sedimentation rates show two periods of very rapid deposition, the early late Miocene (10.1–10.6 Ma; early Tongaporutuan) at 190 m/m.y., and the late late Miocene (6–5 Ma; Kapitean) at 150 m/m.y., separated by intervals of lower accumulation rates. The Pliocene to Holocene rate declined from the Kapitean high to a Quaternary average of 20 m/m.y., though these rates do not take into account a possible a 0.5-m.y. hiatus.

Physical properties at Site 1125 are very uniform, with slow and slight increases in density with depth. The magnetic susceptibility record is relatively featureless. The thermal gradient is 64.9°C/km, and the calculated heat flow is 0.071 W/m<sup>2</sup>.

Because of severe time constraints, just one logging tool was run at Site 1125: the triple combination, comprising gamma radiation, resistivity, and porosity/density sensors. Resistivity and density show little change over the top 500 m of the hole, but the latter jumps from 1950 to 2200 kg/m<sup>3</sup> from around 510 mbsf to the bottom of the hole, accounting for the very slow drilling encountered there. The gamma record exhibits more character, which will be examined by spectral methods.

The upper part of the hole is marked by sulfate reduction, with a decline of sulfate to zero at 200 mbsf and an increase of methane to 500 mbsf in the zone of methanogenesis below. Most other geochemical properties are related to these processes: alkalinity and ammonia increase in the upper 200 m, and calcium decreases as a result of carbonate precipitation, followed by calcium increase and carbonate dissolution in the zone of methanogenesis. Silica concentrations increase steadily downhole, but sharply decrease in the bottom 40 m where particularly hard mudstone was encountered, probably caused by incipient silica cementation.

Site 1125 proved the equal of the other sites on Leg 181 in its capacity to surprise the shipboard scientific party. Two intervals with an astonishing sedimentation rate of over 150 m/m.y. ensured that middle Miocene sediment had not been reached even after 550 m of core penetration. The prospect for high-resolution study of productivity and intermediate water masses in the Southwest Pacific for the last 11 m.y. using Site 1125 materials is excellent. Comparisons between this site, located under subtropical water, and Site 594, just south of Chatham Rise and under subantarctic water, promise to yield a scientific cornucopia.

## REFERENCES

- Alloway, B.W., Pillans, B.J., Sandhu, A.S., and Westgate, J.S., 1993. Revision of the marine chronology in the Wanganui Basin, New Zealand, based on the isothermal plateau fission-track dating of tephra horizons. *Sediment. Geol.*, 82:299–310.
- Andrews, P.B., 1979. Depositional facies and the early phase of ocean basin evolution in the circum-Antarctic region. *Mar. Geol.*, 25:1–13.
- Ballance, P.F., 1976. Evolution of the Upper Cenozoic magmatic arc and plate boundary in northern New Zealand. *Earth Planet. Sci. Lett.*, 28:356–370.
- Barnes, P.M., 1992. Mid-bathyal current scours and sediment drifts adjacent to the Hikurangi deep-sea turbidite channel, eastern New Zealand: evidence from echo character mapping. *Mar. Geol.*, 106:169–187.
- Barnes, P.M., and Mercier de Lepinay, B., 1997. Rates and mechanics of rapid frontal accretion along the very obliquely convergent southern Hikurangi margin, New Zealand. *J. Geophys. Res.*, 102:24931–24952.
- Barrett, P.J., 1996. Antarctic paleoenvironment through Cenozoic times: a review. *Terra Antarct.*, 3:103–119.
- Barron, J., Larsen, B., et al., 1989. *Proc. ODP, Init. Repts.*, 119: College Station, TX (Ocean Drilling Program).
- Berggren, W.A., Kent, D.V., Swisher, C.C., III, and Aubry, M.-P., 1995. A revised Cenozoic geochronology and chronostratigraphy. In Berggren, W.A., Kent, D.V., Aubry, M.-P., and Hardenbol, J. (Eds.), *Geochronology, Time Scales and Global Stratigraphic Correlation*. Spec. Publ.—Soc. Econ. Paleontol. Mineral. (Soc. Sediment. Geol.), 54:129–212.
- Bishop, D.G., and Laird, M.G., 1976. Stratigraphy and depositional environment of the Kyeburn Formation (Cretaceous), a wedge of coarse terrestrial sediments in Central Otago. *J. R. Soc. N. Z.*, 6:55–71.
- Boltovskoy, E., 1980. The age of the Drake Passage. *Alcheringa*, 4:289–297.
- Broecker, W.S., Bond, G., Klas, M., Bonani, G., and Wolfi, W., 1990. A salt oscillator in the glacial Atlantic? 1. The concept. *Paleoceanography*, 5:469–477.
- Bryden, H.L., and Heath, R.A., 1985. Energetic eddies at the northern edge of the Antarctic Circumpolar Current in the Southwest Pacific. *Prog. Oceanogr.*, 14:65–87.
- Campbell, H.J., Andrews, P.B., Beu, A.G., Maxwell, P.A., Edwards, R.A., Laird, M.G., Hornibrook, N. de B., Mildenhall, D.C., Watters, W.A., Buckeridge, J.S., Lee, D.E., Strong, C.P., Wilson, G.J., and Hayward, B.W., 1993. Cretaceous-Cenozoic geology and biostratigraphy of the Chatham Islands, New Zealand. *Inst. Geol. Nucl. Sci. Monogr.*, 2:269.
- Carter, L., and Carter, R.M., 1988. Late Quaternary development of left bank dominant levees in the Bounty Trough, New Zealand. *Mar. Geol.*, 78:185–197.
- , 1993. Sedimentary evolution of the Bounty Trough: a Cretaceous rift basin, southwestern Pacific Ocean. In Ballance, P. (Ed.), *Sedimentary Basins of the World—South Pacific*: Amsterdam (Elsevier), 51–67.
- Carter, L., Carter, R.M., McCave, I.N., and Gamble, J., 1996. Regional sediment recycling in the abyssal Southwest Pacific Ocean. *Geology*, 24:735–738.
- Carter, L., Carter, R.M., Nelson, C.S., Fulthorpe, C.S., and Neil, H.L., 1990. Evolution of Pliocene to Recent abyssal sediment waves on Bounty Channel levees, New Zealand. *Mar. Geol.*, 95:97–109.
- Carter, L., Garlick, R.D., Sutton, P., Chiswell, S., Oien, N.A., and Stanton, B.R., 1998. Ocean circulation New Zealand. *NIWA Chart, Misc. Ser.*, 76.
- Carter, L., and Herzer, R.H., 1979. The hydraulic regime and its potential to transport sediment on the Canterbury continental shelf. *Mem.—N. Z. Oceanogr. Inst.*, 83:1–33.
- Carter, L., and McCave, I.N., 1994. Development of sediment drifts approaching an active plate margin under the SW Pacific deep western boundary current. *Paleoceanography*, 9:1061–1085.



- , 1997. The sedimentary regime beneath the deep western boundary current inflow to the Southwest Pacific Ocean. *J. Sediment. Res.*, 67:1005–1017.
- Carter, L., and Mitchell, J.S., 1987. Late Quaternary sediment pathways through the deep ocean, east of New Zealand. *Paleoceanography*, 2:409–422.
- Carter, L., Nelson, C.S., Neil, H.L., and Froggatt, P.C., 1995. Correlation, dispersal, and preservation of the Kawakawa Tephra and other late Quaternary tephra layers in the Southwest Pacific Ocean. *N. Z. J. Geol. Geophys.*, 38:29–46.
- Carter, L., and Wilkin, J., in press. Abyssal circulation around New Zealand: a comparison between observations and a global circulation model. *Mar. Geol.*
- Carter, R.M., 1985. The mid-Oligocene Marshall Paraconformity, New Zealand: coincidence with global eustatic sea-level fall or rise? *J. Geol.*, 93:359–371.
- , 1988a. Plate boundary tectonics, global sea-level changes and the development of the Eastern South Island Continental Margin, New Zealand, Southwest Pacific. *Mar. Pet. Geol.*, 5:90–107.
- , 1988b. Post-breakup stratigraphy of the Kaikoura Synthem (Cretaceous–Cenozoic), continental margin, southeastern New Zealand. *N. Z. J. Geol. Geophys.*, 31:405–429.
- Carter, R.M., and Carter, L., 1996. The abyssal Bounty Fan and lower Bounty Channel: evolution of a rifted-margin sedimentary system. *Mar. Geol.*, 130:182–202.
- Carter, R.M., Carter, L., and Davy, B., 1994. Geologic and stratigraphic history of the Bounty Trough, southwestern Pacific Ocean. *Mar. Pet. Geol.*, 11:79–93.
- Carter, R.M., Carter, L., and McCave, I.N., 1996. Current controlled sediment deposition from the shelf to the deep ocean: the Cenozoic evolution of circulation through the SW Pacific gateway. *Geol. Rundsch.*, 85:438–451.
- Carter, R.M., and Landis, C.A., 1972. Correlative Oligocene unconformities in southern Australasia. *Nature*, 237:12–13.
- Carter, R.M., and Norris, R.J., 1976. Cainozoic history of southern New Zealand: an accord between geological observations and plate-tectonic predictions. *Earth Planet. Sci. Lett.*, 31:85–94.
- Chiswell, S.M., 1994a. Acoustic Doppler Current Profiler measurements over the Chatham Rise. *N. Z. J. Mar. Freshwater Res.*, 30:1–17.
- , 1994b. Variability in sea surface temperature around New Zealand from AVHRR images. *N. Z. J. Mar. Freshwater Res.*, 28:179–192.
- Cotton, C.A., 1955. Review of the Notocenoic, or Cretaceous-Tertiary of New Zealand. *Trans. R. Soc. N. Z.*, 82:1071–1122.
- Dersch, M., and Stein, R., 1991. Paläoklima und paläoozeanische Verhältnisse im SW-Pazifik während der letzten 6 Mill. Jahre (DSDP-Site 594, Chatham Rücken, Östlich Neuseeland). *Geol. Rundsch.*, 80:535–556.
- Fenner, J., Carter, L., and Stewart, R., 1992. Late Quaternary paleoclimatic and paleoceanographic change over northern Chatham Rise, New Zealand. *Mar. Geol.*, 108:383–404.
- Field, B.D., Uruski, C.I., et al., 1997. Cretaceous-Cenozoic geology and petroleum systems of the East Coast region, New Zealand. *Inst. Geol. Nucl. Sci., Geol. Monogr.*, 19.
- Fleming, C.A., 1975. The geological history of New Zealand and its biota. In Kuschel, G. (Ed.), *Biogeography and Ecology in New Zealand*: The Hague (W. Junk), 1–86.
- Froggatt, P.C., and Lowe, D.J., 1990. A review of late Quaternary silicic and some other tephra formation from New Zealand: their stratigraphy, nomenclature, distribution, volume and age. *N. Z. J. Geol. Geophys.*, 33:89–109.
- Froggatt, P.C., Nelson, C.S., Carter, L., Griggs, G., and Black, K.P., 1986. An exceptionally large late Quaternary eruption from New Zealand. *Nature*, 319:578–582.
- Fulthorpe, C.S., and Carter, R.M., 1991. Continental shelf progradation by sediment drift accretion. *Geol. Soc. Am. Bull.*, 103:300–309.
- Fulthorpe, C.S., Carter, R.M., Miller, K.G., and Wilson, J. 1996. The Marshall Paraconformity: a Southern Hemisphere record of a mid-Oligocene glacioeustatic lowstand. *Mar. Pet. Geol.*, 13:61–77.

- Gordon, A.I., 1986. Inter-ocean exchange of thermocline water. *J. Geophys. Res.*, 91:5037–5046.
- Griggs, G.B., Carter L., Kennett, J.P., and Carter, R.M., 1983. Late Quaternary marine stratigraphy southeast of New Zealand. *Geol. Soc. Am. Bull.*, 94:791–797.
- Heath, R.A., 1985. A review of the physical oceanography of the seas around New Zealand–1982. *N. Z. J. Mar. Freshwater Res.*, 19:70–124.
- Howard, W.R., and Prell, W.L., 1992. Late Quaternary surface circulation of the southern Indian ocean and its relationship to orbital variations. *Paleoceanography*, 7:79–117.
- Kennett, J.P., 1977. Cenozoic evolution of Antarctic glaciation, the circum-Antarctic Ocean, and their impact on global paleoceanography. *J. Geophys. Res.*, 82:3843–3860.
- Kennett, J.P., Burns, R.E., Andrews, J.E., Churkin, M., Jr., Davies, T.A., Dumitrica, P., Edwards, A.R., Galehouse, J.S., Packham, G.H., and van der Lingen, G.J., 1972. Australian-Antarctic continental drift, paleo-circulation change and Oligocene deep-sea erosion. *Nature*, 239:51–55.
- Kennett, J.P., von der Borch, C.C., et al., 1986. *Init. Repts. DSDP*, 90: Washington (U.S. Govt. Printing Office).
- Kowalski, E.A., and Meyers, P.A., 1997. Glacial-interglacial variations in Quaternary production of marine organic matter at DSDP Site 594, Chatham Rise, southeastern New Zealand margin. *Mar. Geol.*, 140:249–263.
- Lawver, L., Gahagan, L., and Coffin, M., 1992. The development of paleoseaways around Antarctica. *Antarct. Res. Ser.*, 56:7–30.
- Lean, C.M.B., and McCave, I.N., 1998. Glacial to interglacial mineral magnetic palaeo-oceanographic changes at Chatham, Southwest Pacific Ocean. *Earth Planet. Sci. Lett.*, 163:247–260.
- Levitus, S., 1982. Climatological Atlas of the World Ocean. *NOAA Prof. Pap.*, 13.
- Lewis, K.B., 1980. Quaternary sedimentation on the Hikurangi oblique-subduction and transform margin, New Zealand. *Spec. Publ. Int. Assoc. Sedimentol.*, 4:171–189.
- , 1994. The 1500-km long Hikurangi Channel: trench-axis channel that escapes its trench, crosses a plateau, and feeds a fan-drift. *Geo-Mar. Lett.*, 14:19–28.
- Lewis, K.B., Bennett, D.J., Herzer, R.H., and von der Borch, C.C., 1986. Seismic stratigraphy and structure adjacent to an evolving plate boundary, western Chatham Rise, New Zealand. In Kennett, J.P., von der Borch, C.C., et al., *Init. Repts. DSDP*, 90: Washington (U.S. Govt. Printing Office), 1325–1337.
- Lewis, K.B., Collott, J.-Y., and Lallemand, S.E., 1998. The dammed Hikurangi Trough: a channel-fed trench blocked by subducting seamounts and their wake avalanches (New Zealand–France GeodyNZ Project). *Basin Res.*, 10:441–468.
- Lewis, K.B., and Kohn, B.P., 1973. Ashes, turbidites and rates of sedimentation on the continental slope off Hawkes Bay. *N. Z. J. Geol. Geophys.*, 16:439–454.
- Lewis, K.B., and Pettinga, J.G., 1993. The emerging frontal wedge of the Hikurangi margin. In Ballance, P.F. (Ed.), *South Pacific Sedimentary Basins*: (Amsterdam) Elsevier, 225–250.
- Lonsdale, P., 1976. Abyssal circulation of the southeastern Pacific and some geological implications. *J. Geophys. Res.*, 81:1163–1176.
- , 1988. Geography and history of the Louisville hotspot chain in the Southwest Pacific. *J. Geophys. Res.*, 93:3078–3104.
- McCave, I.N., and Carter, L., 1997. Recent sedimentation beneath the Deep Western Boundary Current off northern New Zealand. *Deep-Sea Res.*, 44:1203–1237.
- Milliman, J.D., and Syvitski, J.P.M., 1992. Geomorphic/tectonic control of sediment discharge to the ocean: the importance of small mountainous rivers. *J. Geol.*, 100:525–544.
- Molnar, P., Atwater, T., Mammerrickx, J., and Smith, S., 1975. Magnetic anomalies, bathymetry and the tectonic evolution of the South Pacific since the Late Cretaceous. *Geophys. J. R. Astron. Soc.*, 40:383–420.

- Moore, P.R., 1988. Stratigraphy, composition, and environment of deposition of the Whangai Formation and associated Late Cretaceous–Paleocene rocks, eastern North Island, New Zealand. *N.Z. Geol. Surv. Bull.*, 100:1–82.
- Nelson, C.S., Cooke, P.J., Hendy, C.H., and Cuthbertson, A.M., 1993. Oceanographic and climatic changes over the past 160,000 years at Deep Sea Drilling Project Site 594 off southeastern New Zealand, Southwest Pacific Ocean. *Paleoceanography*, 8:435–458.
- Nelson, C.S., Froggatt, P.C., and Gosson, G.J., 1986a. Nature, chemistry, and origin of late Cenozoic megascopic tephra in Leg 90 cores from the southwestern Pacific. In Kennett, J.P., von der Borch, C.C., et al., *Init. Repts. DSDP*, 90: Washington (U.S. Govt. Printing Office), 1161–1171.
- Nelson, C.S., Hendy, C.H., Cuthbertson, A.M., 1994. Oxygen isotope evidence for climatic contrasts between Tasman Sea and Southwest Pacific Ocean during the late Quaternary. In van der Linde, G.R., Swanson, K.M., and Muir, R.J. (Eds.), *Evolution of the Tasman Sea Basin*: Rotterdam (Balkema), 181–196.
- Nelson, C.S., Hendy, C.H., Cuthbertson, A.M., and Jarrett, G.R., 1986b. Late Quaternary carbonate and isotope stratigraphy, subantarctic Site 594, Southwest Pacific. In Kennett, J.P., von der Borch, C.C., et al., *Init. Repts. DSDP*, 90: Washington (U.S. Govt. Printing Office), 1425–1436.
- Nelson, C.S., Hendy, C.H., Jarrett, G.R., and Cuthbertson, A.M., 1985. Near-synchronicity of New Zealand alpine glaciations and Northern Hemisphere continental glaciations during the past 750 kyr. *Nature*, 318:361–363.
- Ninkovich, D., 1968. Pleistocene volcanic eruptions in New Zealand recorded in deep sea sediments. *Earth Planet. Sci. Lett.*, 4:89–102.
- Nodder, S.N., 1998. Particulate fluxes in the Subtropical Convergence region and other marine environments of New Zealand [Ph.D. thesis]. Univ. of Waikato, Hamilton, New Zealand.
- Norris, R.J., Carter, R.M., and Turnbull, I.M., 1978. Cainozoic sedimentation in basins adjacent to a major continental transform boundary in southern New Zealand. *J. Geol. Soc. London*, 135:191–205.
- Oliver, R.L., Finlay, H.J., and Fleming, C.A., 1950. The geology of Campbell Island. *Cape Expedition Ser., Bull.*, 3.
- Orsi, A.H., Whitworth, T., III, and Nowlin, W.D., Jr., 1995. On the meridional extent and fronts of the Antarctic Circumpolar Current. *Deep-Sea Res.*, 42:641–673.
- Pettinga, J.R., 1982. Upper Cenozoic structural history, coastal southern Hawke Bay, New Zealand. *N.Z.J. Geol. Geophys.*, 25:149–191.
- Pudsey, C.J., Barker, P.F., and Hamilton, N., 1988. Weddell Sea abyssal sediments: a record of Antarctic bottom water flow. *Mar. Geol.*, 81:289–314.
- Schmitz, W.J., 1995. On the interbasin-scale thermohaline circulation. *Rev. Geophys.*, 33:151–173.
- Schuur, C.L., Coffin, M.F., Frohlich, C., Mann, P., Massell, C.G., Karner, G.D., Ramsay, D., and Caress, D.W., 1998. Sedimentary regimes at the Macquarie Ridge Complex: interaction of Southern Ocean circulation and plate boundary bathymetry. *Paleoceanography*, 13:646–670.
- Shackleton, N.J., and Kennett, J.P., 1975. Paleotemperature history of the Cenozoic and the initiation of Antarctic glaciation: oxygen and carbon isotope analyses in DSDP Sites 277, 279, and 281. In Kennett, J.P., Houtz, R.E., et al., *Init. Repts. DSDP*, 29: Washington (U.S. Govt. Printing Office), 743–755.
- Shane, P.A.R., 1990. Correlation of some Pliocene tuffs in southern Wairarapa, New Zealand, and the comparison with biostratigraphic and magnetostratigraphic data. *N. Z. J. Geol. Geophys.*, 33:349–355.
- Shane, P.A.R., Black, T.M., Alloway, B.V., and Westgate, J.A., 1996. Early to middle Pleistocene tephrochronology of North Island, New Zealand: implications for volcanism, tectonism, and paleoenvironments. *Geol. Soc. Am. Bull.*, 108:915–925.

- Shane, P.A.R., and Froggatt, P.C., 1991. Glass chemistry, paleomagnetism and correlation of middle Pleistocene tuffs in southern North Island, New Zealand and western Pacific. *N. Z. J. Geol. Geophys.*, 34:203–211.
- Shane, P., Froggatt, P., Black, T., and Westgate, J., 1995. Chronology of Pliocene and Quaternary bioevents and climatic events from fission-track ages on tephra beds, Wairarapa, New Zealand. *Earth Planet. Sci. Lett.*, 130:141–154.
- Stonely, R., 1968. A lower Tertiary decollement on the east coast, North Island, New Zealand. *N.Z.J. Geol. Geophys.*, 11:128–156.
- Suggate, R.P., Stevens, G.R., and Te Punga, M.T., 1978. *The Geology of New Zealand*: Wellington (New Zealand Govt. Printer).
- Sutherland, R., 1995. The Australia-Pacific boundary and Cenozoic plate motions in the SW Pacific: some constraints from Geosat data. *Tectonics*, 14:819–831.
- Thiede, J., Nees, S., Schulz, H., and De Deckker, P., 1997. Oceanic surface conditions recorded on the sea floor of the Southwest Pacific Ocean through the distribution of foraminifers and biogenic silica. *Palaeogeogr., Palaeoclimatol., Palaeoecol.*, 131:207–239.
- Turnbull, I.M., 1985. Sheet D42AC and Part Sheet D43—Te Anau Downs (1st ed.). *Geological Map of New Zealand, Map and Notes*. (1:50,000). New Zealand Dept. Sci. Indust. Res., 1–32.
- Turnbull, I.M., and Uruski, C.I., 1995. Geology of the Monowai–Waitutu area. (1:50,000). *Inst. Geol. Nucl. Sci., Geol. Map*, 19.
- van der Lingen, G.J., 1968. Volcanic ash in the Makara Basin (Upper Miocene), Hawkes Bay, New Zealand. *N. Z. J. Geol. Geophys.*, 11:693–705.
- Vella, P., 1962. Age of the younger marine strata at upper Tengawai River (Appendix). *N. Z. J. Geol. Geophys.*, 5:172–174.
- Walcott, R.I., 1998. Modes of oblique compression: late Cenozoic tectonics of the South Island of New Zealand. *Rev. Geophys.*, 36:1–26.
- Ward, D.M., and Lewis, D.W., 1975. Paleoenvironmental implications of storm-scoured ichnofossiliferous mid-Tertiary limestones, Waihao district, South Canterbury, New Zealand. *N. Z. J. Geol. Geophys.*, 18:881–908.
- Warren, B.A., 1973. TransPacific hydrographic sections at latitudes 43S and 28S; the SCORPIO Expedition—II. Deep water. *Deep-Sea Res.*, 20:9–38.
- , 1981. Deep circulation of the world ocean. In Warren, B.A., and Wunsch, C. (Eds.), *Evolution of Physical Oceanography*: Cambridge, MA (MIT Press), 6–41.
- Watkins, N.D., and Kennett, J.P., 1971. A major sedimentary disconformity as evidence of an upper Cenozoic change in bottom water velocity between Australia, New Zealand, and Antarctica. *Geol. Soc. Am., Abstr.*: 746.
- Watkins, N.D., and Kennett, J.P., 1972. Regional sedimentary disconformities and upper Cenozoic changes in bottom water velocities between Australia and Antarctica. *Antarct. Res. Ser.*, 19:317–334.
- Weaver, P.P.E., Carter, L., and Neil, H., 1998. Response of surface water masses and circulation to late Quaternary climate change, east of New Zealand. *Paleoceanography*, 13:70–83.
- Weaver, P.P.E., Neil, H., and Carter, L., 1997. Sea surface temperature estimates from the Southwest Pacific based on planktonic foraminifera and oxygen isotopes. *Palaeogeogr., Palaeoclimatol., Palaeoecol.*, 131:241–256.

Figure F1. Bathymetric map of the eastern New Zealand region, Southwest Pacific Ocean, showing the location of previous DSDP sites and the location of all sites drilled during Leg 181. Depths in meters.

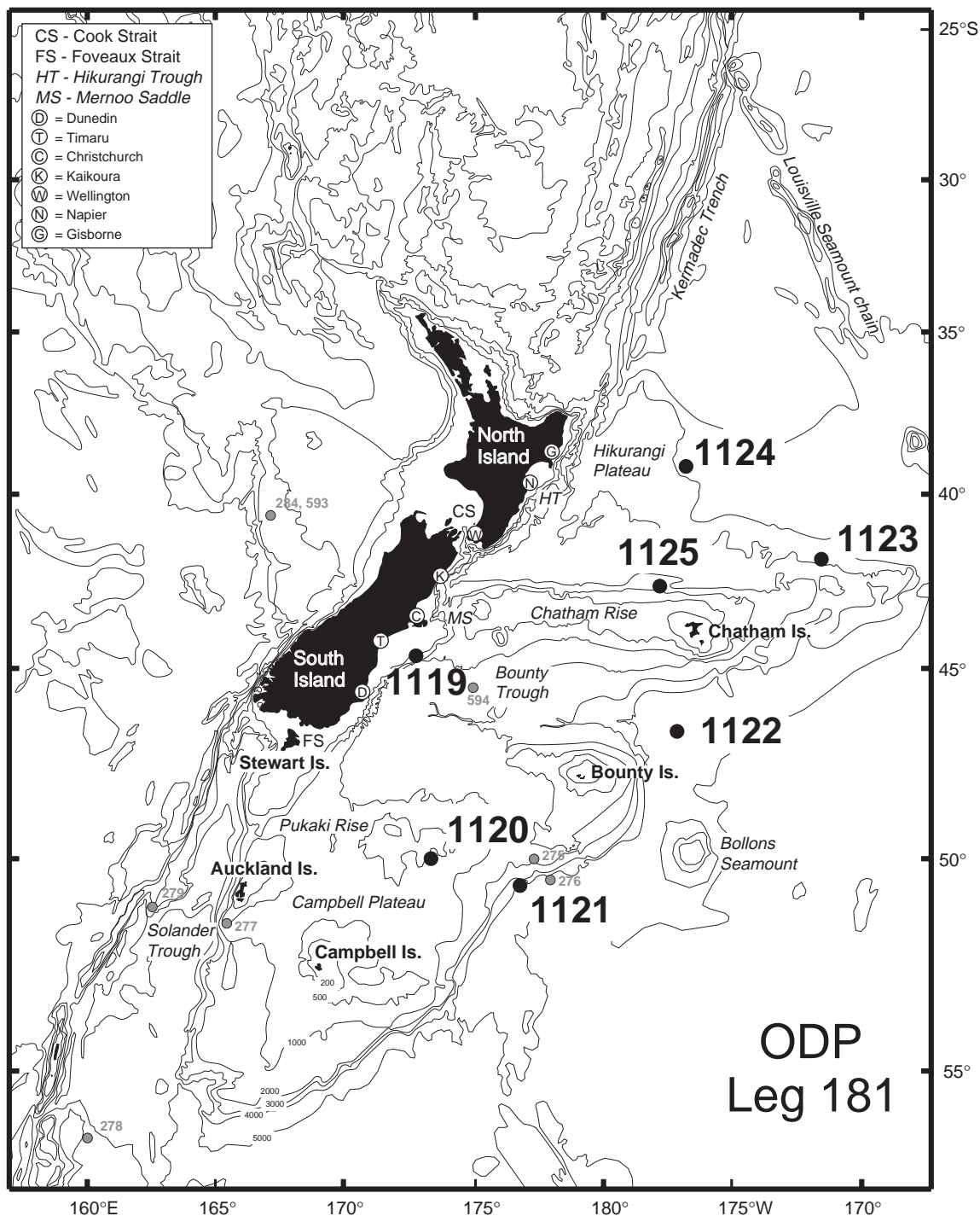




**Figure F2. A.** The bathymetry of the eastern New Zealand region, with the positions of major fronts at the ocean surface (summer temperatures) and the Antarctic Circumpolar (ACC) and Pacific Deep Western Boundary (DWBC) currents indicated. **B.** Meridional salinity cross section through the Pacific Ocean (data after Levitus, 1982), with location of the Leg 181 sites projected onto the plane of section. (Continued on next page.)

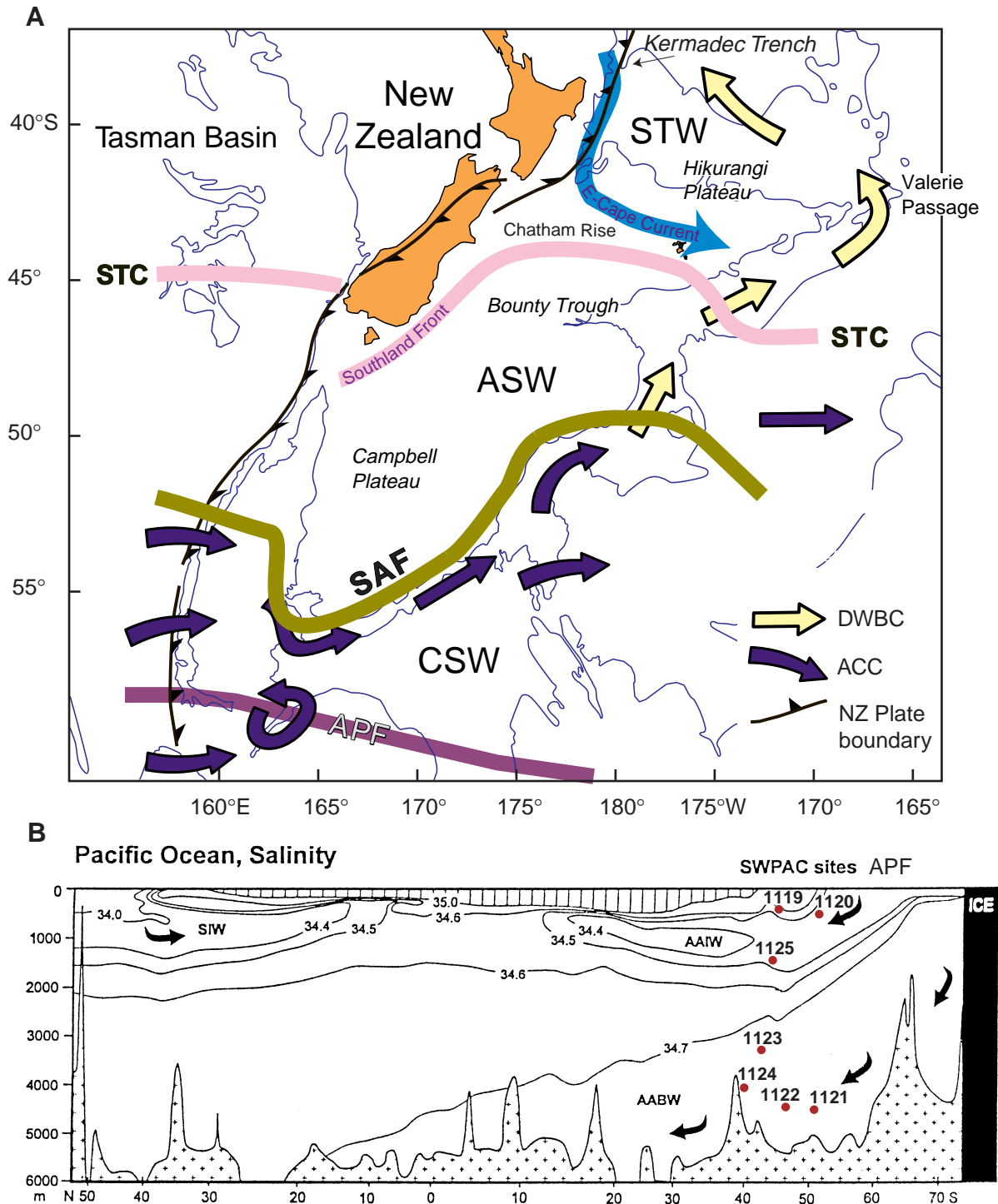


Figure F2 (continued). C. Water masses and fronts of the Southwest Pacific Ocean.

C

MAJOR WATER MASSES AND FRONTS OF THE SOUTHWEST PACIFIC							
Water Mass	Abbr.	Depth (m)	Pot. Density (kg/m <sup>3</sup> )	Salinity	Temp. (°C)	Oxygen (mL/L)	Silica
Subtropical Surface Water	STW	Surface	<div>&gt;15</div>				
<b>Subtropical Convergence</b>	<b>STC</b>		<b>Separates CSTW from ASW at 15° summer surface isotherm</b>				
Australasian Subantarctic Water	ASW	Surface	<div>8-15</div>				
<b>Subantarctic Front</b>	<b>SAF</b>		<b>Separates ASW from CSW at 8° summer surface isotherm</b>				
Circumpolar Surface Water	CSW	Surface	<div>5-8</div>				
<b>Antarctic Polar Front (Convergence)</b>	<b>APF</b>		<b>Separates CSW from Antarctic Water (AAW), with icebergs (&lt;5°C)</b>				
Thermocline water		0-400		34.42-34.90	7.00-11.00	4.40-5.00	
Subantarctic Mode Water	SAMW	400-600	(26.80-27.20)	(34.0-34.2)	(6-10)	(very high)	(very low)
Antarctic Intermediate Water (S min)	AAIW	600-1450	27.20-27.35	34.50-34.36	3.20-7.00	3.20-4.70	
North Pacific Deep Water (O min)	NPDW	1450-2550		34.67-34.50	1.80-3.20	2.80-3.20	
Circumpolar Deep Water (upper)	UCDW	2550-2900	36.50-37.00	34.67-34.71	1.60-1.80	3.03-3.45	
Circumpolar Deep Water (middle) (S max)	MCDW	2900-3800	37.00-45.93	34.71-34.73	0.90-1.60	3.45-3.63	high
Circumpolar Deep Water (lower) (O max)	LCDW	>3800	45.93-46.00	<34.71	0.55-0.90	4.70-4.80	high
Antarctic Circumpolar Current	ACC	0-seafloor	Various <div>-----</div>				
Weddell Sea Deep Water	WSDW		<div>-0.30-0.00</div>				
North Atlantic Deep Water	NADW		As for MCDW <div>-----</div>				
Antarctic Bottom Water	AABW		General term for cold water of Antarctic origin which spreads north into the major ocean basins <div>-----</div>				

Figure F3. Plate tectonic reconstructions of the Southern Hemisphere continents in polar projection for 50, 30, and 20 Ma (after Lawver et al., 1992), with position of inferred currents indicated with arrows.

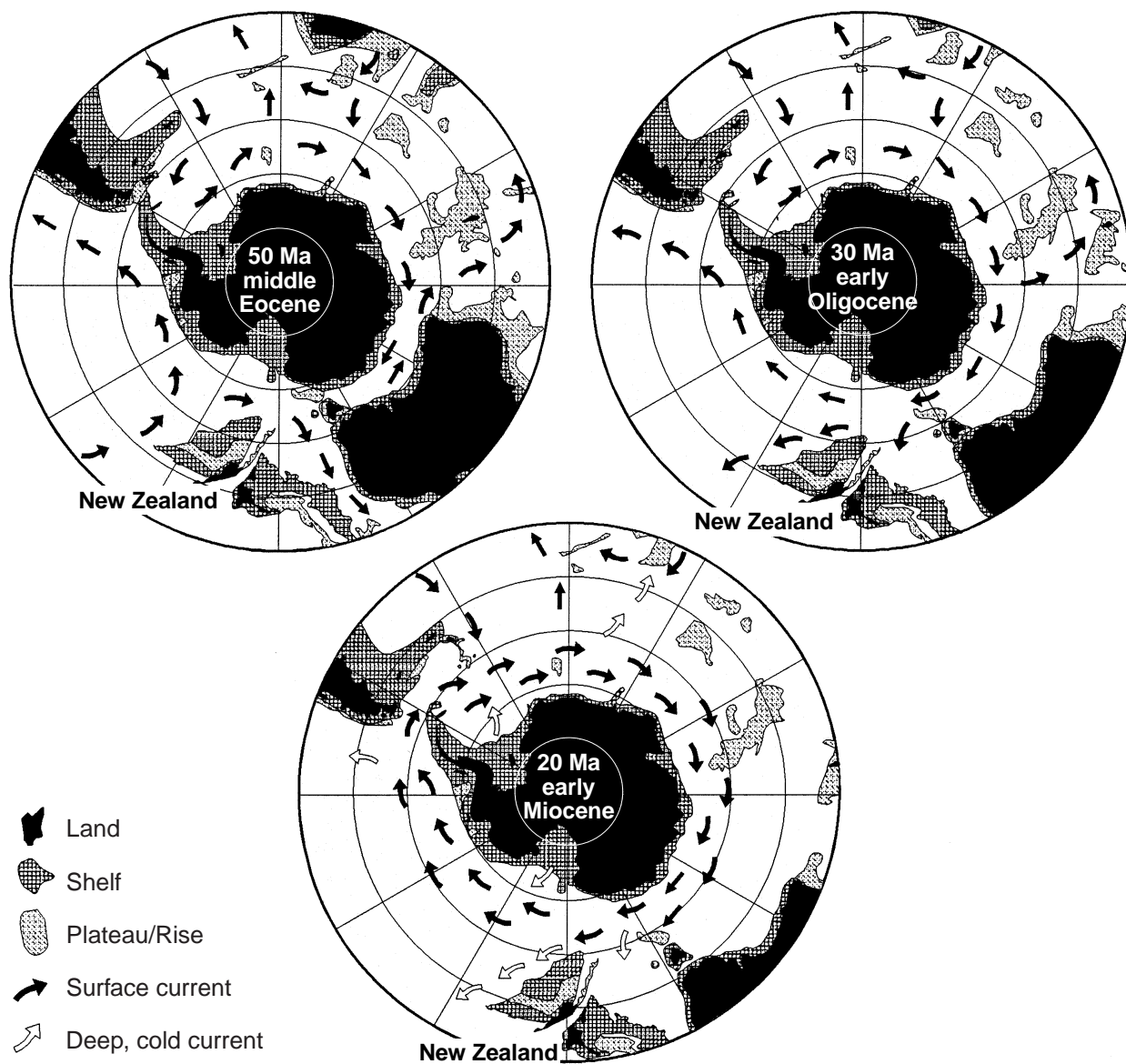


Figure F4. Geologic cross sections (A) through the eastern South Island and adjacent shelf, and (B) from the shelf edge across the Campbell Plateau to the Southwest Pacific abyssal plain. Lst = limestone.

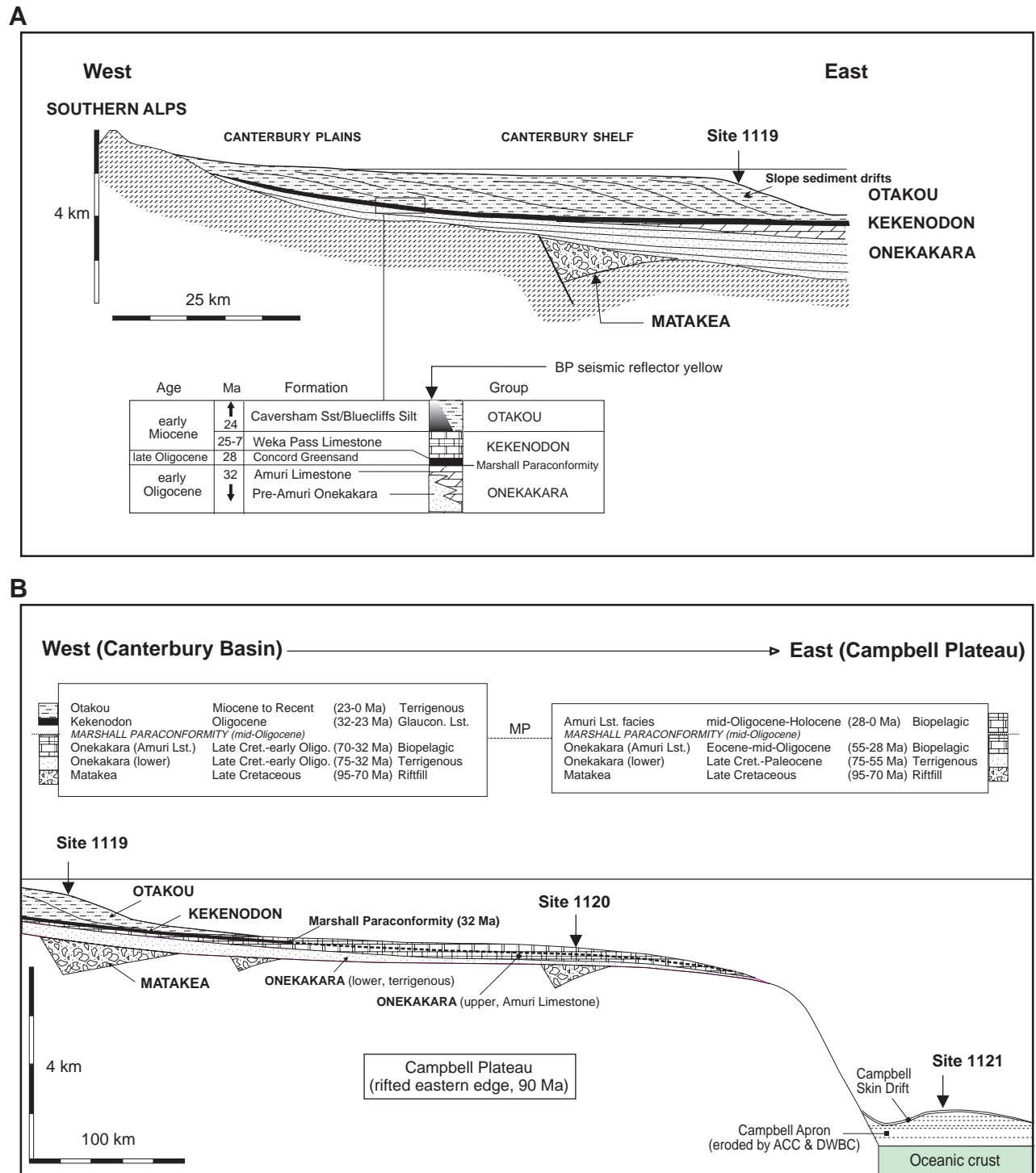


Figure F5. The Eastern New Zealand Oceanic Sedimentary System (ENZOSS), showing the location of the main areas of current scour, sediment supply, and drift deposition related to the ACC-DWBC (after Carter et al., 1996) KC = Kaikoura Canyon; HSZ = Hikurangi Subduction Zone.

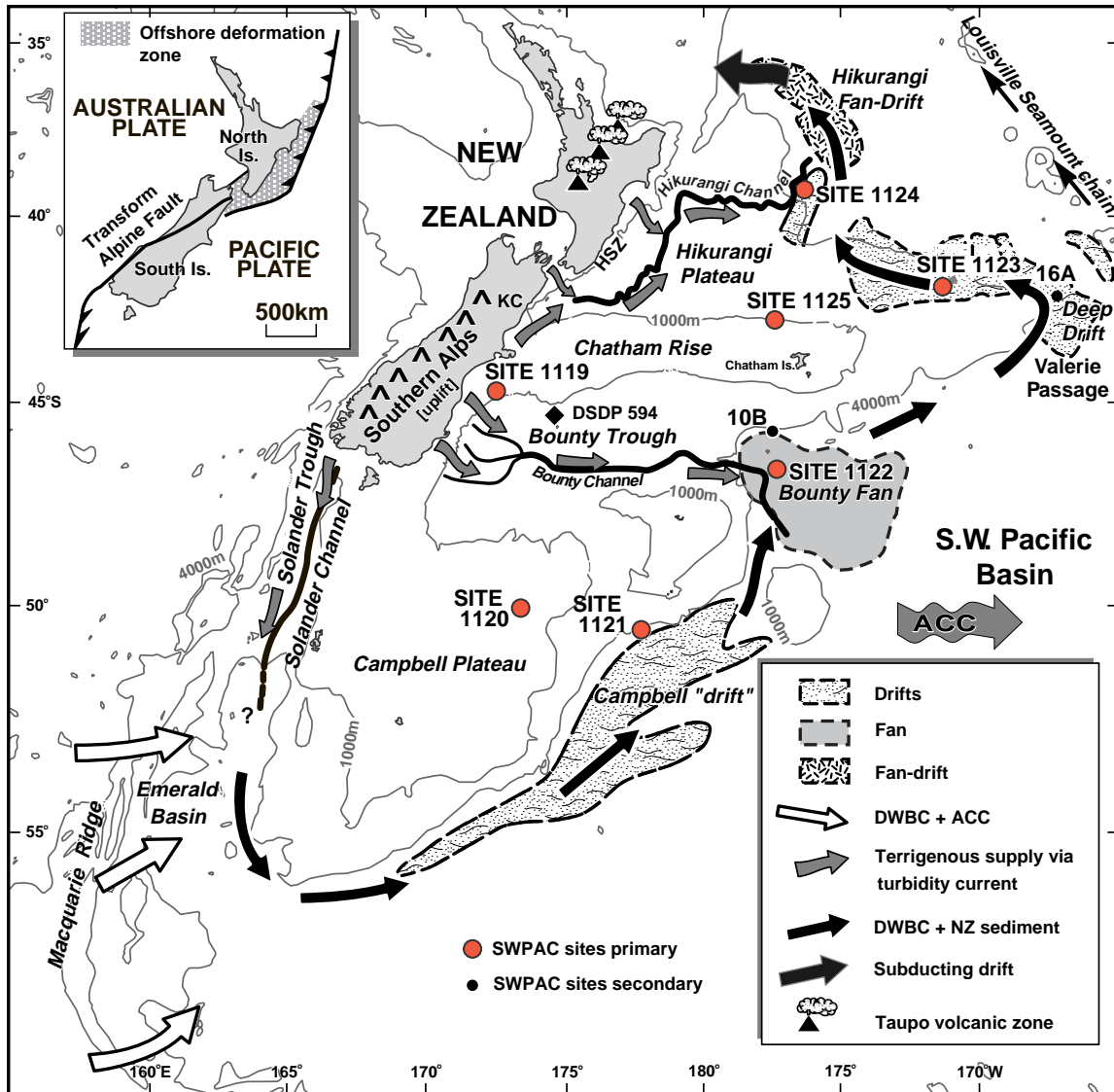
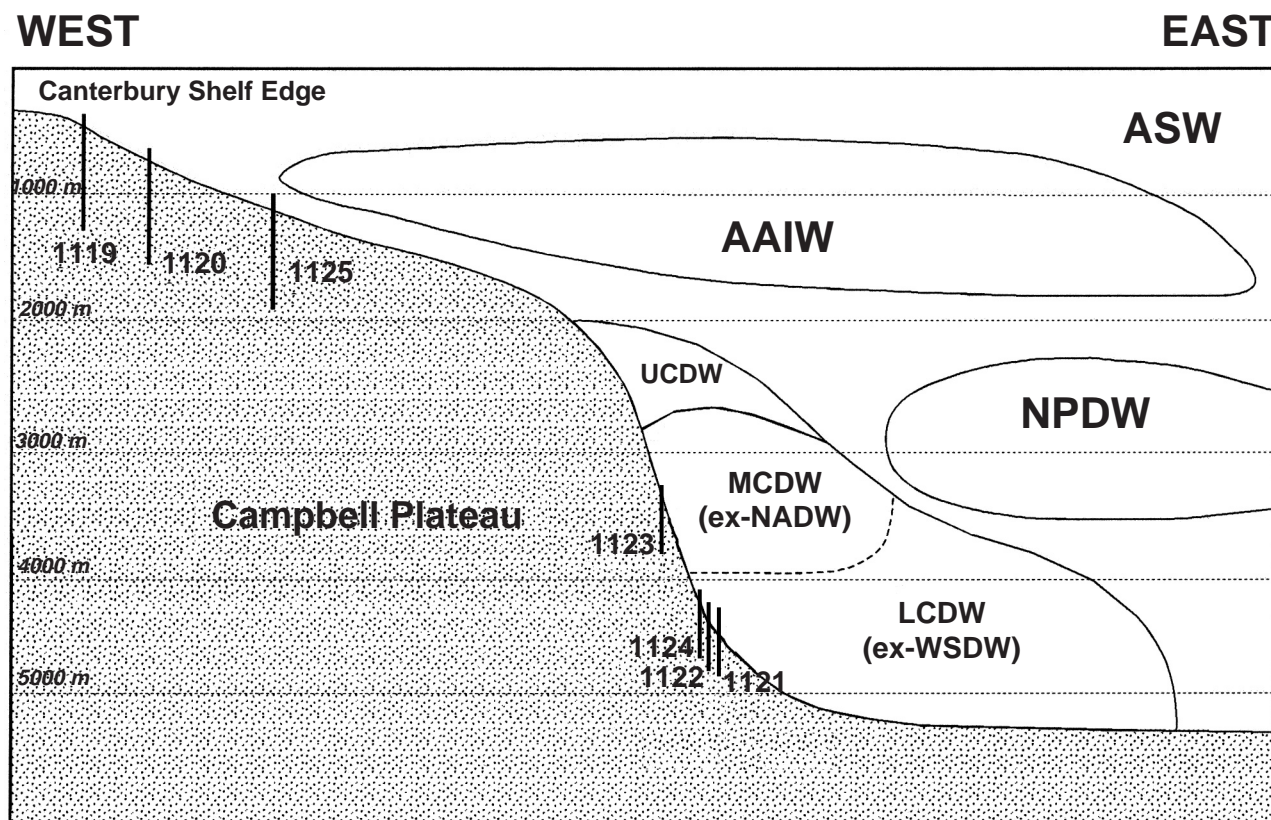
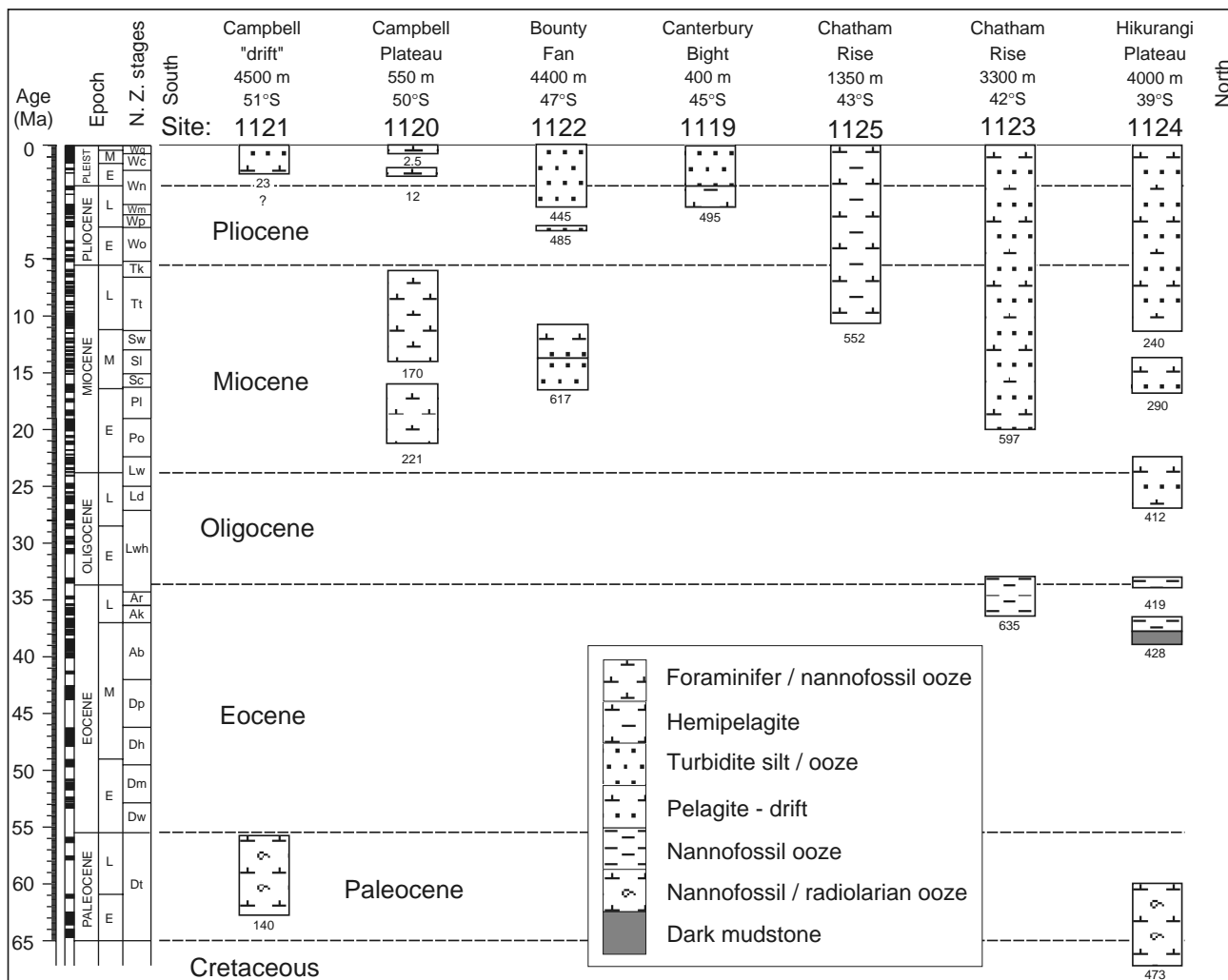




Figure F6. West to east cross section through the major water masses of the Southwest Pacific Ocean at about 45°S, with positions of ODP Leg 181 sites projected onto the plane of section. For abbreviations, see Figure F2C, p. 41.



**Figure F7.** Summary stratigraphy and sediment facies for all sites drilled during Leg 181, arranged broadly in latitudinal order. Small numbers at the base of each section indicate the thickness drilled, in meters, of the overlying section.



**Figure F8.** Summary thickness data, including position and duration of significant unconformities, for all available drill sites in the Southwest Pacific Ocean (DSDP Legs 29, 90; ODP Leg 181).

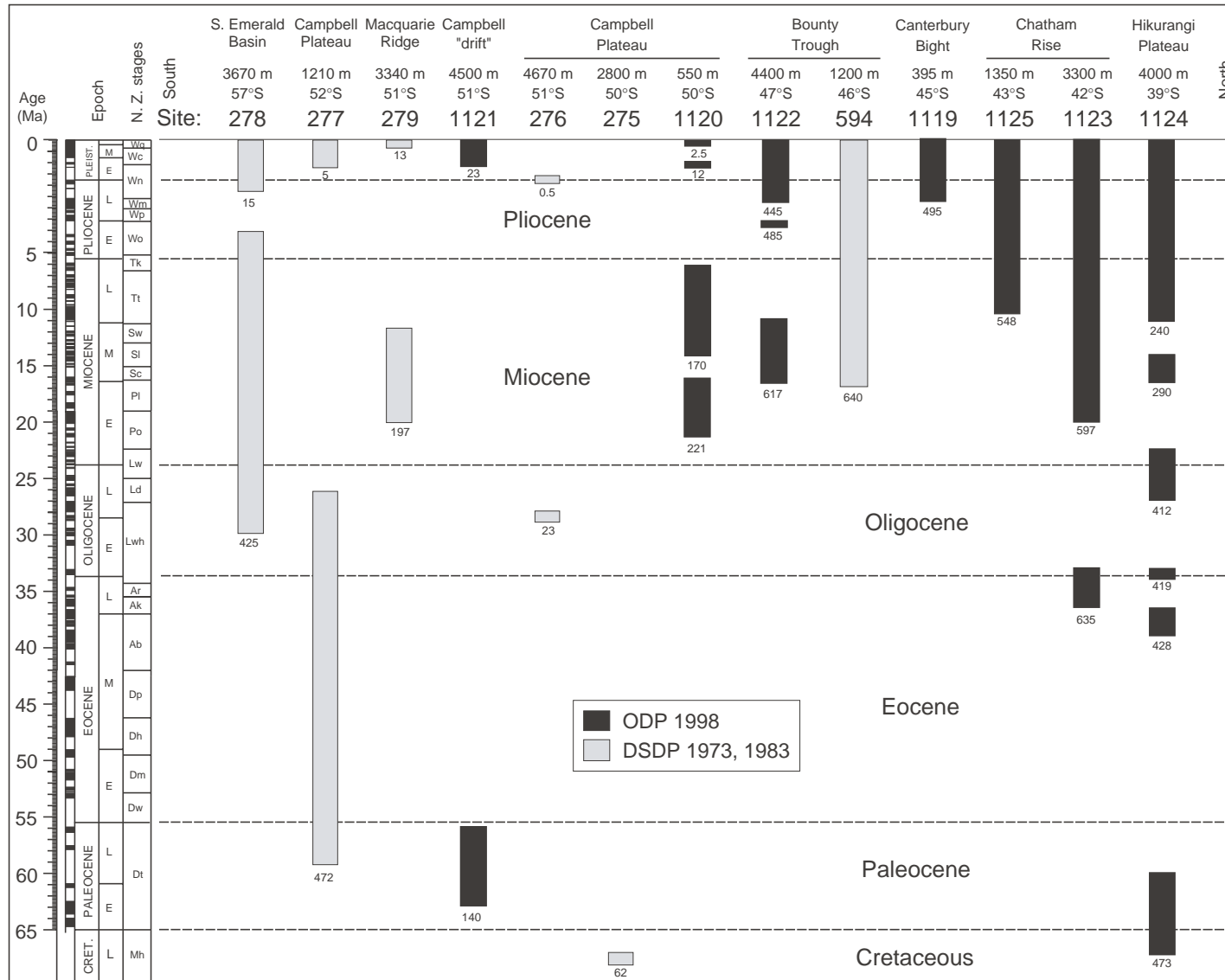
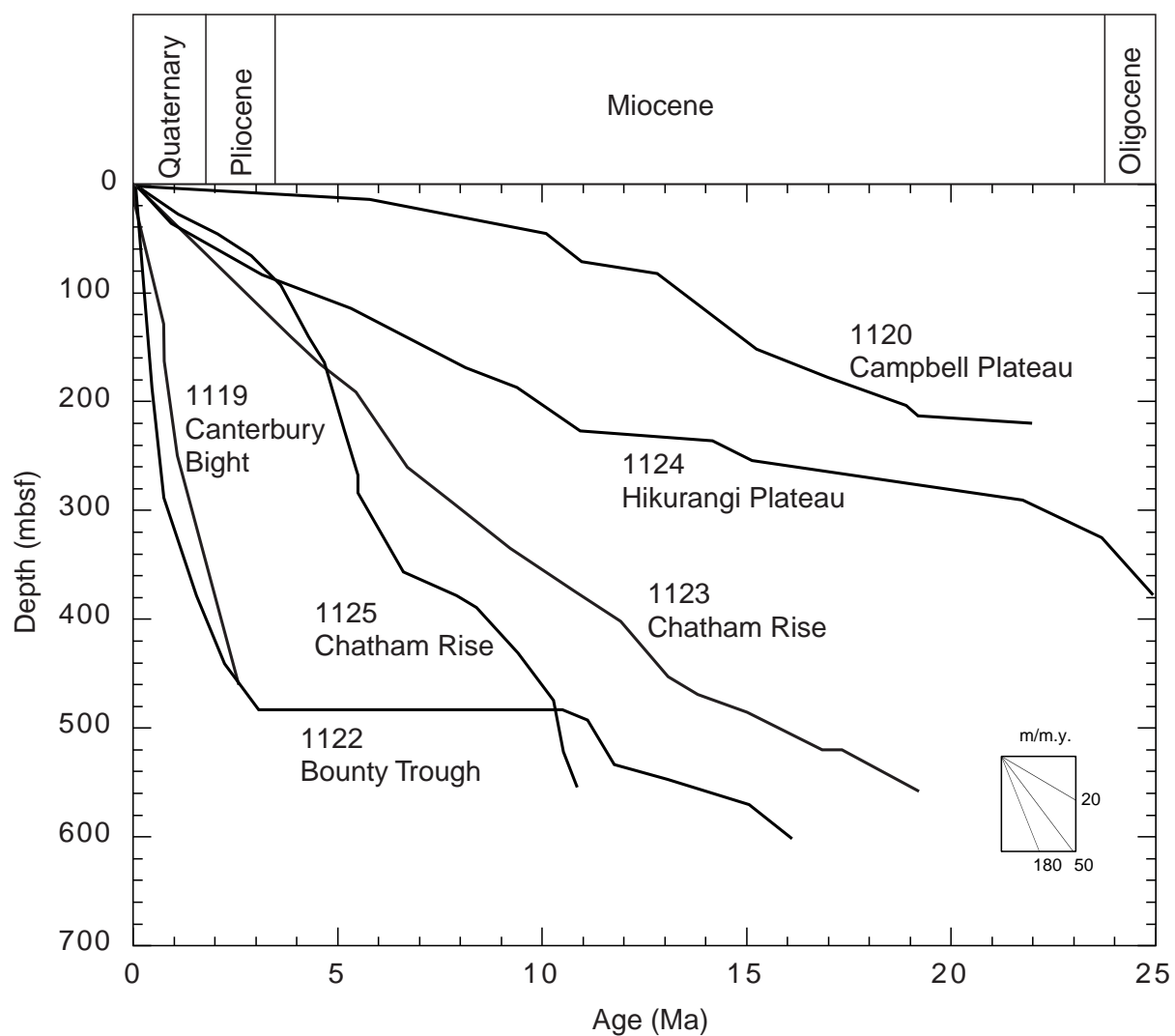


Figure F9. Sedimentation rate summary curves for all sites drilled during Leg 181.



**Figure F10.** Summary log for Site 1119. (Continued on next two pages.)

[illegible]

Figure F10 (continued).

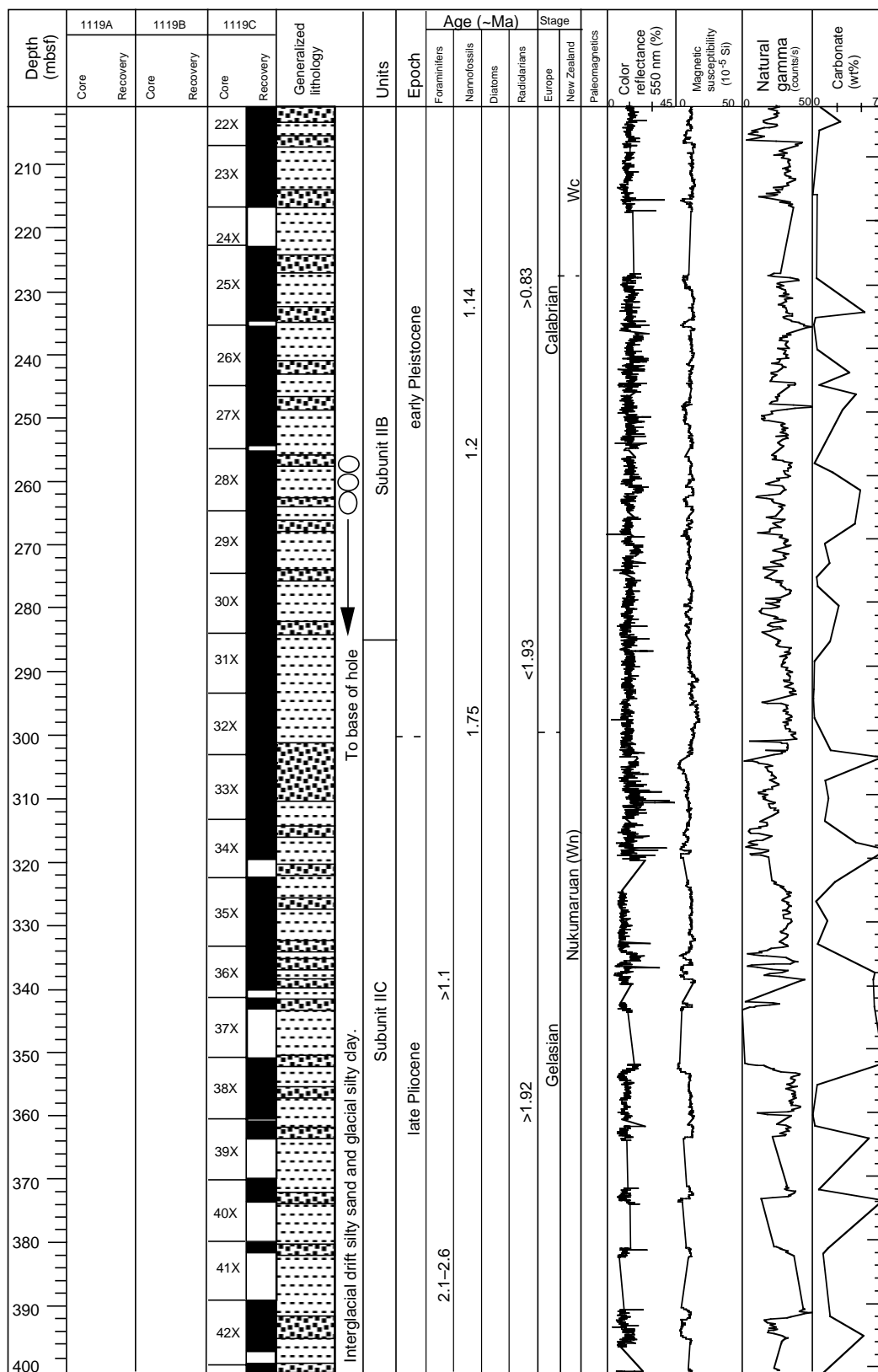
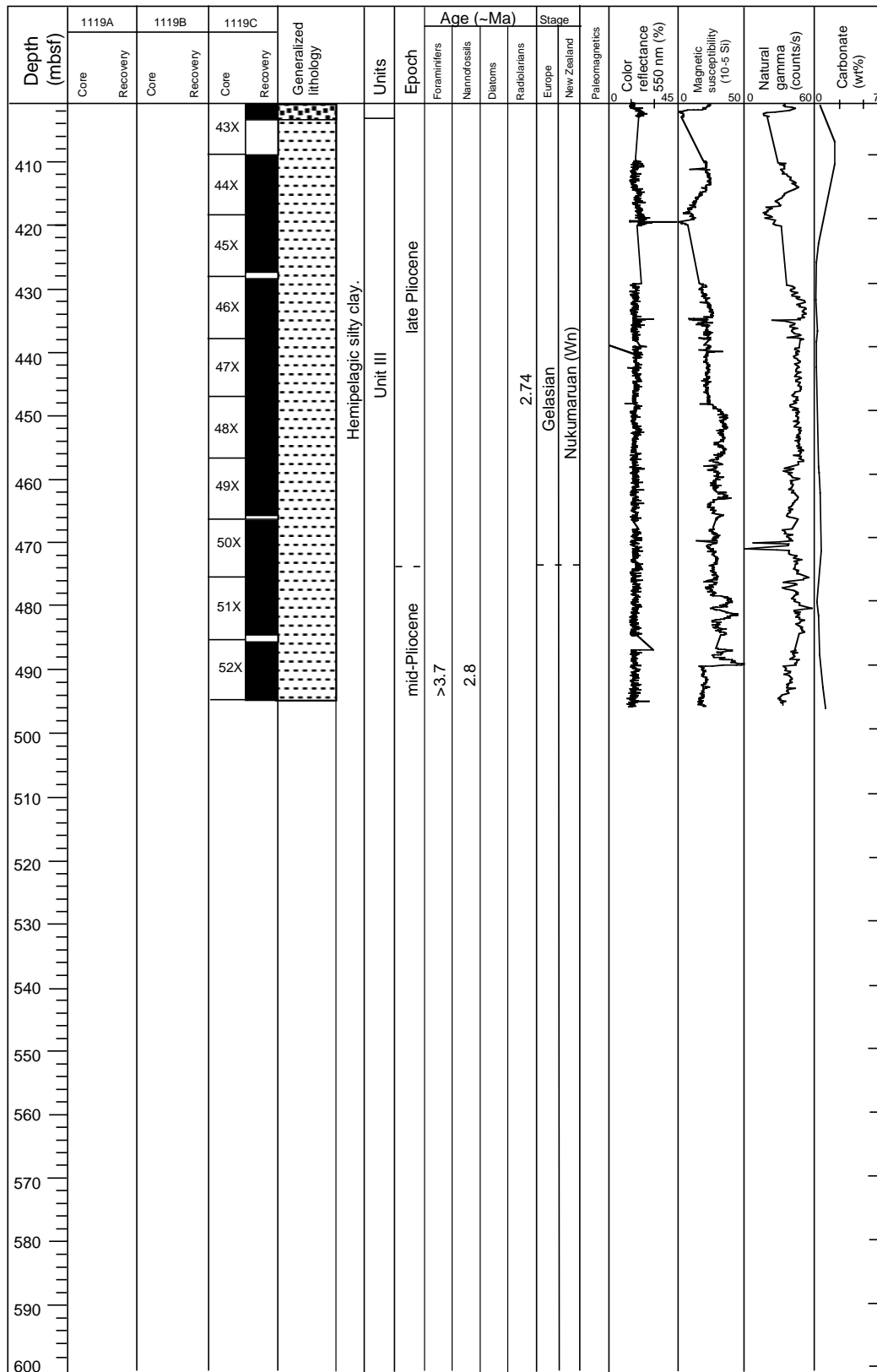




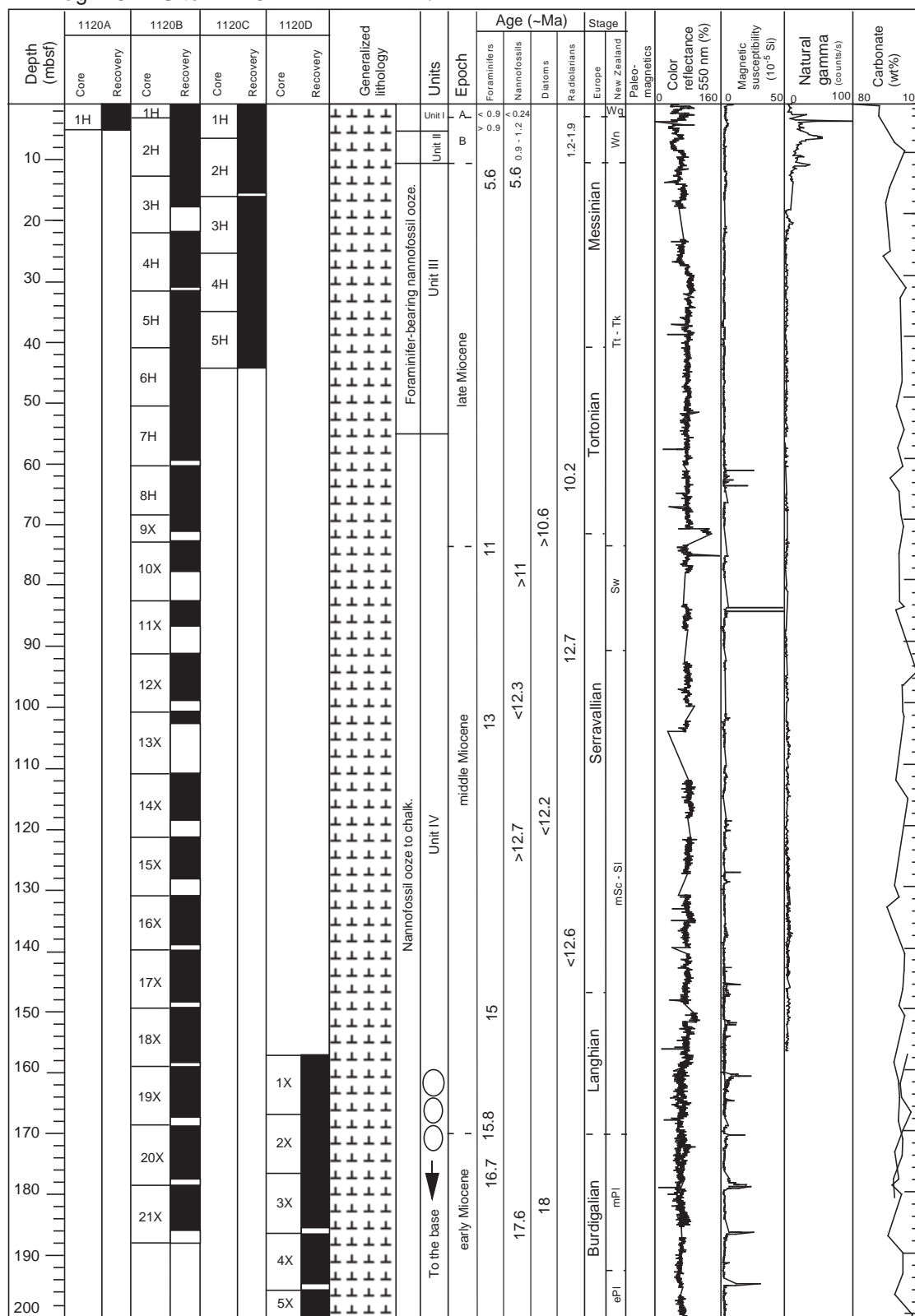
Figure F10 (continued).



## 52

Leg: 181    Site: 1120

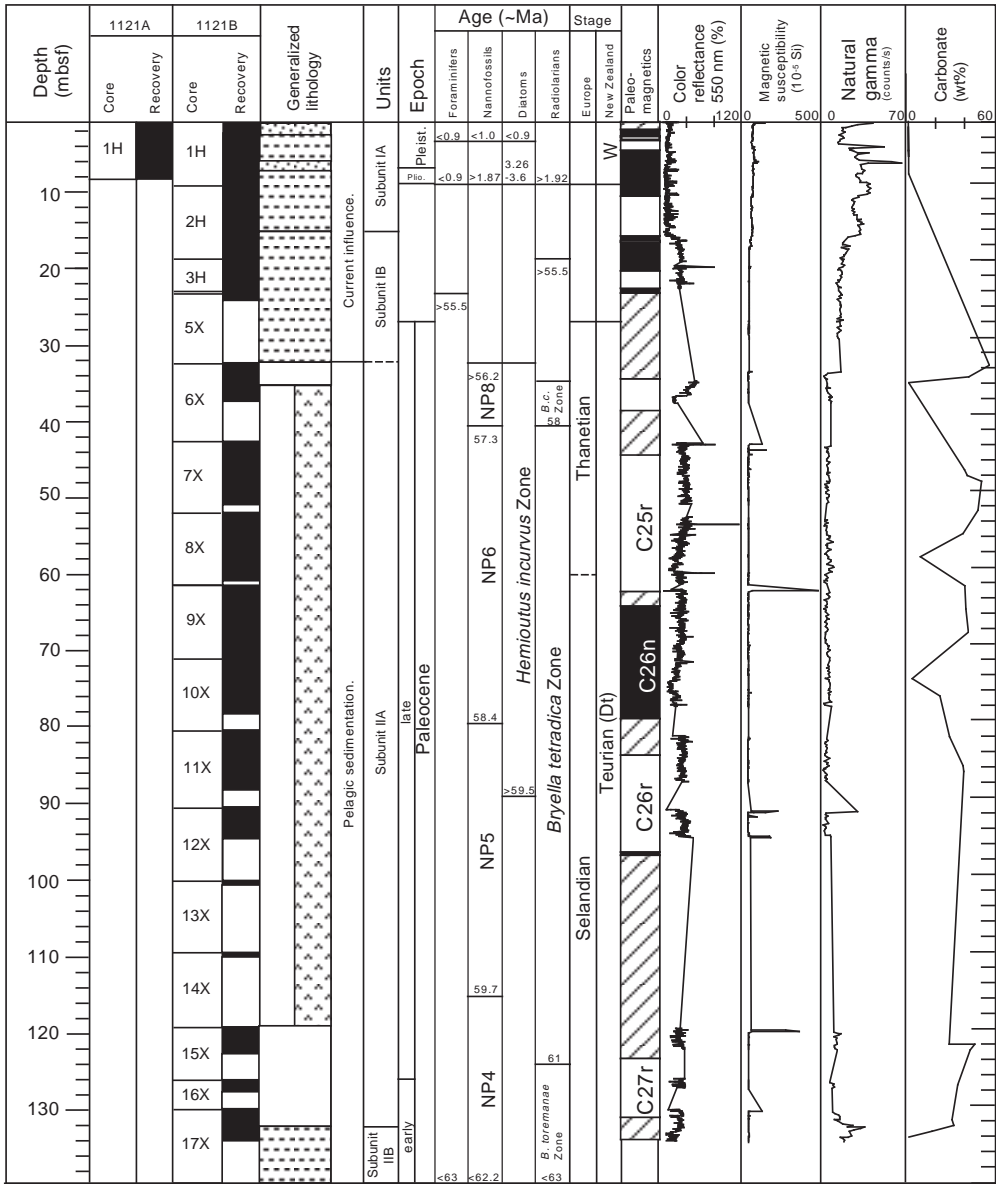
A = latest Pleistocene  
B = early Pleistocene



Depth (mbsf)	1120A		1120B		1120C		1120D		Generalized lithology	Units	Epoch	Age (~Ma)				Stage		Color reflectance	Magnetic susceptibility (10 <sup>-6</sup> SI)	Natural gamma (counts/s)	Carbonate (wt%)
	Core	Recovery	Core	Recovery	Core	Recovery	Core	Recovery				Foraminifers	Nannofossils	Diatoms	Radiolarians	Europe	New Zealand				
210							5X			Unit IV	early Miocene	19	< 21.6	19.2	Burdigalian	Po	ePI				
220						6X															
						7X															
						8X															
230						9X															

Figure F12. Summary log for Site 1121.

Leg: 181 Site: 1121



Leg: 181    Site: 1122

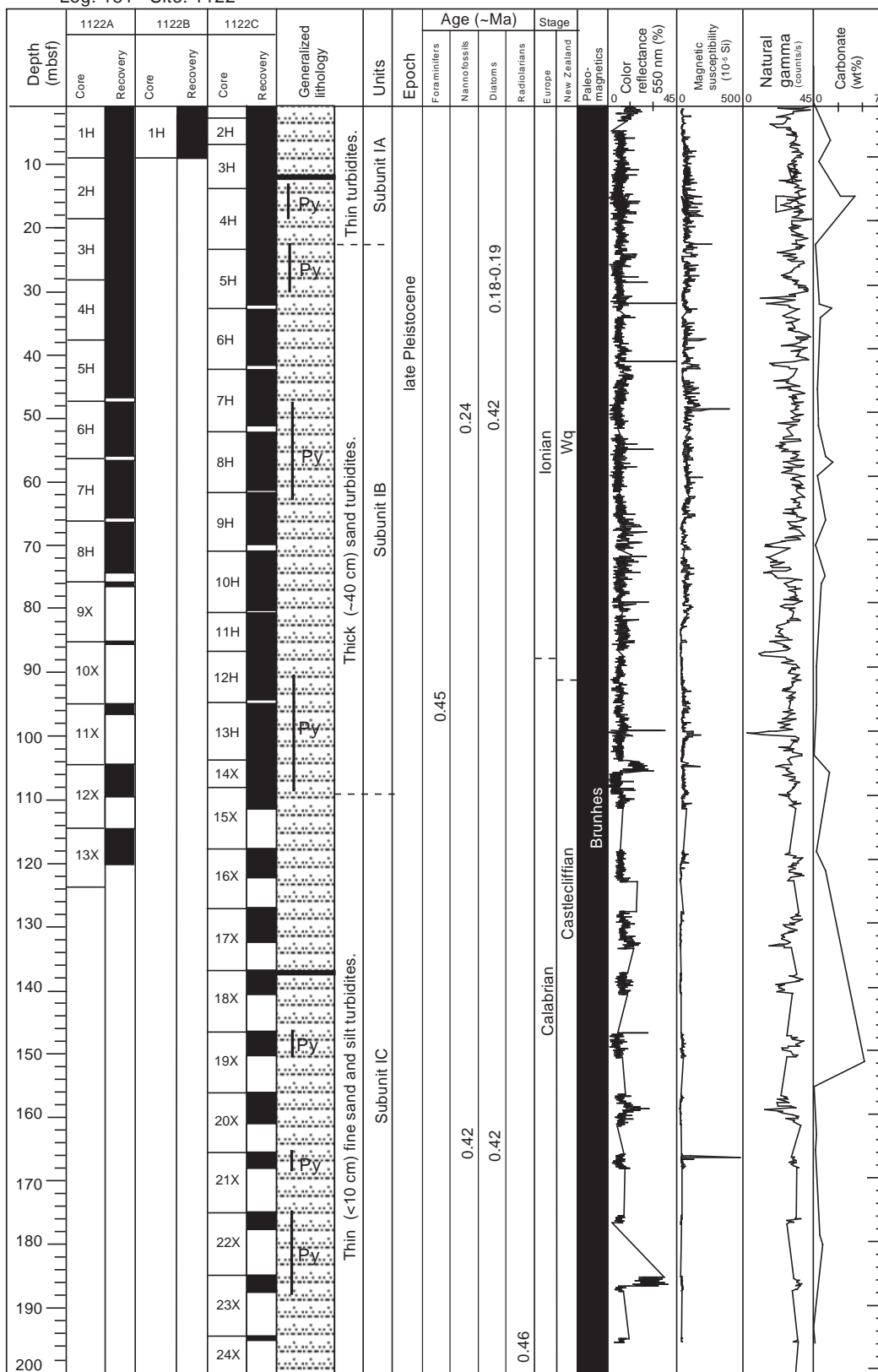
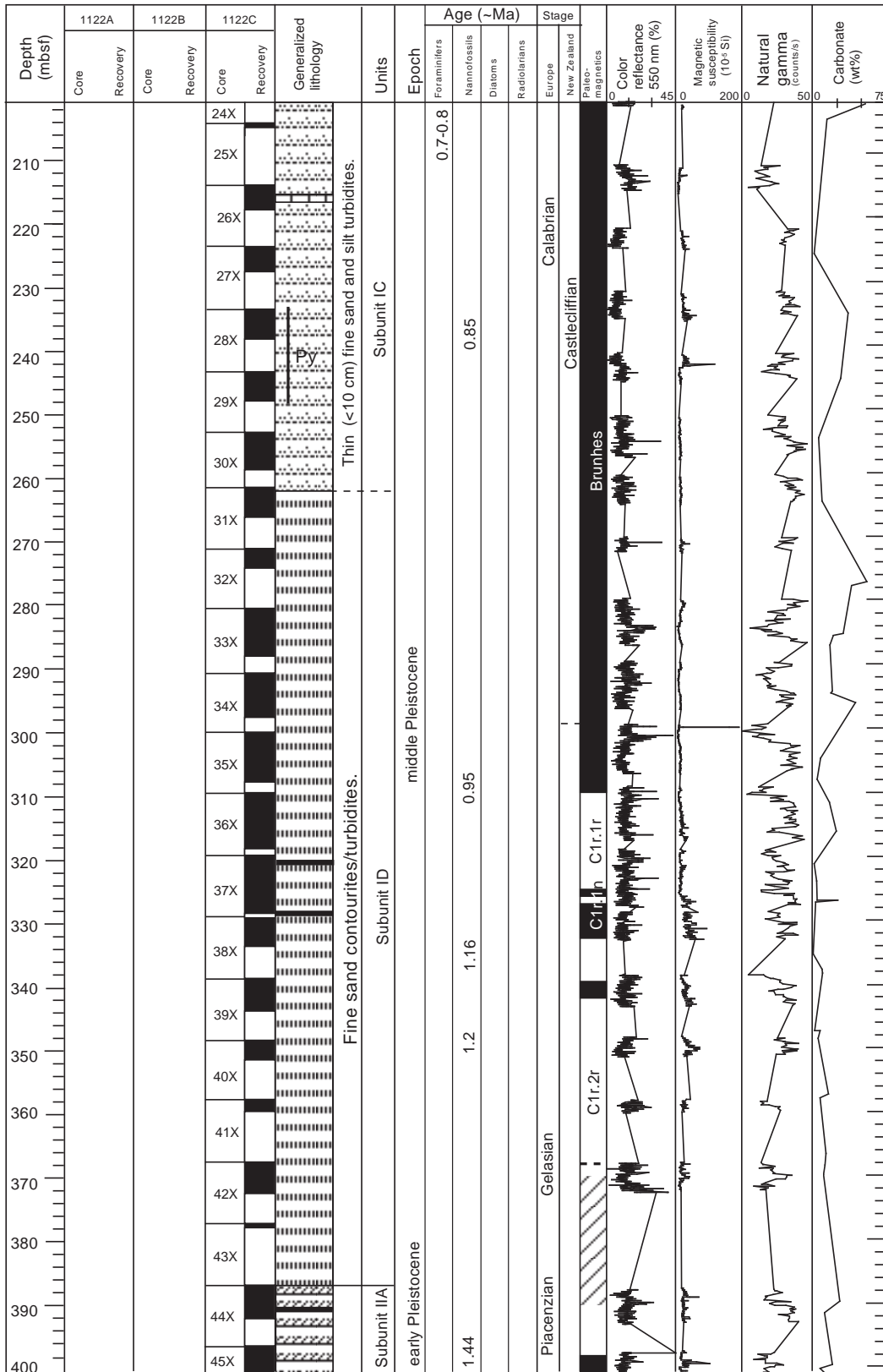
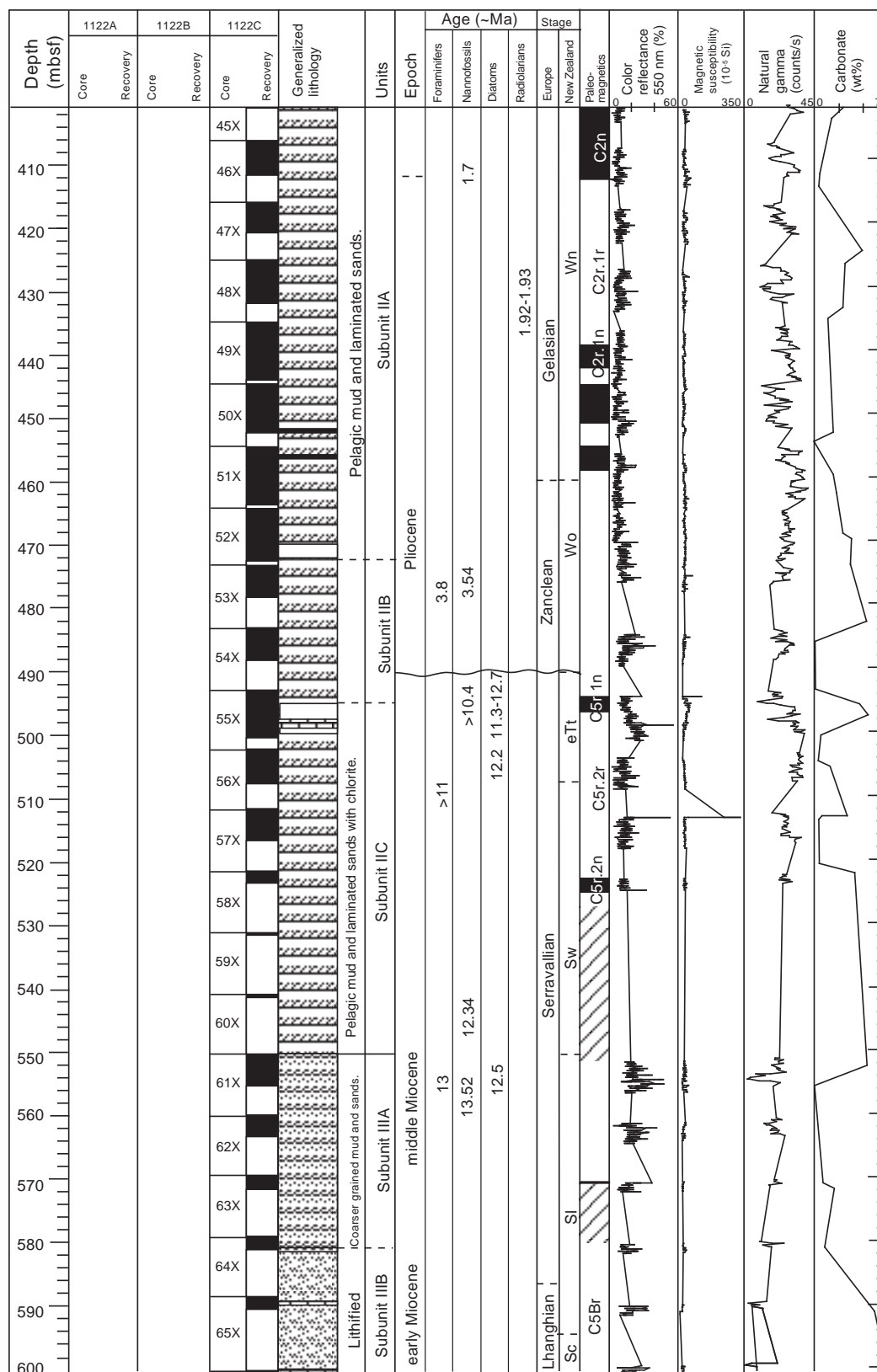


Figure F13 (continued).





**Figure F13 (continued).**




Depth (mbsf)	1122A		1122B		1122C		Generalized lithology
	Core	Recovery	Core	Recovery	Core	Recovery	
							
610							
620							
630							Lithified sediment / debris flows.
640							
650							
660							Subunit IIIB
670							
680							
690							early Miocene
700							
710							
720							16.7
730							
740							
750							<17.4
760							
770							
780							
790							
800							
							Age (~Ma)
							Stage
							Europe New Zealand Paleo-magnetics
							Color reflectance 550 nm (%)  Magnetic susceptibility (10 <sup>-5</sup> SI)  Natural gamma (counts/s)  Carbonate (wt%)

Figure F14. Summary log for Site 1123. (Continued on next three pages.)

Leg: 181 Site: 1123

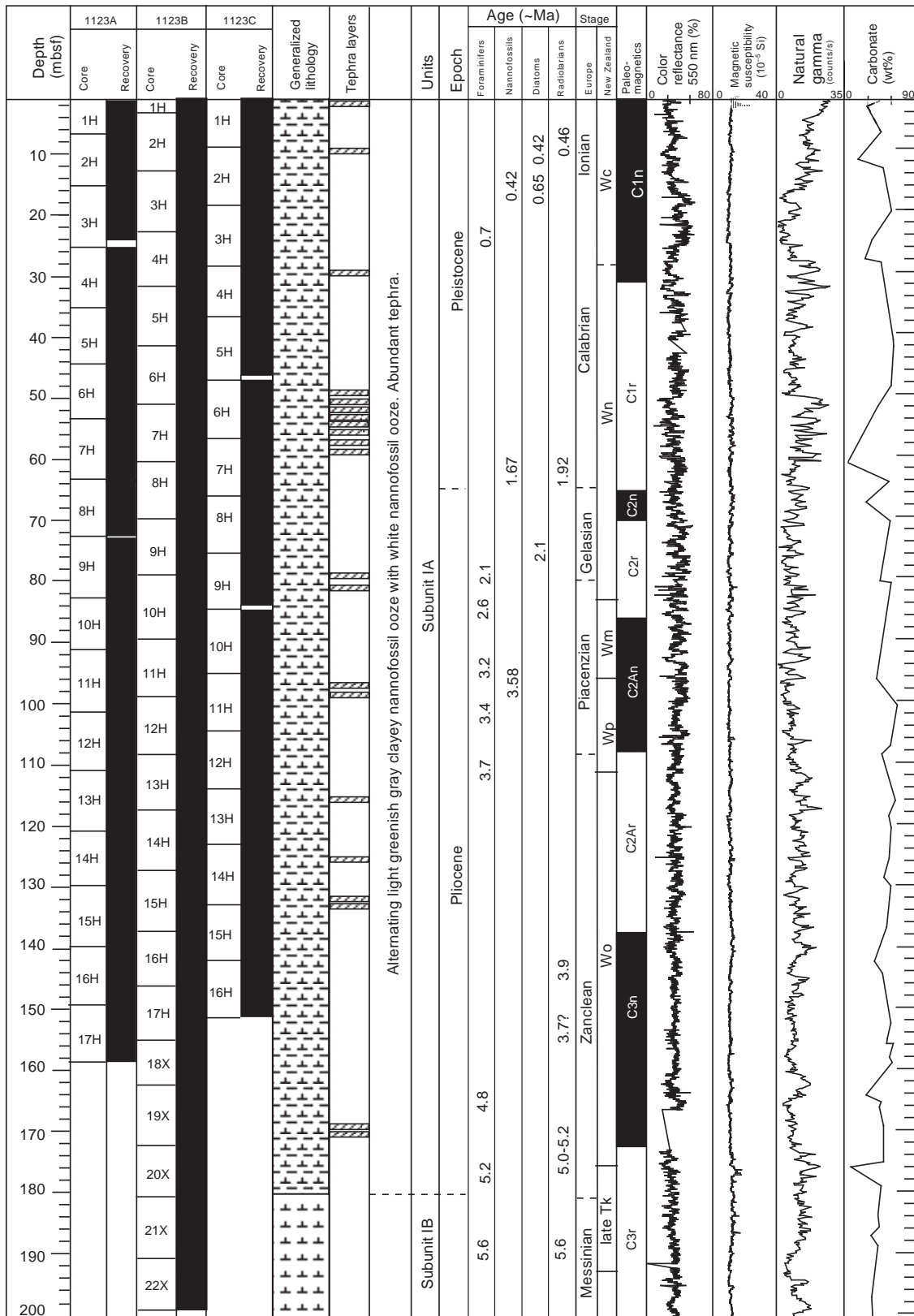
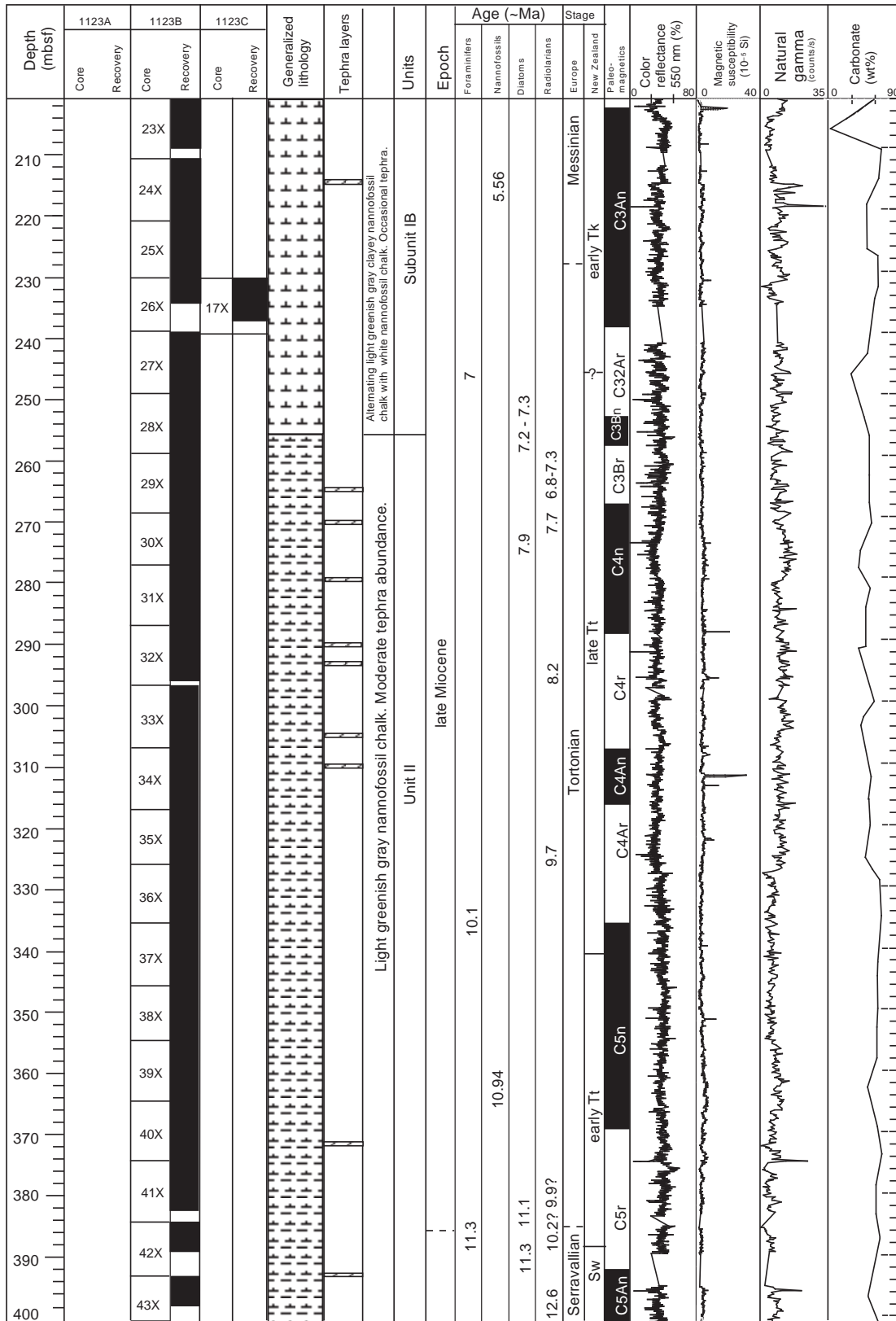
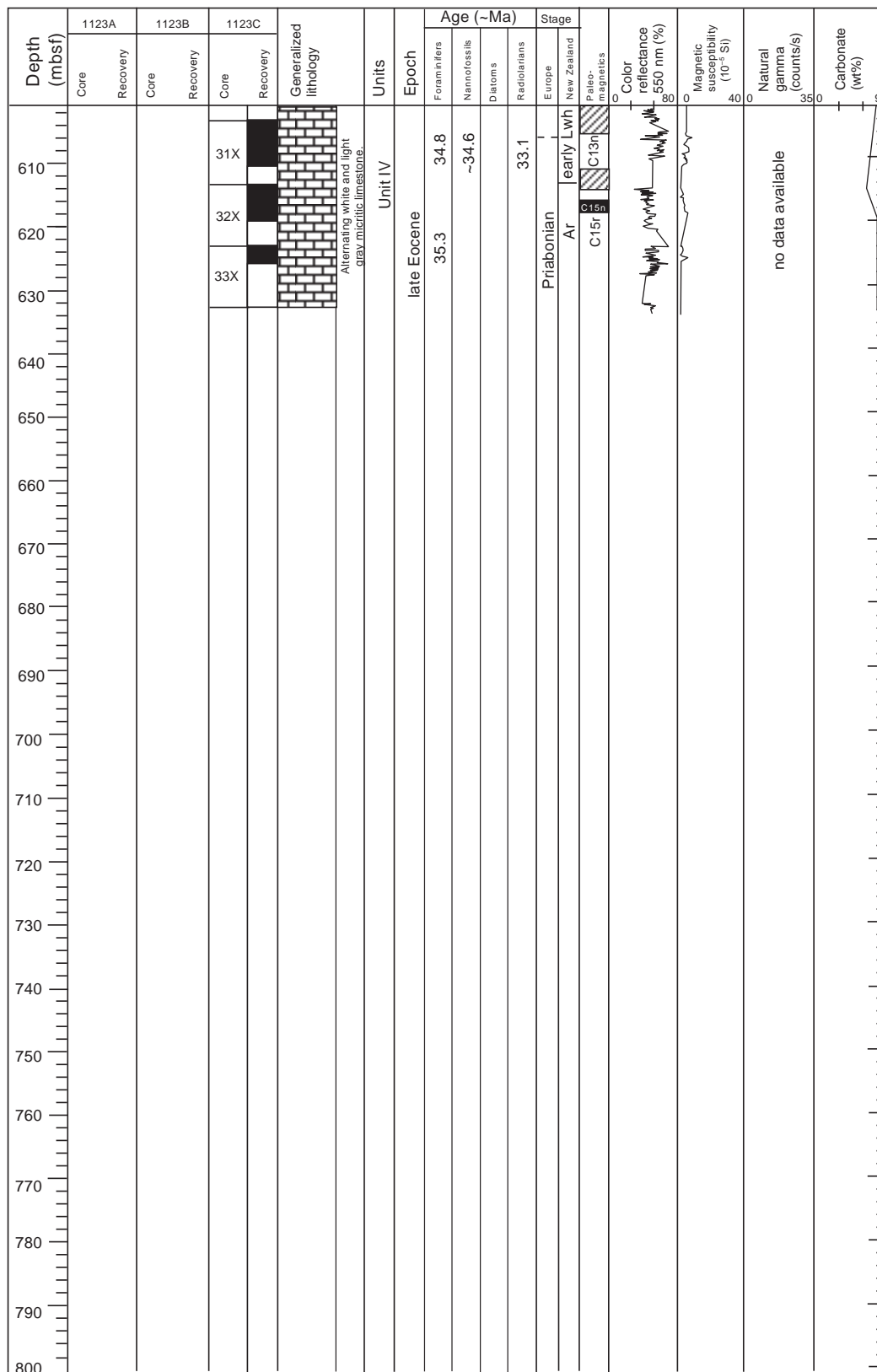


Figure F14 (continued).



Depth (mbsf)	1123A		1123B		1123C		Generalized lithology	Units	Epoch	Age (~Ma)	Stage	Paleo-magnetics	Color reflectance 550 nm (%)	Magnetic susceptibility (10 <sup>-3</sup> SI)	Natural gamma (counts/s)	Carbonate (wt%)
	Core	Recovery	Core	Recovery	Core	Recovery										
410			44X				Alternating greenish gray nanofossil mudstone with light greenish gray clayey nanofossil chalk.	Unit II	middle Miocene	13.0	Serravallian	Sw	C5Ar			
420			45X													
430			46X													
440			47X													
450			48X													
460			49X													
470			50X													
480			51X													
490			52X													
500					18X											
510					19X											
520					20X											
530					21X											
540					22X											
550					23X											
560					24X											
570					25X											
580					26X											
590					27X											
600					28X		Alternating white clay-bearing nanofossil chalk with light greenish gray clayey nanofossil chalk.	Subunit III C	early Miocene	18.6	Burdigalian	mid Pl	C5En			
					29X											
					30X											
							Alternating white clay-bearing nanofossil chalk with light greenish gray clayey nanofossil chalk.	Subunit III B	early Miocene	15.8	Langhian	late Sc	C5Br			
							Alternating white clay-bearing nanofossil chalk with light greenish gray clayey nanofossil chalk.	Subunit III A	early Miocene	15.52	Serravallian	SI	C5ABn			
							Alternating white clay-bearing nanofossil chalk with light greenish gray clayey nanofossil chalk.	Subunit III A	early Miocene	13.5	Serravallian	Sw	C5Ar			
							Alternating white clay-bearing nanofossil chalk with light greenish gray clayey nanofossil chalk.	Subunit III A	early Miocene	17.0	Langhian	late Sc	C5Bn			
							Alternating white clay-bearing nanofossil chalk with light greenish gray clayey nanofossil chalk.	Subunit III A	early Miocene	17.3	Langhian	late Pl	C5Dr			
							Alternating white clay-bearing nanofossil chalk with light greenish gray clayey nanofossil chalk.									

Figure F14 (continued).





Leg: 181    Site: 1124

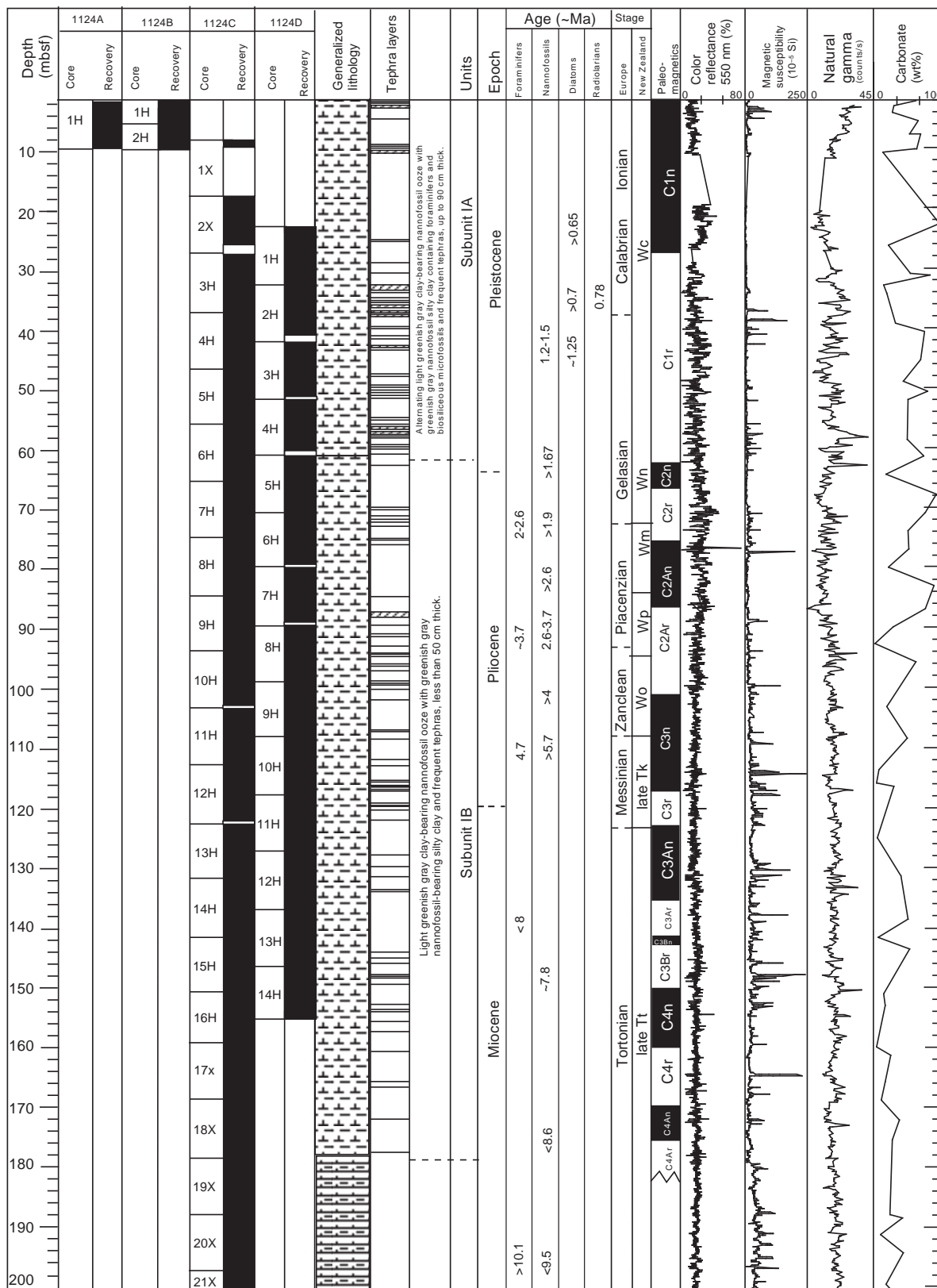


Figure F15 (continued).

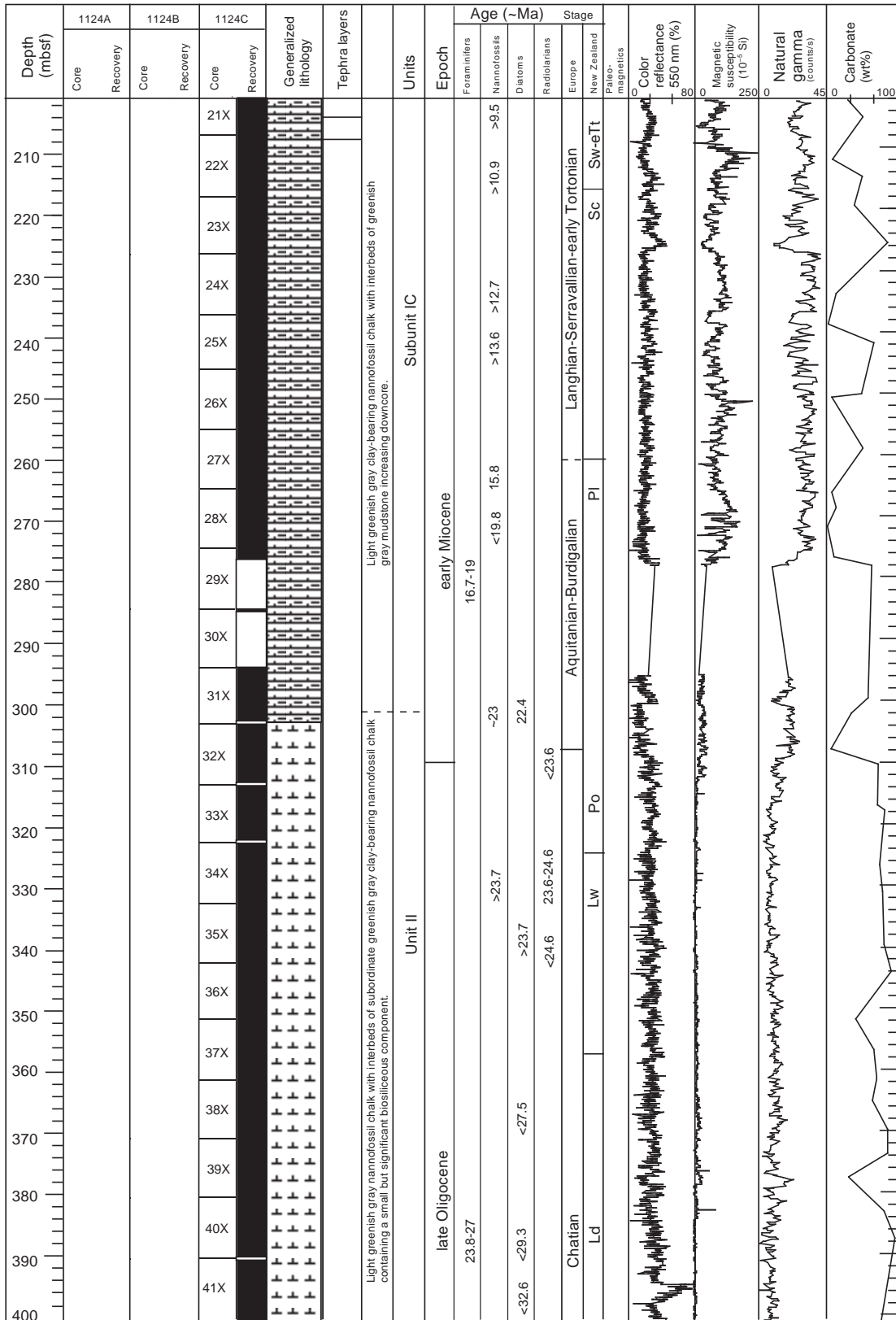


Figure F15 (continued).

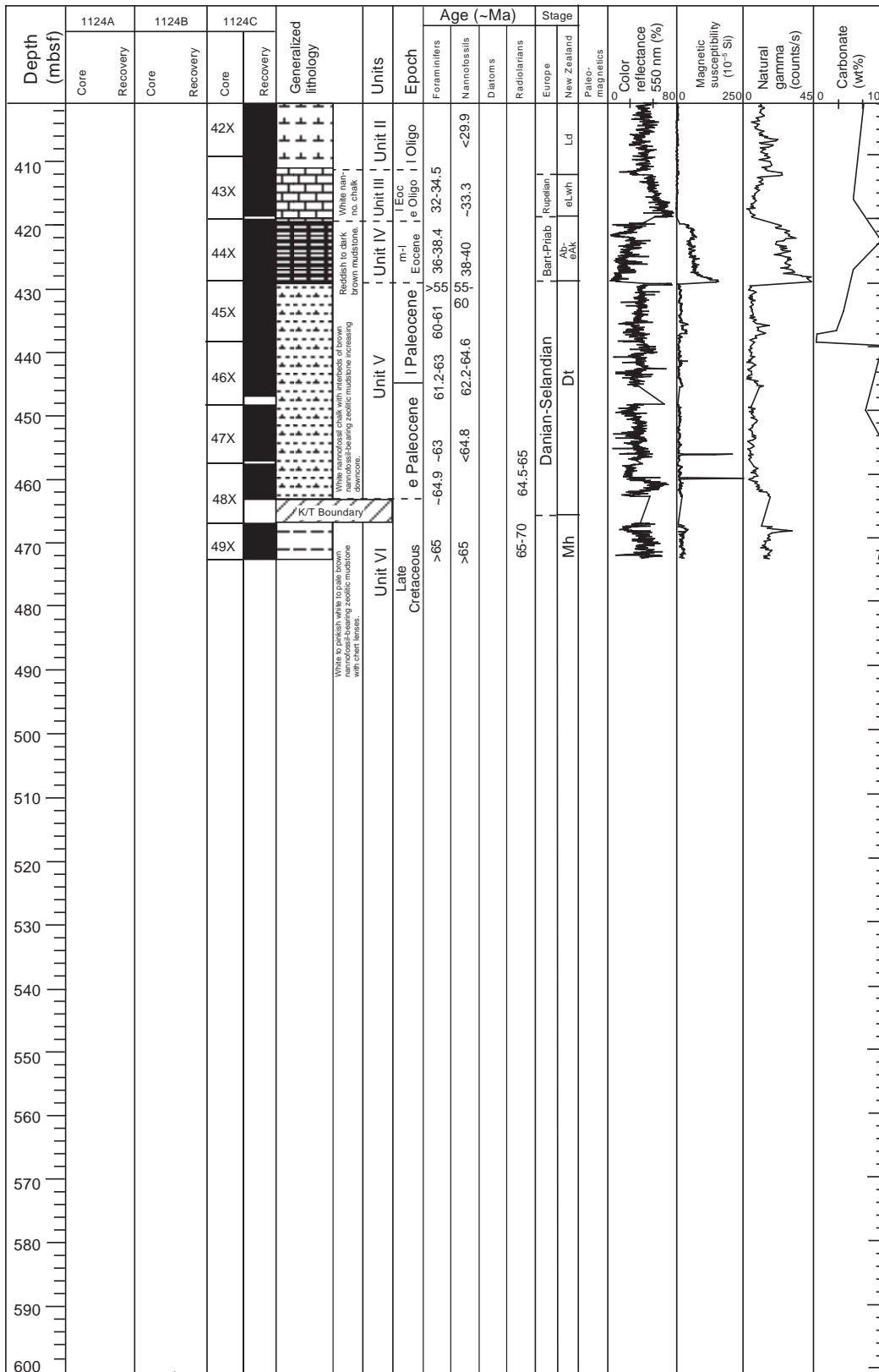


Figure F16. Summary log for Site 1125. (Continued on next two pages.)

Leg: 181 Site: 1125

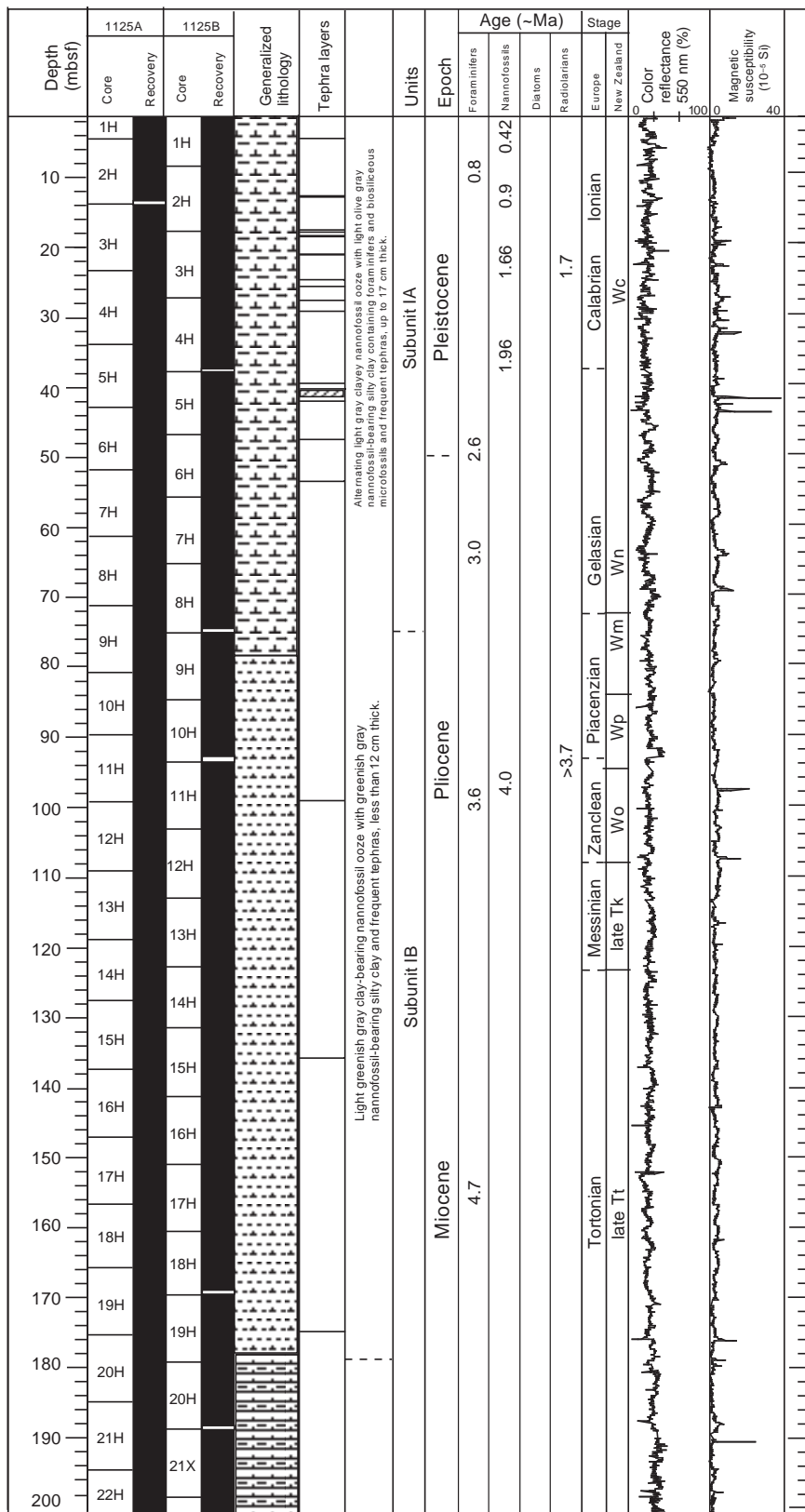


Figure F16 (continued).

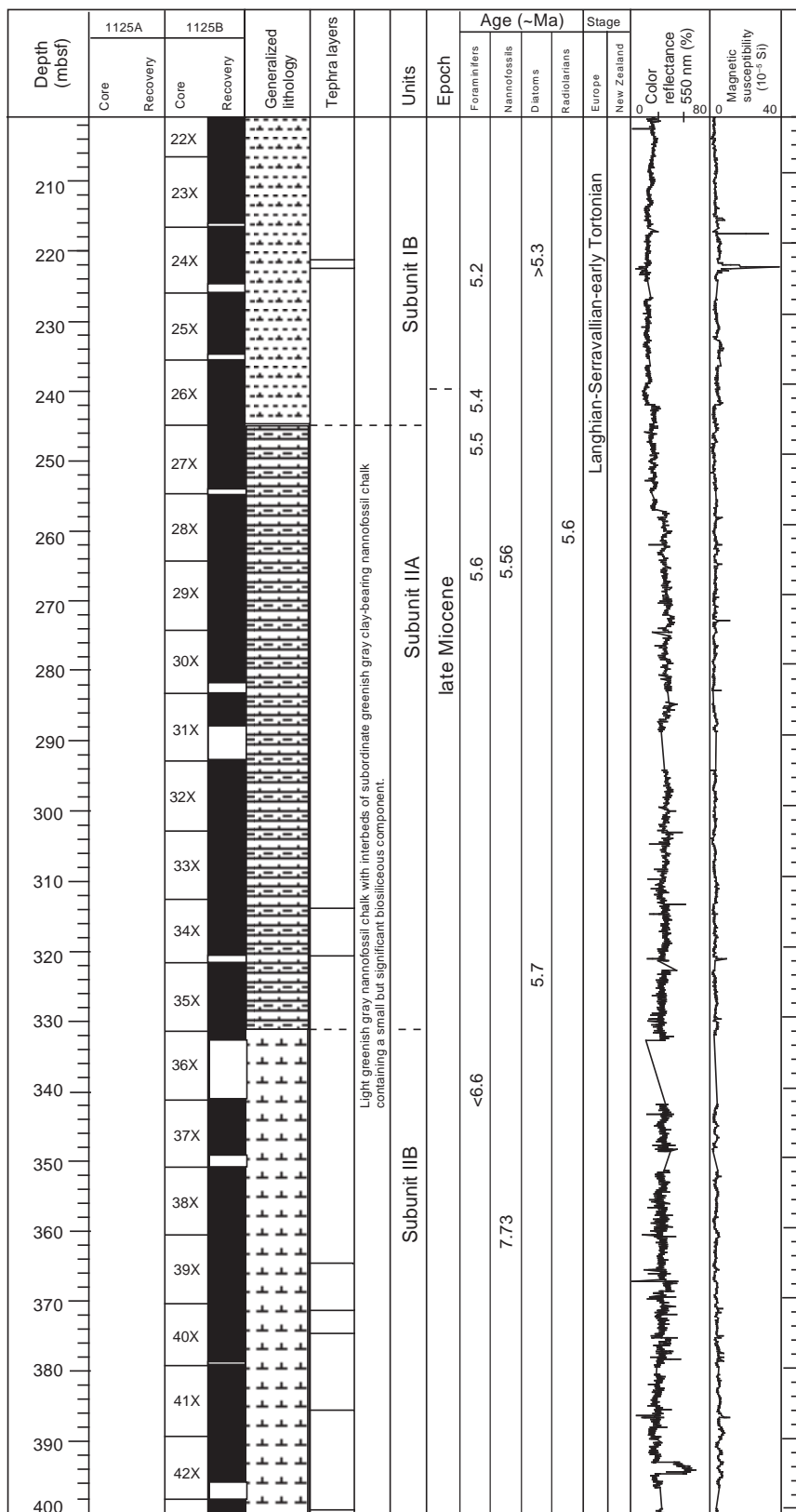
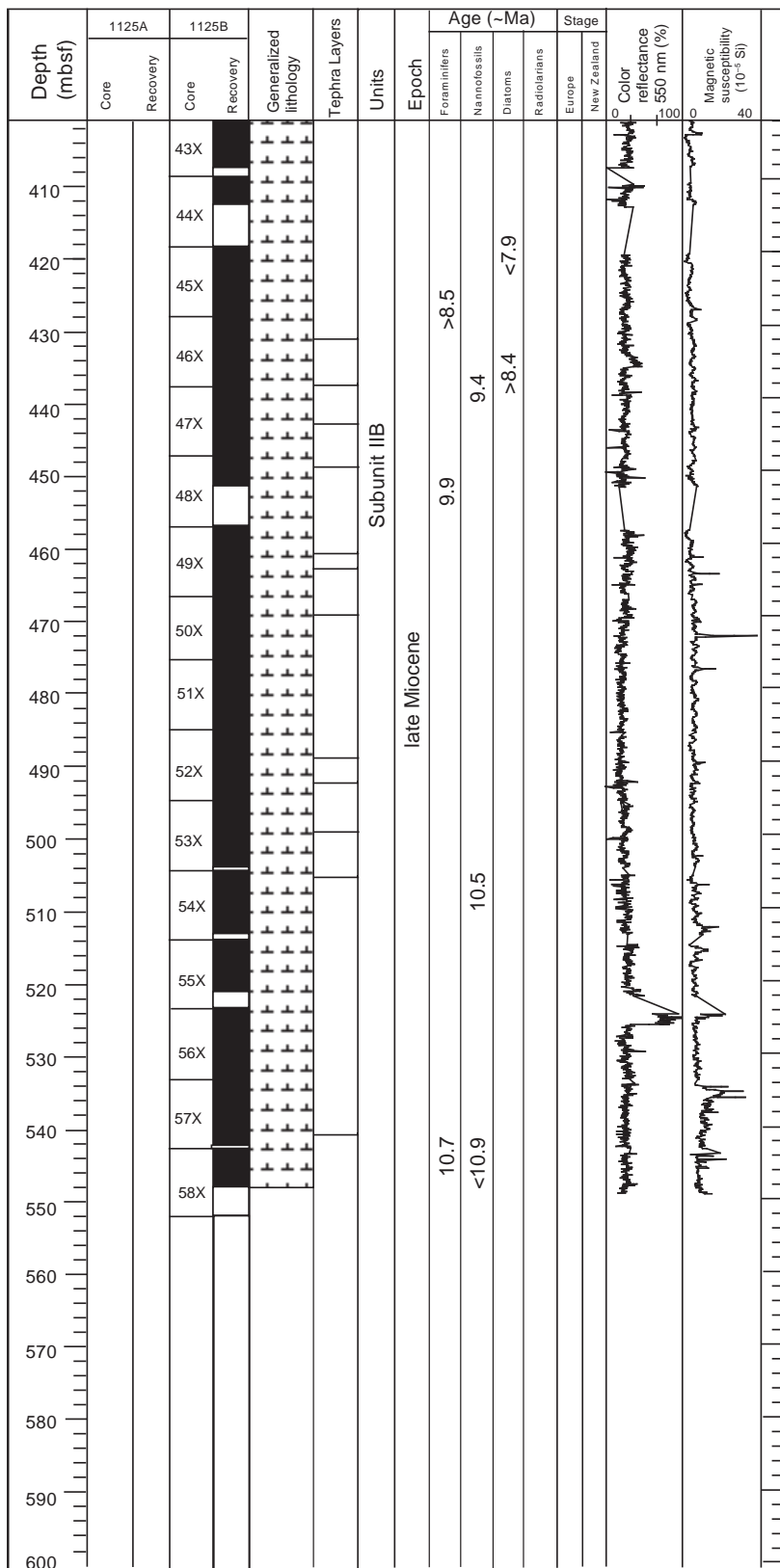


Figure F16 (continued).





**Table T1.** Site 1119 coring summary. (See table note. Continued on next page.)

Core number	Core type	Date (Aug 1998)	Time	Top depth (mbsf)	Bottom depth (mbsf)	Length cored (m)	Length recovered (m)	Recovery (%)
<b>181-119A-</b>								
1	H	23	1025	0.0	6.0	6.0	6.01	100.2
Cored totals:						6.0	6.01	100.17
Drilled:						0.0		
Total:						6.0		
<b>181-119B-</b>								
1	H	23	1055	0.0	4.7	4.7	4.73	100.6
2	H	23	1145	4.7	14.2	9.5	9.88	104.0
3	H	23	1320	14.2	23.7	9.5	10.09	106.2
4	H	23	1417	23.7	33.2	9.5	7.13	75.1
5	H	23	1445	33.2	42.7	9.5	10.27	108.1
6	H	23	1520	42.7	52.2	9.5	10.35	108.9
7	H	23	1600	52.2	61.7	9.5	10.37	109.2
8	H	23	1635	61.7	71.2	9.5	10.44	109.9
9	H	23	1710	71.2	80.7	9.5	10.35	108.9
10	H	23	1805	80.7	90.2	9.5	10.22	107.6
11	H	23	1840	90.2	99.7	9.5	10.24	107.8
12	H	23	1920	99.7	109.2	9.5	10.26	108.0
13	H	23	2005	109.2	118.7	9.5	10.51	110.6
14	H	23	2050	118.7	128.2	9.5	10.33	108.7
15	H	23	2120	128.2	137.7	9.5	10.35	108.9
16	H	23	2200	137.7	147.2	9.5	10.3	108.4
17	H	23	2245	147.2	155.8	8.6	8.65	100.6
Cored totals:						155.8	164.47	105.56
Drilled:						0.0		
Total:						155.8		
<b>181-1119C-</b>								
1	H	24	0105	0	8.3	8.3	8.27	99.6
2	H	24	0135	8.3	17.8	9.5	9.35	98.4
3	H	24	0215	17.8	27.3	9.5	10.08	106.1
4	H	24	0245	27.3	36.8	9.5	10.24	107.8
5	H	24	0315	36.8	46.3	9.5	10.32	108.6
6	H	24	0345	46.3	55.8	9.5	10.4	109.5
7	H	24	0415	55.8	65.3	9.5	10.67	112.3
8	H	24	0450	65.3	74.8	9.5	10.27	108.1
9	H	24	0525	74.8	84.3	9.5	10.48	110.3
10	H	24	0600	84.3	93.8	9.5	10.15	106.8
11	H	24	0630	93.8	103.3	9.5	10.5	110.5
12	H	24	0705	103.3	112.8	9.5	10.19	107.3
13	H	24	0745	112.8	122.3	9.5	10.31	108.5
14	H	24	0820	122.3	131.8	9.5	10.53	110.8
15	H	24	0900	131.8	141.3	9.5	10.28	108.2
16	H	24	0935	141.3	150.8	9.5	11.12	117.1
17	H	24	1020	150.8	160.3	9.5	10.41	109.6
18	X	24	1220	160.3	168.7	8.4	9.9	117.9
19	X	24	1315	168.7	178.3	9.6	7.97	83.0
20	X	24	1345	178.3	187.9	9.6	9.62	100.2
21	X	24	1425	187.9	197.6	9.7	8.67	89.4
22	X	24	1500	197.6	207.2	9.6	9.28	96.7
23	X	24	1530	207.2	216.8	9.6	10.0	104.2
24	X	24	1605	216.8	226.4	9.6	0.0	0.0
25	X	24	1640	226.4	236.0	9.6	9.35	97.4
26	X	24	1725	236.0	245.6	9.6	9.96	103.8
27	X	24	1755	245.6	255.2	9.6	9.08	94.6
28	X	24	1835	255.2	264.8	9.6	9.72	101.3
29	X	24	1915	264.8	274.5	9.7	9.67	99.7
30	X	24	1950	274.5	284.1	9.6	9.55	99.5
31	X	24	2035	284.1	293.8	9.7	9.68	99.8
32	X	24	2110	293.8	303.4	9.6	9.44	98.3
33	X	24	2145	303.4	313.0	9.6	9.48	98.8
34	X	24	2225	313.0	322.3	9.3	6.22	66.9
35	X	24	2255	322.3	331.9	9.6	9.71	101.1
36	X	24	2335	331.9	341.5	9.6	6.98	72.7
37	X	25	0030	341.5	351.1	9.6	1.76	18.3
38	X	25	0110	351.1	360.8	9.7	9.12	94.0
39	X	25	0155	360.8	370.5	9.7	2.69	27.7

**Table T1 (continued).**

Core number	Core type	Date (Aug 1998)	Time	Top depth (mbsf)	Bottom depth (mbsf)	Length cored (m)	Length recovered (m)	Recovery (%)
40	X	25	0240	370.5	380.1	9.6	3.06	31.9
41	X	25	0400	380.1	389.8	9.7	2.19	22.6
42	X	25	0530	389.8	399.4	9.6	6.54	68.1
43	X	25	0630	399.4	409.0	9.6	3.24	33.8
44	X	25	0740	409.0	418.6	9.6	9.9	103.1
45	X	25	0900	418.6	428.2	9.6	0.82	8.5
46	X	25	1045	428.2	437.9	9.7	9.62	99.2
47	X	25	1205	437.9	447.2	9.3	9.62	103.4
48	X	25	1330	447.2	456.8	9.6	9.8	102.1
49	X	25	1500	456.8	466.4	9.6	8.77	91.4
50	X	25	1640	466.4	475.6	9.2	9.67	105.1
51	X	25	1800	475.6	485.2	9.6	8.06	84.0
52	X	25	1945	485.2	494.8	9.6	9.52	99.2
Cored totals:						494.8	442.23	89.38
Drilled:						0.0		
Total:						494.8		

Note: This table is also available in [ASCII format](#).

**Table T2.** Site 1120 coring summary.

Core number	Core type	Date (1998)	Time	Top depth (mbsf)	Bottom depth (mbsf)	Length cored (m)	Length recovered (m)	Recovery (%)
<b>181-1120A-</b>								
1	H	28 Aug	0555	0.0	4.6	4.6	4.6	100
Cored totals:						4.6	4.6	100.00
Drilled:						0.0		
Total:						4.6		
<b>181-1120B-</b>								
1	H	28 Aug	0655	0.0	3.3	3.3	3.36	101.80
2	H	28 Aug	0730	3.3	12.8	9.5	9.58	100.80
3	H	28 Aug	0800	12.8	22.3	9.5	4.90	51.60
4	H	28 Aug	0835	22.3	31.8	9.5	9.26	97.50
5	H	28 Aug	0910	31.8	41.3	9.5	9.64	101.50
6	H	28 Aug	1005	41.3	50.8	9.5	9.78	102.90
7	H	28 Aug	1035	50.8	60.3	9.5	8.66	91.20
8	H	28 Aug	1135	60.3	68.3	8.0	8.03	100.40
9	X	28 Aug	1235	68.3	72.6	4.3	2.57	59.80
10	X	28 Aug	1310	72.6	82.2	9.6	4.86	50.60
11	X	28 Aug	1340	82.2	91.8	9.6	4.45	46.40
12	X	28 Aug	1410	91.8	101.4	9.6	7.40	77.10
13	X	28 Aug	1440	101.4	111.0	9.6	2.21	23.00
14	X	28 Aug	1510	111.0	120.6	9.6	6.56	68.30
15	X	28 Aug	1545	120.6	130.1	9.5	6.28	66.10
16	X	28 Aug	1610	130.1	139.8	9.7	8.73	90.00
17	X	28 Aug	1640	139.8	149.4	9.6	8.49	88.40
18	X	28 Aug	1710	149.4	159.0	9.6	9.23	96.10
19	X	28 Aug	1735	159.0	168.7	9.7	7.93	81.80
20	X	28 Aug	1800	168.7	178.4	9.7	8.44	87.00
21	X	28 Aug	1835	178.4	188.0	9.6	6.15	64.10
Cored totals:						188.0	146.51	77.93
Drilled:						0.0		
Total:						188.0		
<b>181-1120C-</b>								
1	H	30 Aug	300	0.0	6.6	6.6	6.59	99.8
2	H	30 Aug	345	6.6	16.1	9.5	9.12	96.0
3	H	30 Aug	415	16.1	25.6	9.5	9.51	100.1
4	H	30 Aug	455	25.6	35.1	9.5	9.95	104.7
5	H	30 Aug	1055	35.1	44.6	9.5	9.78	102.9
Cored totals:						44.6	44.95	100.78
Drilled:						0.0		
Total:						44.6		
<b>181-1120D-</b>								
1	O	31 Aug	2045	0.0	157.4	0.0	0.0	N/A
1	X	31 Aug	2125	157.4	167.0	9.6	9.63	100.3
2	X	31 Aug	2155	167.0	176.7	9.7	9.73	100.3
3	X	31 Aug	2225	176.7	186.3	9.6	8.28	86.3
4	X	31 Aug	2255	186.3	195.9	9.6	8.48	88.3
5	X	31 Aug	2320	195.9	205.5	9.6	7.77	80.9
6	X	31 Aug	2359	205.5	210.1	4.6	8.72	189.6
7	X	1 Sept	0035	210.1	215.1	5.0	3.55	71.0
8	X	1 Sept	0110	215.1	218.7	3.6	6.75	187.5
9	X	1 Sept	0140	218.7	220.7	2.0	3.26	163.0
Cored totals:						63.3	66.17	104.53
Drilled:						157.4		
Total:						220.7		

Note: This table is also available in [ASCII format](#).

**Table T3.** Site 1121 coring summary.

Core number	Core type	Date (Sept 1998)	Time	Top depth (mbsf)	Bottom depth (mbsf)	Length cored (m)	Length recovered (m)	Recovery (%)
181-1121A-								
1	H	2	1620	0.0	8.4	8.4	8.37	99.6
Cored totals:						8.4	8.37	99.64
Drilled:						0.0		
Total:						8.4		
181-1121B-								
1	H	2	1740	0.0	9.5	9.5	9.92	104.4
2	H	2	1855	9.5	19.0	9.5	9.93	104.5
3	H	2	2025	19.0	23.0	4.0	9.83	245.8
4	X	2	2240	23.0	23.5	0.5	0.28	56.0
5	X	3	0040	23.5	32.7	9.2	0.27	2.9
6	X	3	0150	32.7	42.3	9.6	4.58	47.7
7	X	3	0255	42.3	52.0	9.7	8.35	86.1
8	X	3	0400	52.0	61.6	9.6	9.06	94.4
9	X	3	0455	61.6	71.2	9.6	9.68	100.8
10	X	3	0620	71.2	80.9	9.7	6.18	63.7
11	X	3	0740	80.9	90.5	9.6	6.32	65.8
12	X	3	1045	90.5	100.1	9.6	3.81	39.7
13	X	3	1300	100.1	109.7	9.6	0.39	4.1
14	X	3	1530	109.7	119.4	9.7	0.56	5.8
15	X	3	1745	119.4	126.0	6.6	2.93	44.4
16	X	3	2000	126.0	130.0	4.0	1.30	32.5
17	X	3	2355	130.0	139.7	9.7	4.47	46.1
Cored totals:						139.7	87.86	62.89
Drilled:						0.0		
Total:						139.7		

Note: This table is also available in [ASCII format](#).

**Table T4.** Site 1122 coring summary. (See table note. Continued on next page.)

Core number	Core type	Date (Sept 1998)	Time	Top depth (mbsf)	Bottom depth (mbsf)	Length cored (m)	Length recovered (m)	Recovery (%)
181-1122A-								
1	H	6	1240	0.0	9.3	9.3	9.32	100.2
2	H	6	1355	9.3	18.8	9.5	9.66	101.7
3	H	6	1500	18.8	28.3	9.5	9.77	102.8
4	H	6	1625	28.3	37.8	9.5	10.05	105.8
5	H	6	1730	37.8	47.3	9.5	8.82	92.8
6	H	6	1830	47.3	56.8	9.5	9.06	95.4
7	H	6	1935	56.8	66.3	9.5	9.13	96.1
8	H	6	2045	66.3	75.8	9.5	7.69	80.9
9	X	6	2205	75.8	85.4	9.6	0.81	8.4
10	X	6	2305	85.4	95.0	9.6	0.44	4.6
11	X	7	0025	95.0	104.7	9.7	1.92	19.8
12	X	7	0135	104.7	114.3	9.6	5.02	52.3
13	X	7	0240	114.3	123.9	9.6	5.77	60.1
Cored totals:						123.9	87.46	70.59
Drilled:						0.0		
Total:						123.9		
181-1122B-								
1	H	7	0645	0.0	9.5	9.5	9.81	103.3
Cored totals:						9.5	9.81	103.26
Drilled:						0		
Total:						9.5		
181-1122C-								
1	H	7	0805	0.0	2.5	2.5	2.5	100.4
2	H	7	0930	2.5	9.5	7.0	9.8	139.3
3	H	7	1035	9.5	14.0	4.5	7.6	169.8
4	H	7	1155	14.0	23.5	9.5	9.7	102.1
5	H	7	1310	23.5	33.0	9.5	9.0	94.2
6	H	7	1355	33.0	42.5	9.5	9.2	96.4
7	H	7	1500	42.5	52.0	9.5	8.7	91.8
8	H	7	1610	52.0	61.5	9.5	9.4	99.4
9	H	7	1710	61.5	71.0	9.5	8.7	91.3
10	H	7	1830	71.0	80.5	9.5	9.4	99.3
11	H	7	2000	80.5	86.9	6.4	6.5	101.3
12	H	7	2100	86.9	94.9	8.0	7.9	98.8
13	H	7	2210	94.9	103.7	8.8	8.8	100.0
14	X	7	2330	103.7	108.0	4.3	4.3	100.5
15	X	8	0025	108.0	117.6	9.6	3.4	35.2
16	X	8	0135	117.6	127.2	9.6	5.4	56.0
17	X	8	0240	127.2	136.9	9.7	6.3	64.4
18	X	8	0345	136.9	146.5	9.6	3.7	38.6
19	X	8	0445	146.5	156.1	9.6	4.1	42.5
20	X	8	0545	156.1	165.7	9.6	5.2	54.3
21	X	8	0645	165.7	175.3	9.6	2.4	25.4
22	X	8	0745	175.3	185.0	9.7	1.7	17.8
23	X	8	0850	185.0	194.7	9.7	2.4	24.5
24	X	8	0950	194.7	204.3	9.6	0.8	8.5
25	X	8	1125	204.3	214.0	9.7	0.7	6.9
26	X	8	1230	214.0	223.7	9.7	4.1	42.2
27	X	8	1335	223.7	233.3	9.6	3.5	36.6
28	X	8	1430	233.3	242.9	9.6	4.5	46.7
29	X	8	1530	242.9	252.5	9.6	4.8	50.3
30	X	8	1625	252.5	261.7	9.2	6.7	73.2
31	X	8	1725	261.7	271.3	9.6	4.7	48.9
32	X	8	1830	271.3	280.7	9.4	2.6	27.1
33	X	8	1930	280.7	290.4	9.7	7.3	75.6
34	X	8	2040	290.4	300.0	9.6	7.4	77.5
35	X	8	2150	300.0	309.6	9.6	8.0	83.4
36	X	8	2255	309.6	319.3	9.7	8.7	89.7
37	X	9	0010	319.3	328.9	9.6	9.1	94.5
38	X	9	0120	328.9	338.5	9.6	4.5	46.7
39	X	9	0230	338.5	348.2	9.7	5.3	54.2
40	X	9	0340	348.2	357.9	9.7	3.3	33.6
41	X	9	0445	357.9	367.5	9.6	2.1	21.7
42	X	9	0550	367.5	377.2	9.7	4.7	48.4
43	X	9	0700	377.2	386.9	9.7	0.4	4.4

**Table T4 (continued).**

Core number	Core type	Date (Sept 1998)	Time	Top depth (mbsf)	Bottom depth (mbsf)	Length cored (m)	Length recovered (m)	Recovery (%)
44	X	9	0805	386.9	396.6	9.7	5.7	59.2
45	X	9	0925	396.6	406.2	9.6	6.0	62.6
46	X	9	1035	406.2	415.9	9.7	6.3	65.4
47	X	9	1140	415.9	425.5	9.6	5.7	59.5
48	X	9	1250	425.5	435.2	9.7	7.0	72.3
49	X	9	1400	435.2	444.8	9.6	9.3	97.0
50	X	9	1510	444.8	454.4	9.6	7.4	77.2
51	X	9	1655	454.4	464.1	9.7	9.3	95.5
52	X	9	1835	464.1	473.4	9.3	8.7	93.9
53	X	9	2010	473.4	483.0	9.6	5.0	51.7
54	X	9	2155	483.0	492.7	9.7	5.3	54.1
55	X	9	2340	492.7	502.3	9.6	7.3	75.7
56	X	10	0130	502.3	511.9	9.6	5.6	58.1
57	X	10	0320	511.9	521.5	9.6	5.3	55.6
58	X	10	0510	521.5	531.2	9.7	2.1	21.4
59	X	10	0705	531.2	540.7	9.5	0.1	1.3
60	X	10	0850	540.7	550.4	9.7	0.5	4.7
61	X	10	1030	550.4	560.0	9.6	5.2	54.1
62	X	10	1215	560.0	569.6	9.6	3.4	35.5
63	X	10	1355	569.6	579.3	9.7	1.7	17.7
64	X	10	1545	579.3	588.9	9.6	1.6	16.7
65	X	10	1735	588.9	598.5	9.6	1.8	18.5
66	X	10	1920	598.5	608.2	9.7	1.0	9.8
67	X	10	2100	608.2	617.8	9.6	1.0	10.5
68	X	10	2245	617.8	627.4	9.6	0.1	0.5
Cored totals:						627.4	351.44	56.02
Drilled:						0.0		
Total:						627.4		

Note: This table is also available in [ASCII format](#).



**Table T5.** Site 1123 coring summary. (See table note. Continued on next page.)

Core number	Core type	Date (Sept 1998)	Time	Top depth (mbsf)	Bottom depth (mbsf)	Length cored (m)	Length recovered (m)	Recovery (%)
181-1123A-								
1	H	14	0445	0.0	6.1	6.1	6.1	100
2	H	14	0545	6.1	15.6	9.5	9.61	101.2
3	H	14	0640	15.6	25.1	9.5	7.71	81.2
4	H	14	0825	25.1	34.6	9.5	9.7	102.1
5	H	14	0930	34.6	44.1	9.5	9.69	102
6	H	14	1025	44.1	53.6	9.5	9.72	102.3
7	H	14	1125	53.6	63.1	9.5	9.65	101.6
8	H	14	1225	63.1	72.6	9.5	8.97	94.4
9	H	14	1325	72.6	82.1	9.5	9.83	103.5
10	H	14	1420	82.1	91.6	9.5	9.83	103.5
11	H	14	1515	91.6	101.1	9.5	9.64	101.5
12	H	14	1610	101.1	110.6	9.5	9.76	102.7
13	H	14	1700	110.6	120.1	9.5	9.14	96.2
14	H	14	1800	120.1	129.6	9.5	9.66	101.7
15	H	14	1855	129.6	139.1	9.5	9.99	105.2
16	H	14	1955	139.1	148.6	9.5	9.61	101.2
17	H	14	2250	148.6	158.1	9.5	10.02	105.5
Core totals:						158.1	158.63	100.34
Drilled:						0.0		
Total:						158.1		
181-1123B-								
1	H	15	0130	0.0	3.4	3.4	3.36	98.8
2	H	15	0220	3.4	12.9	9.5	9.45	99.5
3	H	15	0315	12.9	22.4	9.5	9.84	103.6
4	H	15	0415	22.4	31.9	9.5	9.8	103.2
5	H	15	0535	31.9	41.4	9.5	9.77	102.8
6	H	15	0630	41.4	50.9	9.5	9.78	102.9
7	H	15	0750	50.9	60.4	9.5	10.12	106.5
8	H	15	0845	60.4	69.9	9.5	9.79	103.1
9	H	15	0945	69.9	79.4	9.5	9.76	102.7
10	H	15	1045	79.4	88.9	9.5	9.79	103.1
11	H	15	1155	88.9	98.4	9.5	9.91	104.3
12	H	15	1255	98.4	107.9	9.5	9.76	102.7
13	H	15	1350	107.9	117.4	9.5	9.88	104.0
14	H	15	1445	117.4	126.9	9.5	9.58	100.8
15	H	15	1540	126.9	136.4	9.5	9.91	104.3
16	H	15	1855	136.4	145.9	9.5	9.46	99.6
17	H	15	2040	145.9	155.4	9.5	9.78	102.9
18	X	15	2145	155.4	162.7	7.3	8.39	114.9
19	X	15	2225	162.7	172.3	9.6	9.59	99.9
20	X	15	2330	172.3	181.9	9.6	9.65	100.5
21	X	16	0735	181.9	191.6	9.7	9.47	97.6
22	X	16	0840	191.6	201.2	9.6	9.87	102.8
23	X	16	0955	201.2	210.8	9.6	7.76	80.8
24	X	16	1110	210.8	220.4	9.6	9.75	101.6
25	X	16	1220	220.4	230.0	9.6	9.7	101.0
26	X	16	1330	230.0	239.6	9.6	4.18	43.5
27	X	16	1440	239.6	249.2	9.6	9.82	102.3
28	X	16	1545	249.2	258.8	9.6	9.59	99.9
29	X	16	1820	258.8	268.4	9.6	9.79	102.0
30	X	16	1940	268.4	278.1	9.7	9.65	99.5
31	X	16	2045	278.1	287.7	9.6	9.49	98.9
32	X	16	2145	287.7	297.3	9.6	8.71	90.7
33	X	16	2305	297.3	306.9	9.6	9.65	100.5
34	X	17	0010	306.9	316.5	9.6	9.78	101.9
35	X	17	0120	316.5	325.9	9.4	9.62	102.3
36	X	17	0230	325.9	335.5	9.6	9.67	100.7
37	X	17	0350	335.5	345.1	9.6	9.8	102.1
38	X	17	0510	345.1	354.7	9.6	9.79	102.0
39	X	17	0625	354.7	364.4	9.7	9.88	101.9
40	X	17	0740	364.4	374.1	9.7	9.76	100.6
41	X	17	1020	374.1	383.7	9.6	8.2	85.4
42	X	17	1145	383.7	393.4	9.7	4.84	49.9
43	X	17	1335	393.4	403.0	9.6	6.22	64.8
44	X	17	1525	403.0	412.6	9.6	5.42	56.5
45	X	17	1710	412.6	422.2	9.6	4.06	42.3

**Table T5 (continued).**

Core number	Core type	Date (Sept 1998)	Time	Top depth (mbsf)	Bottom depth (mbsf)	Length cored (m)	Length recovered (m)	Recovery (%)
46	X	17	1855	422.2	431.8	9.6	6.21	64.7
47	X	17	2045	431.8	441.5	9.7	5.26	54.2
48	X	17	2255	441.5	450.8	9.3	4.25	45.7
49	X	18	0220	450.8	460.4	9.6	6.41	66.8
50	X	18	0420	460.4	470.0	9.6	8.35	87.0
51	X	18	0625	470.0	479.3	9.3	9.72	104.5
52	X	18	0835	479.3	489.0	9.7	9.36	96.5
Core totals:						489	451.4	92.31
Drilled:						0		
Total:						489		
181-1123C-								
1	H	19	1155	0.0	9.0	9.0	9.02	100.2
2	H	19	1250	9.0	18.5	9.5	9.53	100.3
3	H	19	1355	18.5	28.0	9.5	9.79	103.1
4	H	19	1450	28.0	37.5	9.5	9.59	100.9
5	H	19	1545	37.5	47.0	9.5	8.85	93.2
6	H	19	1645	47.0	56.5	9.5	9.91	104.3
7	H	19	1740	56.5	66.0	9.5	9.85	103.7
8	H	19	1845	66.0	75.5	9.5	9.82	103.4
9	H	19	1935	75.5	85.0	9.5	8.65	91.1
10	H	19	2035	85.0	94.5	9.5	9.94	104.6
11	H	19	2130	94.5	104.0	9.5	9.71	102.2
12	H	19	2225	104.0	113.5	9.5	9.87	103.9
13	H	19	2325	113.5	123.0	9.5	9.74	102.5
14	H	20	0025	123.0	132.5	9.5	10.05	105.8
15	H	20	0125	132.5	142.0	9.5	9.59	100.9
16	H	20	0240	142.0	151.5	9.5	9.79	103.1
17	O	20	0630	151.5	230.0	0.0	0.00	N/A
17	X	20	0740	230.0	239.6	9.6	6.39	66.6
18	O	20	1945	239.6	484.0	0.0	0.00	N/A
18	X	20	2125	484.0	488.5	4.5	4.95	110.0
19	X	20	2310	488.5	498.1	9.6	9.7	101.0
20	X	21	0115	498.1	507.7	9.6	8.44	87.9
21	X	21	0320	507.7	517.4	9.7	9.41	97.0
22	X	21	0510	517.4	527.0	9.6	9.81	102.2
23	X	21	0710	527.0	536.6	9.6	9.81	102.2
24	X	21	0905	536.6	546.2	9.6	9.76	101.7
25	X	21	1050	546.2	555.7	9.5	9.66	101.7
26	X	21	1230	555.7	565.4	9.7	9.67	99.7
27	X	21	1410	565.4	575.1	9.7	9.66	99.6
28	X	21	1555	575.1	584.7	9.6	8.78	91.5
29	X	21	1815	584.7	594.3	9.6	8.71	90.7
30	X	21	2035	594.3	603.9	9.6	5.44	56.7
31	X	21	2305	603.9	613.6	9.7	7.28	75.1
32	X	21	0340	613.6	623.2	9.6	5.61	58.4
33	X	22	0710	623.2	632.8	9.6	2.66	27.7
Core totals:						309.9	289.44	93.40
Drilled:						322.9		
Total:						632.8		

Note: This table is also available in [ASCII format](#).

Table T6. Site 1124 coring summary. (See table note. Continued on next page.)

Core number	Core type	Date (1998)	Time	Top depth (mbsf)	Bottom depth (mbsf)	Length cored (m)	Length recovered (m)	Recovery (%)
181-1124A-								
1	H	26 Sept	0325	0.0	9.5	9.5	9.51	100.1
Core totals:						9.5	9.51	100.11
Drilled:						0.0		
Total:						9.5		
181-1124B-								
1	H	26 Sept	0530	0.0	5.4	5.4	5.41	100.2
2	H	26 Sept	1740	5.4	9.9	4.5	4.48	99.6
Core totals:						9.9	9.89	99.90
Drilled:						0.0		
Total:						9.9		
181-1124C-								
1	O	27 Sept	0325	0.0	8.0	0.0	0.0	N/A
1	X	27 Sept	0330	8.0	17.6	9.6	1.51	15.7
2	X	27 Sept	0430	17.6	27.2	9.6	7.68	80.0
3	H	27 Sept	0540	27.2	36.7	9.5	10.0	105.3
4	H	27 Sept	0645	36.7	46.2	9.5	9.74	102.5
5	H	27 Sept	0810	46.2	55.7	9.5	9.99	105.2
6	H	27 Sept	0915	55.7	65.2	9.5	9.58	100.8
7	H	27 Sept	1040	65.2	74.7	9.5	9.99	105.2
8	H	27 Sept	1155	74.7	84.2	9.5	9.75	102.6
9	H	27 Sept	1315	84.2	93.7	9.5	10.04	105.7
10	H	27 Sept	1420	93.7	103.2	9.5	9.12	96.0
11	H	27 Sept	1535	103.2	112.7	9.5	9.85	103.7
12	H	27 Sept	1640	112.7	122.2	9.5	9.15	96.3
13	H	27 Sept	1745	122.2	131.7	9.5	9.91	104.3
14	H	27 Sept	1850	131.7	141.2	9.5	9.51	100.1
15	H	27 Sept	1955	141.2	150.7	9.5	9.45	99.5
16	H	27 Sept	2100	150.7	159.2	8.5	8.72	102.6
17	X	27 Sept	2220	159.2	168.8	9.6	9.6	100.0
18	X	27 Sept	2325	168.8	178.4	9.6	9.58	99.8
19	X	28 Sept	0040	178.4	188.0	9.6	9.87	102.8
20	X	28 Sept	0145	188.0	197.7	9.7	9.67	99.7
21	X	28 Sept	0250	197.7	207.3	9.6	9.76	101.7
22	X	28 Sept	0400	207.3	216.9	9.6	9.76	101.7
23	X	28 Sept	0505	216.9	226.5	9.6	9.79	102.0
24	X	28 Sept	0615	226.5	236.2	9.7	9.66	99.6
25	X	28 Sept	0720	236.2	245.8	9.6	9.78	101.9
26	X	28 Sept	0830	245.8	255.4	9.6	9.7	101.0
27	X	28 Sept	0935	255.4	265.1	9.7	9.65	99.5
28	X	28 Sept	1040	265.1	274.7	9.6	9.62	100.2
29	X	28 Sept	1150	274.7	284.3	9.6	1.81	18.9
30	X	28 Sept	1300	284.3	294.0	9.7	0.15	1.5
31	X	28 Sept	1410	294.0	303.6	9.6	9.18	95.6
32	X	28 Sept	1520	303.6	313.3	9.7	9.45	97.4
33	X	28 Sept	1625	313.3	322.9	9.6	9.48	98.8
34	X	28 Sept	1740	322.9	332.6	9.7	9.69	99.9
35	X	28 Sept	1850	332.6	342.2	9.6	9.84	102.5
36	X	28 Sept	2000	342.2	351.9	9.7	9.61	99.1
37	X	28 Sept	2110	351.9	361.5	9.6	9.74	101.5
38	X	28 Sept	2225	361.5	371.2	9.7	9.66	99.6
39	X	28 Sept	2330	371.2	380.8	9.6	9.85	102.6
40	X	29 Sept	0040	380.8	390.4	9.6	9.37	97.6
41	X	29 Sept	0200	390.4	400.1	9.7	9.57	98.7
42	X	29 Sept	0315	400.1	409.7	9.6	9.74	101.5
43	X	29 Sept	0450	409.7	419.3	9.6	9.05	94.3
44	X	29 Sept	0635	419.3	429.0	9.7	9.77	100.7
45	X	29 Sept	0820	429.0	438.7	9.7	9.72	100.2
46	X	29 Sept	1005	438.7	448.3	9.6	7.18	74.8
47	X	29 Sept	1145	448.3	457.9	9.6	9.26	96.5
48	X	29 Sept	1350	457.9	467.4	9.5	5.52	58.1
49	X	29 Sept	1620	467.4	473.1	5.7	5.72	100.4
Core totals:						465.1	433.79	93.27
Drilled:						8.0		
Total:						473.1		

**Table T6 (continued).**

Core number	Core type	Date (1998)	Time	Top depth (mbsf)	Bottom depth (mbsf)	Length cored (m)	Length recovered (m)	Recovery (%)
181-1124D-								
1	O	30 Sept	2050	0.0	22.6	0.0	0.0	N/A
1	H	30 Sept	2150	22.6	32.1	9.5	9.56	100.6
2	H	30 Sept	2255	32.1	41.6	9.5	7.75	81.6
3	H	30 Sept	2355	41.6	51.1	9.5	8.97	94.4
4	H	1 Oct	0100	51.1	60.6	9.5	8.52	89.7
5	H	1 Oct	0205	60.6	70.1	9.5	9.77	102.8
6	H	1 Oct	0315	70.1	79.6	9.5	9.3	97.9
7	H	1 Oct	0420	79.6	89.1	9.5	9.95	104.7
8	H	1 Oct	0525	89.1	98.6	9.5	9.01	94.8
9	H	1 Oct	0630	98.6	108.1	9.5	9.88	104.0
10	H	1 Oct	0730	108.1	117.6	9.5	9.72	102.3
11	H	1 Oct	0835	117.6	127.1	9.5	9.89	104.1
12	H	1 Oct	0940	127.1	136.6	9.5	9.73	102.4
13	H	1 Oct	1040	136.6	146.1	9.5	10.04	105.7
14	H	1 Oct	1155	146.1	155.6	9.5	9.75	102.6
Core totals:						133.0	131.84	99.13
Drilled:						22.6		
Total:						155.6		

Note: This table is also available in [ASCII format](#).

**Table T7.** Site 1125 coring summary. (See table note. Continued on next page.)

Core number	Core type	Date (Oct 1998)	Time	Top depth (mbsf)	Bottom depth (mbsf)	Length cored (m)	Length recovered (m)	Recovery (%)
181-1125A-								
1	H	3	0405	0.0	4.3	4.3	4.31	100.2
2	H	3	0445	4.3	13.8	9.5	9.17	96.5
3	H	3	0515	13.8	23.3	9.5	9.9	104.2
4	H	3	0550	23.3	32.8	9.5	9.63	101.4
5	H	3	0640	32.8	42.3	9.5	9.88	104.0
6	H	3	0715	42.3	51.8	9.5	9.42	99.2
7	H	3	0805	51.8	61.3	9.5	10.07	106.0
8	H	3	0840	61.3	70.8	9.5	9.18	96.6
9	H	3	0930	70.8	80.3	9.5	10.06	105.9
10	H	3	1015	80.3	89.8	9.5	9.71	102.2
11	H	3	1055	89.8	99.3	9.5	10.12	106.5
12	H	3	1130	99.3	108.8	9.5	9.88	104.0
13	H	3	1215	108.8	118.3	9.5	10.09	106.2
14	H	3	1250	118.3	127.8	9.5	9.91	104.3
15	H	3	1335	127.8	137.3	9.5	10.0	105.3
16	H	3	1415	137.3	146.8	9.5	9.45	99.5
17	H	3	1455	146.8	156.3	9.5	9.99	105.2
18	H	3	1535	156.3	165.8	9.5	9.82	103.4
19	H	3	1620	165.8	175.3	9.5	9.92	104.4
20	H	3	1650	175.3	184.8	9.5	9.72	102.3
21	H	3	1730	184.8	194.3	9.5	9.62	101.3
22	H	3	1820	194.3	203.5	9.2	9.22	100.2
Cored totals:						203.5	209.07	102.74
Drilled:						0		
Total:						203.5		
181-1125B-								
1	H	3	2145	0.0	8.3	8.3	8.30	100.00
2	H	3	2210	8.3	17.8	9.5	9.65	101.60
3	H	3	2245	17.8	27.3	9.5	9.51	100.10
4	H	3	2320	27.3	36.8	9.5	9.38	98.70
5	H	3	2355	36.8	46.3	9.5	9.86	103.80
6	H	4	0035	46.3	55.8	9.5	9.73	102.40
7	H	4	0110	55.8	65.3	9.5	9.95	104.70
8	H	4	0145	65.3	74.8	9.5	9.12	96.00
9	H	4	0230	74.8	84.3	9.5	9.85	103.70
10	H	4	0305	84.3	93.8	9.5	8.50	89.50
11	H	4	0345	93.8	103.3	9.5	9.93	104.50
12	H	4	0420	103.3	112.8	9.5	9.65	101.60
13	H	4	0455	112.8	122.3	9.5	9.90	104.20
14	H	4	0535	122.3	131.8	9.5	9.94	104.60
15	H	4	0620	131.8	141.3	9.5	9.92	104.40
16	H	4	0755	141.3	150.8	9.5	9.97	104.90
17	H	4	0840	150.8	160.3	9.5	10.06	105.90
18	H	4	0920	160.3	169.8	9.5	9.39	98.80
19	H	4	1005	169.8	179.3	9.5	9.98	105.10
20	H	4	1100	179.3	188.8	9.5	9.03	95.10
21	X	4	1235	188.8	197.2	8.4	9.74	116.00
22	X	4	1315	197.2	206.8	9.6	9.81	102.20
23	X	4	1400	206.8	216.4	9.6	9.47	98.60
24	X	4	1435	216.4	226.0	9.6	7.50	78.10
25	X	4	1520	226.0	235.6	9.6	8.82	91.90
26	X	4	1600	235.6	245.2	9.6	9.72	101.30
27	X	4	1640	245.2	254.8	9.6	8.75	91.10
28	X	4	1725	254.8	264.4	9.6	9.74	101.50
29	X	4	1810	264.4	274.1	9.7	9.64	99.40
30	X	4	1900	274.1	283.7	9.6	8.23	85.70
31	X	4	1945	283.7	293.3	9.6	4.68	48.80
32	X	4	2030	293.3	303.0	9.7	9.82	101.20
33	X	4	2110	303.0	312.6	9.6	9.79	102.00
34	X	4	2205	312.6	321.9	9.3	8.44	90.80
35	X	4	2255	321.9	331.5	9.6	9.89	103.00
36	X	4	2340	331.5	341.1	9.6	1.28	13.30
37	X	5	0055	341.1	350.7	9.6	7.31	76.10
38	X	5	0150	350.7	360.4	9.7	9.77	100.70
39	X	5	0235	360.4	370.1	9.7	9.69	99.90
40	X	5	0320	370.1	379.7	9.6	9.02	94.00

**Table T7 (continued).**

Core number	Core type	Date (Oct 1998)	Time	Top depth (mbsf)	Bottom depth (mbsf)	Length cored (m)	Length recovered (m)	Recovery (%)
41	X	5	0405	379.7	389.4	9.7	9.76	100.60
42	X	5	0450	389.4	399.0	9.6	6.67	69.50
43	X	5	0535	399.0	408.6	9.6	7.83	81.60
44	X	5	0620	408.6	418.3	9.7	3.53	36.40
45	X	5	0735	418.3	427.9	9.6	9.61	100.10
46	X	5	0830	427.9	437.5	9.6	9.82	102.30
47	X	5	0915	437.5	446.8	9.3	9.63	103.50
48	X	5	1030	446.8	456.4	9.6	4.07	42.40
49	X	5	1145	456.4	466.0	9.6	9.60	100.00
50	X	5	1255	466.0	475.2	9.2	9.15	99.50
51	X	5	1405	475.2	484.9	9.7	9.80	101.00
52	X	5	1515	484.9	494.5	9.6	9.69	100.90
53	X	5	1625	494.5	504.1	9.6	9.13	95.10
54	X	5	1755	504.1	513.8	9.7	8.73	90.00
55	X	5	2005	513.8	523.4	9.6	7.28	75.80
56	X	5	2230	523.4	533.0	9.6	9.59	99.90
57	X	6	0030	533.0	542.6	9.6	9.32	97.10
58	X	6	0315	542.6	552.1	9.5	5.72	60.20
Cored totals:						552.1	511.66	92.68
Drilled:						0		
Total:						552.1		

Note: This table is also available in [ASCII format](#).